UNIVERSITY OF SOUTHAMPTON
SCHOOL OF OCEAN AND EARTH SCIENCE

OCEAN-CLIMATE PROCESSES RECORDED IN HOLOCENE LAMINATED SEDIMENTS FROM THE GOTLAND DEEP, BALTIC SEA

BY

IAN TERENCE BURKE

Completed in partial fulfilment of the requirements for admission to the degree of Doctor of Philosophy

September 2001

ABSTRACT

The Gotland Deep is an isolated deep basin within the shallow and enclosed Baltic Sea. Due to a limited exchange with oxygenated surface water with stagnant deep water, the Gotland Deep has been commonly anoxic and laminated sediments have been intermittently deposited throughout the last ~8100^{14}Cyr. Using Scanning electron microscope techniques, individual laminae, down to 50μm in thickness, with distinct mineralogical, micropalaeontological, or geochemical composition have been identified and described. Depositional laminae sequences in the form of couplets, triplets, and quadruplets of diatomaceous and lithogenic laminae are observed with a thickness range commonly between 0.45-1.25mm (mean 0.75mm). Examination of the diatom assemblages suggests that these sequences of laminae represent annual deposits, or varves. Varves are relatively uncommon and typically occur in small intervals of 2-5 varves, which are interrupted by more indistinctly laminated and homogeneous sediments.

The varves occurring in the Littorina sequence allow the placing of early diagenetic Ca-rhodochrosite laminae within the seasonal cycle as an exclusively winter-early spring deposit. This is in agreement with the seasonal distribution of major Baltic inflow events in historical records, and a direct causal link between saline inflows and Ca-rhodochrosite deposition is implied. Benthic foraminifera tests are also found to be encrusted with Ca-rhodochrosite, implying that benthic re-colonisation during oxidation events occurs concurrently with Ca-rhodochrosite formation.

Many trace metals including; Mn, Fe, Mo, U, V, Cd, Pb, Co, Ni, Cu, As and Zn, are observed to be enriched within both Ca-rhodochrosite and Fe-sulphide rich laminae. This is most likely to be caused by scavenging by particulate Fe-sulphides and Mn-oxides in the Gotland Deep, providing an effective sedimentary sink for these elements.

The relatively common occurrence of small (50-100μm) hexagonal γ Mn-sulphide pseudomorphs is reported here for the first time. Although Mn-sulphide crystals are not usually preserved in these sediments, initial formation of Mn-sulphide may be more common than previous reports suggest. Several Mn-sulphide laminae, although heavily oxidised during sampling, are indeed directly observed within a

single organic-carbon rich interval. This demonstrates that Mn-sulphide is formed and preserved, at the expense of Ca-rhodochrosite, under more reducing conditions. The exact proportions of Ca-rhodochrosite and Mn-sulphide that may be produced following a major Baltic inflow event as a result of the progressive rapid microbial reduction of a Mn-oxy-hydroxide laminae, is primarily controlled by variation in pore-water redox conditions.

Although there is much interannual variation in formation and preservation, sedimentary Mn-enrichments represent a good record of groups of saline inflow events. Centimetre-scale periodic variation in Mn-enrichment is observed, which most likely relates to decadal-scale variation in saline inflows to the Baltic Sea, and by extension to variation in North Atlantic climate.

To my parents, Terry and Carole Burke

GRADUATE SCHOOL OF THE
SOUTHAMPTON OCEANOGRAPHY CENTRE

This PhD dissertation by

IAN T. BURKE

has been produced under the supervision of the following persons

Supervisor

Prof. Alan Kemp

Chair of Advisory Panel

Prof. John Murray

Members of Advisory Panel

Prof. John Thomson Dr. Andy Roberts

This research was funded by the award of NERC studentship GT4/98/ES/266.

ACKNOWLEDGEMENTS

Very special thanks to Alan Kemp for his help and advice throughout my PhD studies here in Southampton.

Cheers! to Ivo Grigorov, author of the excellent pilot-study which kick-started this project, and the co-author on my first ever paper.

Many thanks to John Thomson for his patient advice on all things geochemical, and whose comments greatly improved Chapters 4, 5 and 6.

Special thanks also to Eelco Rohling and John Murray, for their help in foraminiferal identification. Eelco also provided stimulating advice which helped in the drafting of Chapter 7. As my advisory panel chairman, John also provided sage advice at all times.

Thanks also to Andy Roberts, who also sat on my advisory panel, and shared palaeomagnetic data.

Thanks to Kay Emeis of the Institute of Baltic Research, Warnemünde, Germany, who provided core material making this study possible, and Ulrick Struck also of the Institute of Baltic Research for sharing radiocarbon data.

Richard Pearce, Steve Cooke, Ross Williams and Andy Milton are thanked for their time and advice.

An earlier version of Chapter 3 was greatly improved by comments made in review by H. Chamley, S. Björck and A. Lepland.

Earlier drafts of Chapter 4 were greatly improved by pre-review comments from Chris German, and comments made in review by S. Calvert and an anonymous reviewer.

This thesis was also greatly improved by copy editing and advice from Linda Strickler.

Finally to Airasa Maughan-Strickler , who against all odds, continues to put up with me.

CONTENTS

LIST OF FIGURES

All figures are included as separate plates at the end of each chapter

LIST OF TABLES

All tables are included in the text of each chapter

1 INTRODUCTION

With 2 figures

1.1 RATIONALE AND OBJECTIVES

The Baltic Sea is a shallow enclosed basin, much of which is less than 50m deep. There are a few isolated deep basins including the Gotland Deep (250m), and the Bornholm Deep (80m) (Fig. 1.1). The Baltic Sea drains a watershed more than four times its area and there is limited exchange of saline North Sea water, producing the largest brackish water body in the world. As a result of this freshwater surplus, the Baltic Sea has a very strong salinity stratification, in which a low salinity, well-mixed, surface water layer (~2-8‰), is separated from more saline deep water (~11-15‰) by a permanent halocline at 60-80m (Manheim, 1961; Kullenberg, 1981) that effectively restricts the mixing of surface and deep waters (Matthäus, 1990), and the deep basins are only flushed during periodic saline inflows of North Sea water (Matthäus, 1995). Sedimentation below the halocline in the Gotland Deep is characterised by accumulation of fine grained organic carbon-rich muds (Ignatius et al., 1981; Sohlenius, 1996) that have been intermittently laminated throughout the last ~8100 ^{14}C yr.

The laminated Gotland Deep sediments represent a good record of climatic and environmental changes affecting the entire Baltic Sea (Rahm, 1988), and provide an opportunity to investigate the nature and origin of variability in ocean-climate processes on seasonal to centennial time scales. This study has utilised sediment core material collected by the Institute of Baltic Sea Research at Warnemuende (IOW), Germany, as part of the Gotland Basin Experiment (GOBEX) (Emeis and Struck, 1998). SEM based techniques have been used to resolve the composition of these sediments down to laminae scales in order to characterise processes relating to:

1. Individual sedimentation events, determining variation in biogenic production (diatoms) and lithogenic input.
2. Relating these individual sedimentation events and sequences of sedimentation events to seasonal/annual processes and from this to develop an understanding of inter-annual variability and sedimentation rates.

3. Documentation of early diagenetic Ca-rhodochrosite laminae and their relationship to redox processes occurring in the Gotland Deep.
4. Collection and analysis of continuous time-series data in order to delimit inter-annual, decadal, and centennial scale variability in ocean-climate processes affecting the Baltic Sea.

1.2 The Late Pleistocene and Holocene history of the Baltic Sea

Since the onset of deglaciation, Baltic Sea stratigraphy has been controlled by the balance between global eustatic sea level rise and local isostatic uplift, leading to continual fluctuation of Baltic shorelines and connectivity to the North Sea (Fig. 1.2). The Late Pleistocene and Holocene history (approx. 13K ^{14}C years BP—present) of the Baltic Sea and corresponding sediments are traditionally divided into the 5 Stages summarised in Table 1.1.

Baltic Ice Lake—An early ice-damned lake with sediments dominated by varved glaciogenic ice marginal sedimentation (Ignatius et al., 1981). These sediments are transgressive from south to north as the ice sheet retreated, producing thick (>200mm), coarse-grained, proximal varves close to the ice margin, and ever thinner and finer-grained distal varves (0.2-2mm) with increasing distance from the ice margin (Wastegård et al., 1995). Sediments have a low organic carbon content at approx. 0.5wt% (Danyushevskaya, 1992).

Yoldia Sea—Formed after a catastrophic switch of outflow thresholds as the ice sheet retreated, causing a 25m drop in lake level down to Yoldia sea level (Björck, 1995). Despite the name 'Yoldia sea', brackish conditions persisted for only 200-300yr during mid Yoldia times (Mörner, 1995; Wastegård et al., 1995), where the dwarf marine bivalve, *Portlandia 'Yoldia' arctica* (Raukas, 1995), and brackish water diatom assemblages are preserved in a sub-millimetre micro-varved clay.

Ancylus Lake—Rapid isostatic uplift then closed the connection to the North Sea through central Sweden and created this final lacustrine stage, during which a transitional clay facies was deposited. Although still dominated by glacially derived sediment from a distant ice sheet (Ignatius et al., 1981), the transitional sediments are homogeneous and have been post-depositionally stained grey by sulphide minerals due to downwards diffusion of sulphide from the later deposited Littorina sediments above (Ignatius et al., 1981). Sediments contain a moderate ~1.2wt% organic carbon (Danyushevskaya, 1992).

Littorina Sea—Connection to the North Atlantic, initiated by rapid eustatic sea level rise, established the brackish conditions that have persisted to the present day (Sohlenius et al., 1996a). The salt-water intrusion led to the progressive development of a strong salinity stratification between fresher surface waters and more saline bottom waters (Sohlenius et al., 2001). This permanent halocline inhibits vertical mixing and the Baltic's deep basins tend to be isolated and prone to anoxia, therefore, laminated sediments are common throughout the post-glacial Littorina muds. Littorina sediments are enriched in organic carbon, possibly due to increased biogenic production (Sohlenius et al., 1996a; Westman and Sohlenius, 1999), and contain 3.0-5.5wt% organic carbon (Danyushevskaya, 1992). These sediments are rich in early diagenetic Fe-sulphides and Ca-rhodochrosite, indicating a reducing sedimentary environment (Berner and Raiswell, 1983; Boesen and Postma, 1988; Huckriede and Meischner, 1996).

Modern Baltic (or Limnaea Sea)—Essentially this stage represents a continuation of Littorina conditions, however isostatic uplift of the sill region has led to the restriction of saline inflow, reducing salinity in the Baltic Sea from approx. 15-20‰ to 2-8‰ (Ignatius et al., 1981; Mörner, 1995; Sohlenius et al., 1996a). Baltic conditions have remained fairly stable over the last 3000 ^{14}C yr.

Table 1.1 Stratigraphic stages of the Baltic Sea

Baltic Stage[1,3,7,9,11] ^{14}C Ka BP	Sediment Type[1]	Organic Carbon (wt%)[2]	Salinity (‰)[3]	Fossil Assemblage	Environmental Conditions
Modern Baltic (or Limnaea Sea) Present—3Ka BP	mixed laminated and homogeneous clay gyttja	3.0-5.5	6-9	Brackish water diatoms[3]	Continuation of Littorina stage, however slow isostatic uplift of sill region led to the restriction of saline inflow, reducing salinity[1,8]
Littorina Sea (inc. Mastogloia) 3Ka—8.1Ka BP	laminated and homogeneous clay gyttja	3.0-5.5	Up to 20	Brackish water diatoms[3]	Initiated by rapid eustatic sea level rise, connection to the North Atlantic established the brackish conditions and salinity stratification that have persisted to the present day[3]. A 2-5% enrichment in manganese is due to the occurrence of rhodochrosite laminae[10]
Ancylus Lake 8.1—9.5Ka BP	homogeneous sulphide stained clay	1.2	Fresh Water	Fresh water mollusc *Ancylus fluviatilis*[6]	Final lacustrine stage initiated by rapid isostatic uplift[6,7,8]
Yoldia Sea 9.3—10.0Ka BP	glaciogenic micro-varved clay	0.4	~10%	Brackish water diatoms and dwarf marine bivalve *Portlandia 'Yoldia' arctica*[6]	Formed after a catastrophic 25m drop in lake level down to Yoldia sea level[7], brackish conditions persisted for only 200-300yr. during mid Yoldia times[8,9]
Baltic Ice Lake 10.0— ~13Ka BP	glaciogenic ice marginal varved clay	0.5	Fresh Water	Sparse cold water Diatoms[4]	Early ice-damned lake, formed from melt-water from the Weichselian Ice Sheet[5]

[1]Ignatius et al., 1981; [2]Danyushevskaya, 1992; [3]Sohlenius et al., 1996a; [4]Kabailiené, 1995; [5]Raukas, 1995; [6]Zenkevitch, 1963; [7]Björck, 1995; [8]Mörner, 1995; [9]Wastegård et al., 1995; [10]Huckriede and Meischner, 1996; [11]Björck et al., 1996

1.3 THESIS STRUCTURE AND MANUSCRIPTS RELATED TO THIS STUDY

This thesis has been prepared as a series of 5 papers suitable for publication in peer reviewed journals. These 5 papers are linked by a common theme, i.e. the exploration of different aspects of the laminated sediments found in the Gotland Deep. Essentially Chapters 3-7 are almost identical to those manuscripts; however, some of the common background material, and methods, which are described in Chapters 1 and 2 have been omitted from chapters 3-7 to avoid duplication.

Chapter 3 presents a discussion of the biogenic and lithogenic laminae that occur in Gotland Deep sediments, placing them into the context of seasonal flux events and varves. Chapter 4 presents a sub-millimetre scale fabric and geochemical study of the occurrence of Ca-rhodochrosite laminae, relating Ca-rhodochrosite laminae to seasonal scale diagenetic processes; the occurrence of Mn-sulphide pseudomorphs are also reported. Chapter 5 explores the possible trace metal associations occurring within Ca-rhodochrosite laminae.

Chapter 6 builds further on the work presented in chapter 4, presenting millimetre scale geochemical record, and discusses in detail the diagenetic processes that cause Ca-rhodochrosite and Mn-sulphide to form in Gotland Deep sediments. Chapter 7 uses the millimetre scale geochemical record of Mn-enrichments presented in chapter 6 as a proxy-record of seasonal variations in Gotland Deep redox conditions, and relates this to variations in North Atlantic climate. Chapters 8 and 9 contain a short summary of the results and a brief outline of possible directions for further work following from this study. All figures are included at the end of each chapter as a series of separate plates.

Two manuscripts relating directly to this study have now been accepted for publication, and are included in full on the data CD-ROM:

Burke, I.T., Grigorov, I. and Kemp, A.E.S. (in press) Micro-fabric study of biogenic and terrigenous deposition in laminated sediments from the Gotland Deep, Baltic Sea. Marine Geology, (Chapter 3).

Burke, I.T. and Kemp, A.E.S. A micro-fabric analysis of Ca-rhodochrosite laminae deposition, and Mn-sulphide formation in the Gotland Deep, Baltic Sea. Geochimica et Cosmochimica Acta, (Chapter 4).

Chapters 6 and 7 are also currently in preparation for publication.

Figure 1.1 Bathymetry Map of Baltic Sea showing location of: 1. Darrs Strait; 2. Arkona Basin; 3. Bornholm Basin; 4. Stolpe Channel and the Gotland Deep.

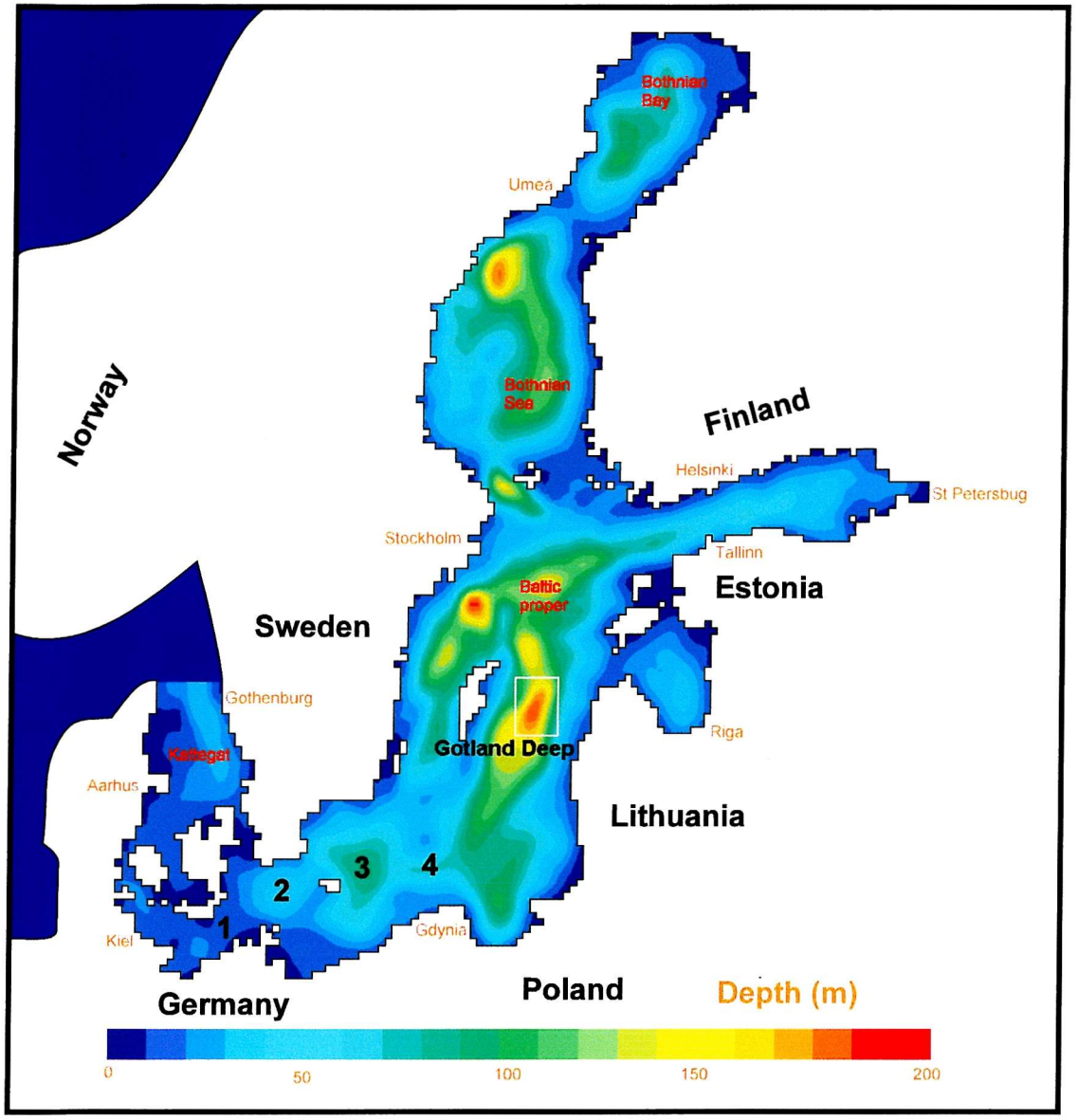

Figure 1.2 Late Pleistocene and Early Holocene development of The Baltic Sea, modified from Lindström et al. (1994), and Sohlenius (1996).

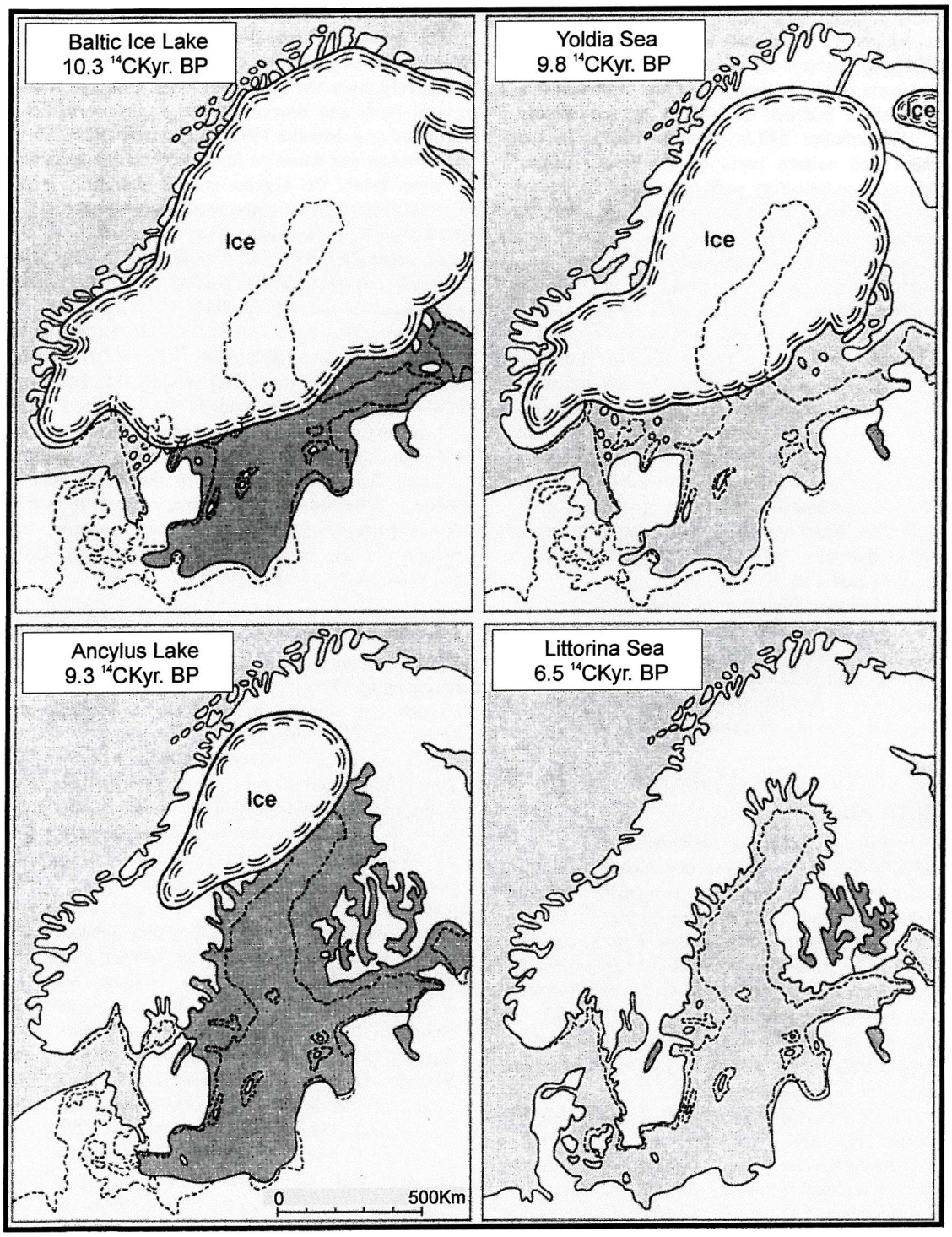

2 METHODS AND MATERIALS

With 4 figures

2.1 CORE LOCATION AND INITIAL TREATMENT

As part of the Gotland Basin Experiment (GOBEX), (Emeis and Struck, 1998), a 5.64m gravity Core, 20001-5, was collected in the Central Gotland Basin at 57°18.33N, 20°03.00E (Fig. 2.1), in a water depth of 243m, during cruise 94.44.13.2 of R/V *Alexander Von Humboldt* in August 1994. Initial core description and sub-sampling was undertaken by staff of the Institute of Baltic Research at Warnemünde, Germany, where the core was sub-sampled into 25cm wet sediment slabs and X-ray exposures were taken. The wet sediment slabs were vacuum packed in polythene bags to prevent desiccation. A radiocarbon ^{14}C-AMS age was obtained from a fish bone recovered from 205cm in core 20001-5 for Dr. U Struck (Institute of Baltic Research, Warnemünde), with a reservoir correction of -400yrs. Two kasten cores, 201301-5 and 201302-5, were also collected as part of GOBEX during cruise 4.3-13.3.96 of R/V *Poseidon* in February 1996, at 57°20.10N, 19°57.50E (water depth 237m) and 57°15.14N, 20°11.99E (water depth 249m) respectively. Preliminary fabric descriptions were prepared from X-ray images in Emeis and Struck (1998) for the post-Ancylus sections of 201301-5 and 201302-5, and these are presented with core 20001-5 in Figure 2.2 only for reference purposes.

2.2 SAMPLE PREPARATION

Only material from core 20001-5 was prepared from SEM analysis. Sediment samples from four slabs, Slab 4 (71-93cm), Slab 6 (118-144cm), and Slabs 8 and 9 (165-216cm), were prepared for SEM study by embedding in epoxy resin using a fluid displacive impregnation technique modified from that described in Pike and Kemp (1996a), by Kemp et al. (1998). After partial desiccation during transit to the UK, Slab 4 showed signs of oxidation, and growths of gypsum crystals were observed on the sediment surface. The yellow Ca-rhodochrosite laminae were not evident in Slab 4, however, the sediment fabric was otherwise undisturbed, allowing examination of the primary sedimentary micro-structure. In contrast, many yellow Ca-rhodochrosite laminae were evident in Slab 6. Fluid displacive embedding allows thin section

preparation with minimal fabric disturbance. Polished thin sections were prepared using an oil-based lubricant prior to fabric analysis carried out under the SEM.

2.3 SCANNING ELECTRON MICROSCOPY

The polished thin sections were examined in the SEM using back-scattered electron (BSE) imagery. BSE images reveal the minerals, textures and fabrics of sediments and rocks in much greater detail than is possible with conventional optical microscopy (Krinsley et al., 1998). Back-scattered electrons undergo elastic collisions and are subsequently directed back out of the sample. The ratio of back-scattered/ incident electrons defines the back-scattering coefficient (η), which is a function of the atomic number of the sample. Thus, for highly polished flat specimens, the brightness within the BSE image is proportional to the atomic number of the sample. Minerals with high mean atomic number such as pyrite ($\eta = 0.247$) are very bright (Fig. 3.3b), while those with intermediate mean atomic number such as dolomite ($\eta = 0.133$) are mid grey (Fig. 3.3b) and the epoxy resin is black (Krinsley et al., 1998). Since the epoxy resin has been absorbed into all pore spaces in the sediment, the overall distribution of brightness or darkness within an image is effectively a porosity map of the specimen. In lower magnification images (e.g., Fig. 3.4, 3.5), the less porous clay-rich sediment laminae stand out from the darker diatomaceous laminae, in which the resin has pervasively entered the more open diatom framework.

Counterparts of the sediment prepared as polished thin sections were broken off, dried, mounted on stubs, and examined under SEM to produce topographic BSE images (analogous to secondary electron images) to aid identification of microfossils, mineral habits and sediment fabrics (Fig. 3.2).

2.4 ENERGY DISPERSIVE X-RAY MICROANALYSIS (EDS)

Non-destructive major element analysis was performed on thin sections using the Energy Dispersive X-ray Microanalysis (EDS) tool fitted to the SEM under standard conditions (count time 40sec; voltage 15kV; beam current $5x10^{-6}$A). Comparison to standard spectra produced quantitative data with errors of less than 10% down to 0.5wt%; below 0.5wt% errors can increase up to 25%. The sampled excitation volume using this technique can be as little as $2\mu m^3$. A $2\mu m^3$ spot analysis can be used to determine individual grain composition, but a $100\mu m^2$, or even $500\mu m^2$, raster was more commonly used in order to average compositional data over a greater area and

produce a better representation of the composition of individual laminae, or bundles of laminae. Profiles were produced by analysing a row of contiguous 100μm^2 or 500μm^2 rasters.

2.5 X-RAY DIFFRACTION (XRD)

XRD analysis was used to determine the mineral composition of 2g sediment samples on the 'Phillips PW17-10 x-ray diffractometer', by Ross Williams (University of Southampton). Most mineral phases were identified by comparison to standard spectra, however, Ca-rhodochrosite was determined by comparison to spectra in Heiser et al. (2001).

2.6 FORAMINIFERAL ANALYSIS

Foraminifera were collected from a single horizon (depth, 117-119cm) by sieving through a 125μm sieve to remove the clay fraction but retain foraminifera. Foraminiferal tests were examined under the SEM to aid identification and to determine surface features.

2.7 ION COUPLED PLASMA MASS SPECTROMETRY (ICP-MS)

Destructive trace element analysis was carried out on selected thin sections on the VG Plasmaquad ICP-MS, fitted with a laser ablation sampling tool, collected under standard conditions (spot 18μm diameter, count time 20s). Rows of ablated spots were taken in order to produce profiles of trace element composition across Ca-rhodochrosite laminae (Fig. 2.3). Three separate profiles were averaged in each sample area in order to produce compositional data that better represents the composition of individual laminae. Comparison to count rates produced from the NIST glass (basalt composition) standard produced quantitative data with standard errors of less than 5%.

2.8 BIOTURBATION INDEX

A bioturbation index (Fig. 2.4) was established for Gotland Deep sediments following the scheme of Behl and Kennett (1996), where sediment fabric is linked to the tolerance of burrowing organisms to variations in benthic oxygenation levels. The bioturbation index values were produced by visual inspection of low magnification (x5) back-scattered electron images. A bioturbation index of 4 equates to very well laminated sediment fabric and benthic oxygen levels <0.1ml per litre. Conversely, at

index level 1, the sediments are completely homogenised by benthic organisms, indicating oxygen levels >0.3ml per litre. This index is relatively sensitive to changes between oxic and anoxic benthic conditions, but does not record extremes in either oxic or anoxic conditions.

Figure 2.1 Bathymetry of the Gotland Basin (after Emeis and Struck, 1998) and core locations for 20001-5, 201301-5, and 201302-5.

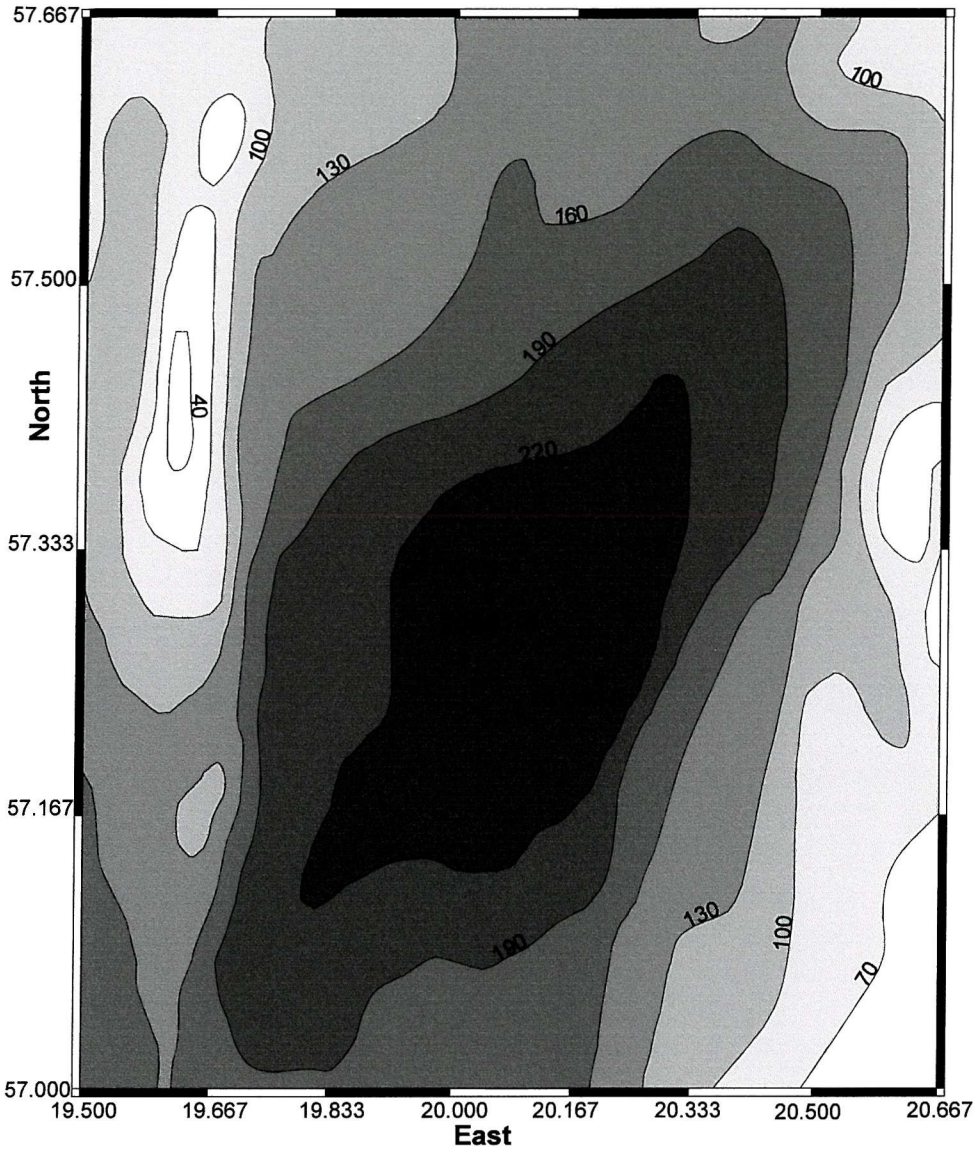

Figure 2.2 Lithology and Stratigraphy of cores 20001-5, 201301-5 and 21302-5. Logged from X-ray images in Emeis and Struck (1998) by I. Burke

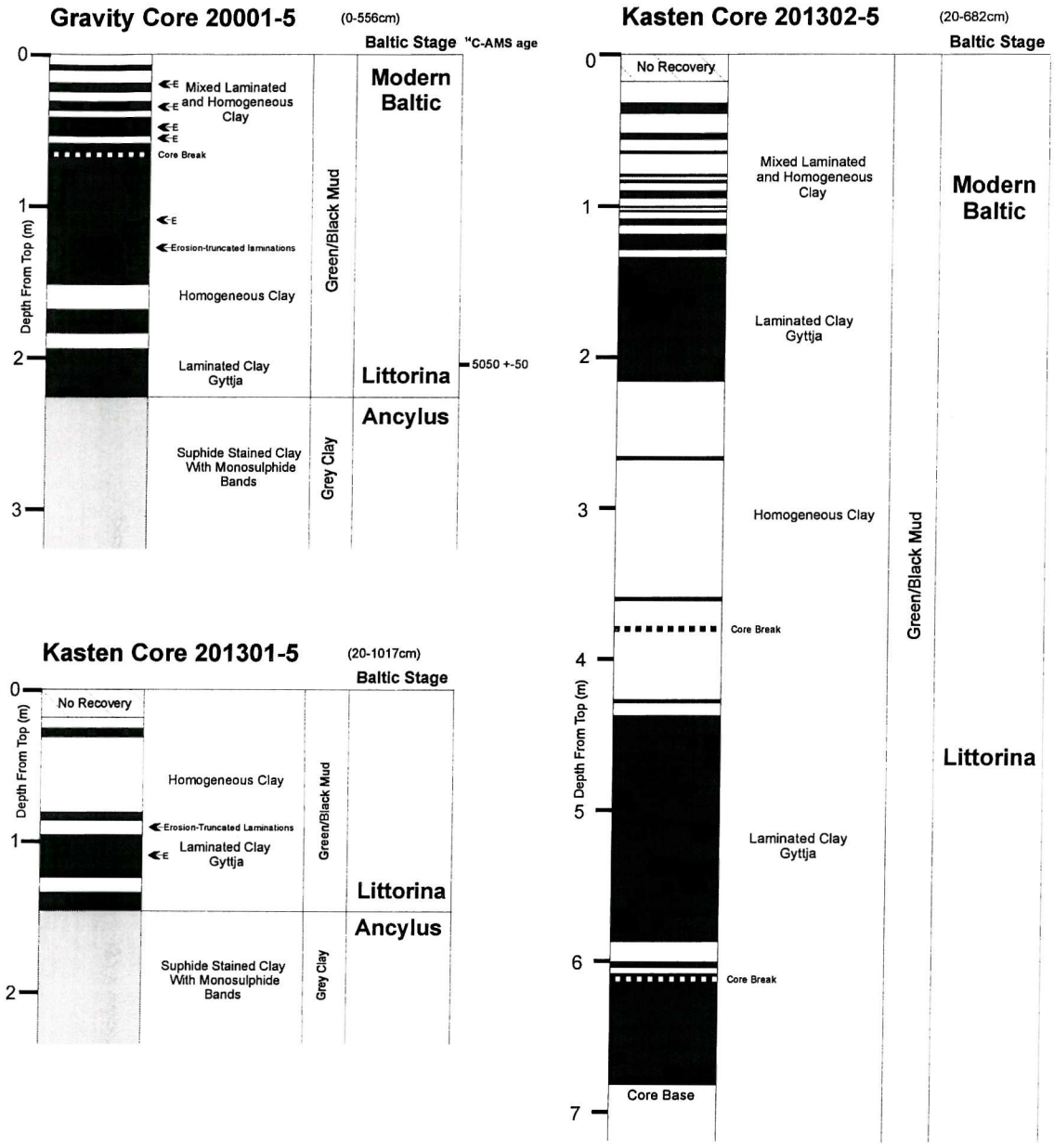

Figure 2.3 Row of pits produced by laser ablation of Gotland Deep sediments embedded in resin. The ablated material from each spot is carried by a Ne/Ar mix into a plasma and then analysed for multiple trace elements using a quadrapole mass spectrometer.

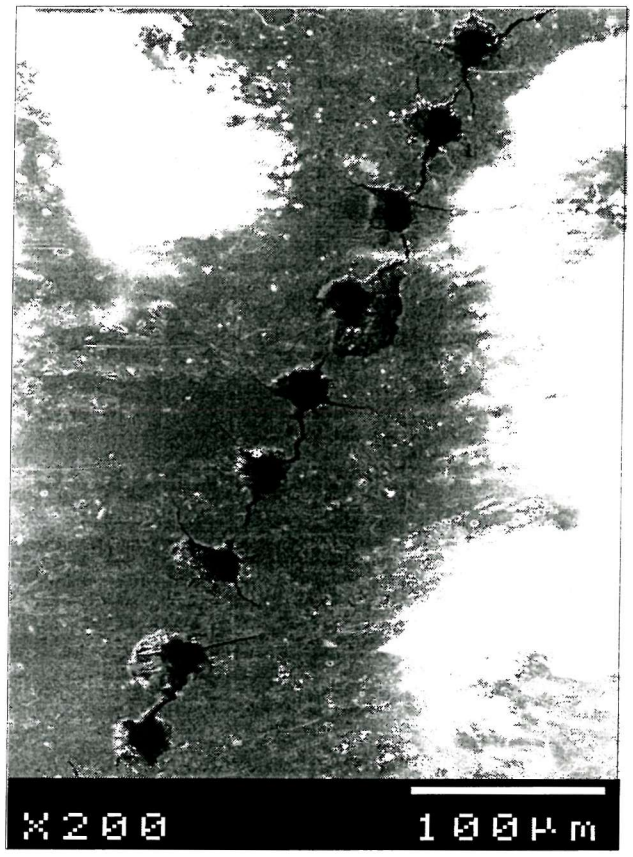

Figure 2.4 Bioturbation index based on sediment fabric disturbance (after Behl and Kennet, 1996).

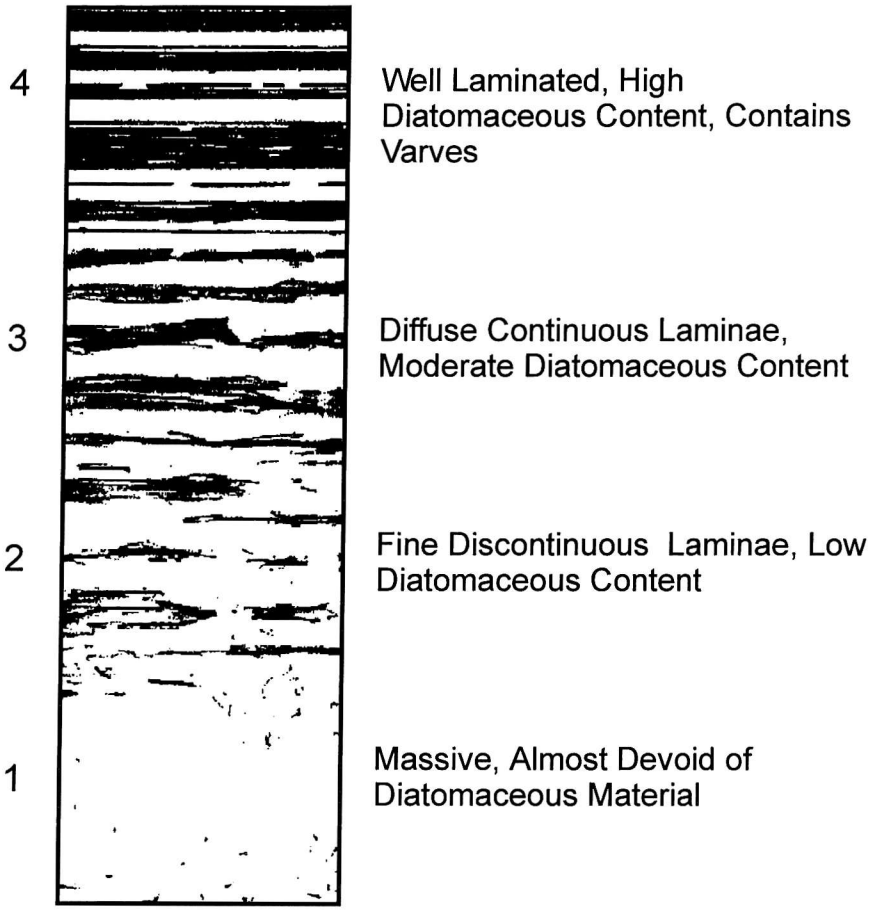

3 MICRO-FABRIC STUDY OF DIATOMACEOUS AND LITHOGENIC DEPOSITION

With 6 figures

3.1 INTRODUCTION

The accumulation of laminated sediments in the Gotland Deep represent a good record of climatic and environmental changes affecting the entire Baltic Sea (Rahm, 1988). The origin and succession of lamina, however, have proved difficult to describe using traditional diatom and sedimentological methods (Morris et al., 1988; Yemelyanov et al., 1995; Sohlenius and Westman, 1998). High-resolution SEM-based techniques using back-scattered electron images (BSE images) have been employed successfully to study laminated sediment fabrics in a wide range of other settings (e.g., Grimm, 1992; Kemp and Baldauf, 1993; Kemp, 1996; Pike and Kemp, 1996b; Pearce et al., 1998; Dean et al., 1999). The results of a SEM-based micro-fabric study of the laminated Littorina sediments of the Gotland Deep are presented below.

3.2 FABRIC DESCRIPTION

Laminated sediments occur in core 20001-5, from the Ancylus-Littorina boundary at 229cm upwards, throughout most of the core (Fig. 2.2). There are two intervals of homogeneous, bioturbated sediments in the lower Littorina section, from 143-166cm and from 182-194cm. The remaining laminated sediments contain relatively thin (1-3cm) well-laminated intervals interbedded with thicker intervals of indistinctly laminated sediments. The Modern Baltic sediments, which occur from 0-66cm, are characterised by mixed packets of laminated and homogeneous sediments. There are at least six occurrences of macro-scale erosional features observable within the post-Ancylus muds, where laminations are clearly truncated. The fine-scale sediment fabric becomes apparent upon examination of low magnification (x5) BSE image base maps (Fig. 3.1). Laminae observed in Slab 6 are presented in table 3.1 and can be divided into six main lamina types. The same lamina types were observed in Slab 4, with the exception of Ca-rhodochrosite laminae, which were absent.

Table 3.1 Lamina Type Descriptions, Core 20001-5, Slab 6, 118-144cm

Lamina Type	Number of occurrences	Thickness range (μm)	Average Thickness (μm)	Description
Diatom Ooze	82	<100–1800	325	More than 80% diatom frustules, monospecific or mixed diatom assemblage.
Diatomaceous Mud	198	200–800	380	Diatom rich, 50-80% diatom frustules, mixed assemblage.
Clay-rich Mud	165	150–1000	425	More than 50% Clay matrix, minor diatom assemblage.
Barren Mud	64	100–2900	600	More than 90% Clay matrix.
Silt-rich Mud	30	50-150	90	Clay-rich matrix with more than 20% silt grains.
Ca-rhodochrosite	95	<80–350	135	Dense aggregates of distinctively bright crystals.

3.3 MINERAL COMPOSITION.

XRD analysis was performed on five representative 1cm intervals from Slab 6 in order to determine general mineral composition: 1.Well-laminated mud; 2. Mixed laminated and homogeneous mud; 3. Homogeneous mud; 4. Well-laminated mud with visible yellow Ca-rhodochrosite laminae; 5. Homogeneous mud with visible yellow Ca-rhodochrosite laminae. All XRD traces show peaks representing the primary clastic minerals; quartz, illite, plagioclase feldspar, and kaolinite, with smectite present in samples 1-3. This is typical of Gotland Deep mineral assemblages (Gingele and Leipe, 1997). The presence of Ca-rhodochrosite was determined in samples 4 and 5 by comparison to XRD traces presented in Heiser et al. (2001). Peaks representing gypsum occurred in samples 1-3 and 5. The occurrence of gypsum is most likely to relate to oxidation in transit (see Chapter 2, section 2.2), and not to primary sedimentation or diagenetic processes.

3.4 DIATOMACEOUS LAMINAE

In thin section, diatomaceous material can easily be recognised in BSE images due to their distinctive shapes, although identification to species level is only possible

in three dimensional topographic BSE images. EDS spot analysis of diatom frustules produced compositions rich in Si and O, as expected for opaline silica. Diatomaceous laminae may be subdivided on the basis of diatom content into two distinct lamina types:

Diatom ooze laminae (>80% diatom frustules)

Diatom ooze laminae contain mixed species assemblages or, less commonly, near-monospecific oozes of *Thalassionema nitzschioides* (Fig. 3.3b) or of *Pseudosolenia calcar-avis* frustules. While *T. nitzschioides* frustules are still intact, *P. calcar-avis* girdle bands are always separated (Fig. 3.2b). The diatom frustules appear to be well preserved and even lightly silicified rhizosolenid girdle bands are observed intact. Diatom identification to species level in *P. calcar-avis* deposits is only possible where a high density of terminal processes can be observed. Laminae of *Thalassionema nitzschioides* are usually very thick (300-600μm); in contrast laminae of *Pseudosolenia calcar-avis* are usually much thinner (100-200μm). *Chaetoceros* spp. resting spores also form ooze deposits, but are rarely monospecific. The resting spores of *Chaetoceros lorenzianus* and *Chaetoceros diadema* were found to co-occur with *T. nitzschioides* (Fig. 3.2d). Other *Chaetoceros* spp. resting spores formed minor constituents, but were observed rarely. There is no apparent vertical succession between the *C. lorenzianus* and *C. diadema* resting spores. The weakly silicified *Chaetoceros* spp. vegetative cells are very rarely present. Small centric (<50 μm) *Thalassiosira* spp. frustules (Fig. 3.2e), also occur in *Chaetoceros* spp. oozes. The frustules are well preserved, with no signs of dissolution, and are rarely broken.

Diatomaceous mud laminae (50-80% diatom frustules)

Diatomaceous muds most commonly contain mixed *Chaetoceros* spp. resting spores (Fig. 3.3c), although rhizosolenids and chrysophyte cysts (Fig. 3.2c) can also be present. Again, there is no apparent vertical succession; commonly two or more species of variable abundance are mixed homogeneously. Occasionally up to five species are found in diatomaceous mud laminae. There is commonly a progressive increase in the proportion of clay material present towards the lamina top.

3.5 LITHOGENIC LAMINAE

In most BSE images the most common material observed consists of aggregates of very small (less than 2μm) crystals that create a grey background in many images. No distinct crystal shapes are evident; however, EDS spot analysis of this material

revealed that it is composed largely of Al, Si, and O, with variable minor amounts Fe, Mg, K, Na and Ca, and was inferred to represent the clay minerals determined by XRD. Separate feldspar grains were not observed by EDS spot analysis and may form part of the fine background matrix. In this study, the term 'silt' simply refers to any clastic mineral grain larger than 2μm. Silt grains are commonly irregular and angular in BSE images, and Si and O-rich (quartz, centre Fig. 3.3d), and Ca, Mg, C and O-rich (dolomite, centre Fig. 3.3a) grains, were the two main types determined by EDS spot analysis. All clay-rich laminae are usually massive, with no apparent grain size grading and pellets are very rarely observed. Based on the dominance of clay matrix, diatom, and silt content clay-rich laminae may be divided into three distinct types:

Clay-rich mud laminae (50 - 90% clay matrix)

Clay-rich mud laminae commonly contain the large centric diatom (greater than 50 μm) *Actinocyclus* spp. (Fig. 4f and 5d), either distributed evenly throughout the lamina or as a continuous sub-lamina. Often small amounts of *Chaetoceros* spp. resting spores and chrysophyte cysts are also observed within clay-rich laminae. There is commonly an upward increase in the amount of clay material present towards the lamina top.

Barren mud laminae (>90% clay matrix)

These are distinguished from clay-rich mud laminae by very low diatom content.

Silt-rich laminae

Distinct, thin (50-150μm) silt-rich mud laminae occur irregularly and infrequently with a >20% silt fraction.

3.6 DIAGENETIC MINERALS AND LAMINAE

Ca-rhodochrosite laminae

Diagenetic Ca-rhodochrosite laminae occur regularly throughout the Littorina sediments of the Gotland Deep. Ca-rhodochrosite laminae contain aggregates of 2-10μm globular crystallites (Fig. 3.2a), which in BSE images appear as bright, rounded, often hollow grains (Fig. 3.3a). Ca-rhodochrosite crystallites are also occasionally observed as overgrowths on detrital dolomite grains or encrusting benthic foraminifera tests, but are not observed to encrust diatom frustules. There is normally large thickness variation within individual Ca-rhodochrosite laminae, and dense nodular aggregates may occur both within Ca-rhodochrosite laminae and in isolation within other laminae.

In well-laminated sections, Ca-rhodochrosite laminae usually have well defined upper and lower transitions, but within the more massive intervals, Ca-rhodochrosite may occur in dispersed bands, (although individual Ca-rhodochrosite laminae can still be distinguished). In some cases, Ca-rhodochrosite crystallites appear to be distributed across the contact between other laminae (e.g., Fig. 3.4). Rare tests of the benthic foraminifera, *Elphidium excavatum* (Terquem), *Elphidium albiumbilicatum* (Weiss), *Ammonia* sp., *Spiroloculina canaliculata* (d'Orbigny) and *Cassidulina* sp., are found encrusted in Ca-rhodochrosite, associated with rhodochrosite laminae. For a full discussion of Ca-rhodochrosite formation mechanisms in the Gotland Deep see Huckriede and Meischner (1996), Sohlenius et al. (1996), Neumann et al. (1997) and Sternbeck and Sohlenius (1997).

Fe-sulphides

The very brightest individual grains in BSE images, when determined by EDS spot analysis, were found to be rich in Fe and S, and inferred to represent Fe-sulphides. Small (2-10μm) Fe-sulphide crystallites were observed to occur in both rounded framboidal (e.g., centre Fig. 3.3b) and cubic forms (e.g., dispersed below Ca-rhodochrosite laminae Fig. 3.3a). Fe-sulphides do not form distinct laminae, rather they occur finely dispersed more or less continually throughout all laminae in the section. See Boesen and Postma (1988), Neumann et al. (1997), and Sternbeck and Sohlenius (1997) for detailed discussion of Fe-sulphide formation in the Gotland Deep.

3.7 SUCCESSION OF LAMINAE

Throughout the laminated sections of Slab 4 and Slab 6, there are short 1-4mm intervals containing distinct diatomaceous and clay-rich laminae, intercalated with intervals of indistinct laminae or massive sediment. Figures 3.4 and 3.5 show examples of two such intervals, one containing (Fig. 3.4), and one without Ca-rhodochrosite laminae (Fig. 3.5). Most commonly laminae are organised in simple couplets of alternating diatomaceous mud laminae and clay-rich mud laminae, but triplets and occasionally quadruplets are also observed, defined by the presence of additional distinct diatom ooze or barren mud laminae (Fig. 3.6). A common feature of these couplets, triplets, and quadruplets is an increase in clay material upward at the expense of diatom content, as can be seen clearly for sequence 1 in Figure 3.4. Thus, when distinct diatom ooze laminae occur, they are present at the base of the sequence; and conversely, when barren muds occur, they are at the top. The upper boundaries of

clay-rich laminae are commonly well defined. Ca-rhodochrosite laminae occur in Figure 3.4, sequence1-3. Of the 95 Ca-rhodochrosite laminae occurrences in Slab 6 (Table 3.1), 31 are within recognisable couplets, triplets, or quadruplets. Ca-rhodochrosite laminae always occur either towards the top part of the clay-rich mud laminae, or between the clay-rich laminae and the following diatomaceous laminae.

Figure 3.6 shows the abundance of couplets, triplets, and quadruplets observed in Slab 4 and Slab 6. Simple couplets of diatomaceous mud laminae and clay-rich mud laminae are most common, accounting for 104 sequences. Triplets make up 48 sequences. There are 24 occurrences each of either the simple couplet plus an extra basal diatom ooze lamina generally of *Thalassionema nitzschioides* and *Chaetoceros* spp. resting spores (Triplet A), or an extra upper barren mud laminae (Triplet B). Only 8 quadruplets containing four separate laminae were observed. A total of 160 couplets, triplets and quadruplets were observed in Slab 4 (103) and in Slab 6 (57). The average thickness of these groups of laminae in Slab 4 and Slab 6 is approx. 680μm, and 750μm, respectively, producing an overall average thickness of approx. 700μm. In Slab 4 and Slab 6 these depositional sequences account for approx. 16% and 31% of the record respectively, and typically only 2-5 groups of laminae occur continuously in any one section.

3.8 DIATOM PALAEOECOLOGY AND OCCURRENCE IN THE ANNUAL SEDIMENTATION CYCLE

The diatom assemblages observed in this study are distinctly different from those described in modern Baltic assemblages. This is possibly due to changes in Baltic environmental conditions since Littorina times (Sohlenius et al., 1996a), and the effects of silica dissolution, which can modify the species composition occurring in the water column when compared to that preserved in the sediments (Sancetta, 1989; Heiskanen and Kononen, 1994). There is a large surface water salinity difference between modern Baltic conditions, 2-8‰, and Littorina conditions of up to 20‰ (Sohlenius et al., 1996a). Therefore salinity-sensitive species, such as *P. calcar-avis* which is common throughout Littorina sediments (Yemelyanov et al., 1995), are not present in modern Baltic water column and sediment assemblages (Zenkevitch, 1963; Hallfors et al., 1981; Morris et al., 1988; Jansson, 1989; Heiskanen and Kononen, 1994). Also, *Chaetoceros* spp. resting spores are very common within Littorina sediments, but the delicate vegetative cells and *setae* are very rarely observed. It is

therefore possible for lightly silicified species, which do not employ a well-silicified stage in their life cycle, to be missing from the record.

The palaeoecology of Baltic Littorina diatom assemblages may be inferred from numerous other studies of either modern or fossil assemblages. Mixed diatomaceous laminae, containing *C. lorenzianus*, *C. diadema* resting spores, *Thalassiosira* spp and *Thalassionema nitzschioides*, are common in Littorina sediments. A common feature of these species is their small size, typical of rapid-growing diatoms in spring blooms or upwelling pulses (Margalef, 1967; Kemp et al., 2000). The fabric of the deposits also suggests that the assemblages were formed and deposited out of the water column rapidly before grazing could break the frustules (Figs. 3.2d and 3.2e). In the Littorina sediments these diatomaceous laminae are thought to represent rapid sedimentation from diatom spring blooms.

Following the water column studies by Alldredge and Gotschalk (1989) of aggregation of *Chaetoceros* spp. blooms, Grimm et al. (1996; 1997) ascribed large concentrations of *Chaetoceros* spp. resting spores in sediment laminae to 'self sedimentation' at the end of bloom events. Bull and Kemp (1995) also attribute the formation of *Chaetoceros*-rich deposits to the mass flocculation of *Chaetoceros* spp. resting spores following bloom events. While *C. lorenzianus* and *C. diadema* resting spores very often co-occur in diatom ooze or diatomaceous laminae, there is some uncertainty about the overlap between the ecological requirements of each species , as inferred from modern assemblage studies. Canonical correspondence analysis of laminated sediments from Saanich Inlet, British Columbia, suggests that *C. lorenzianus* has low temperature and high salinity optima (McQuoid and Hobson, 1997). In Narragansett Bay, Rhode Island, *C. diadema* is commonly found in early spring but rarely in the autumn (Rines and Hargraves, 1988). *Thalassiosira* spp. typical of northern, cold water regions are often found in early spring diatom water column assemblages (Morris et al., 1988; McQuoid and Hobson, 1997; Pike and Kemp, 1997). *T. nitzschioides* is most abundant in late spring/early summer water column assemblages (McQuoid and Hobson, 1997), and *T. nitzschioides* is commonly found as a component of a mixed assemblage ooze with *Chaetoceros* spp. in other settings (Brodie and Kemp, 1994; Bull and Kemp, 1995; Pearce et al., 1998).

Chrysophyte cysts are typically found in the upper part of diatomaceous mud laminae or within clay-rich laminae, and are reported to bloom in great abundance during early summer in the Baltic Sea (Hallfors et al., 1981).

Thin laminae of *Pseudosolenia calcar-avis* ooze are occasionally observed with an irregular occurrence. These near-monospecific ooze laminae are thought to form by rapid diatom deposition following disruption of stratification in autumn/early winter. In contrast to the 'spring bloom' species, *P. calcar-avis* is slow growing (Guillard and Kilham, 1978) and adapted to stratified, oligotrophic conditions, yet recent studies have shown that it may be a major component of flux to the sea floor. Many rhizosolenids can regulate their buoyancy to retrieve nutrients from the thermocline/nutricline (Villareal et al., 1993), and may occur in positively buoyant macroscopic aggregates up to 30cm in size (Villareal and Carpenter, 1989). A sediment-trap time series study off the coast of Oregon, showed maximum *P. calcar-avis* fluxes during late autumn and winter in three consecutive years (Sancetta et al., 1991). Kemp et al. (1999) have also reported near-monospecific *P. calcar-avis* ooze laminae in Mediterranean sapropels, which are attributed to late autumn/early winter flux events. In a new synthesis of diatom flux observations from laminae and from sediment traps, Kemp et al. (2000) attribute such flux events to break down of the summer thermocline and rapid deposition of the rhizosolenid diatoms in an autumn or 'fall dump' (Smetacek, 2000).

Clay-rich laminae containing *Actinocyclus* spp. are commonly found following the spring/summer diatomaceous laminae. Although not identified to species level in this study, Sohlenius et al. (1996) found that *Actinocyclus octonarius* and *A. ehrenbergii* are the most common in Gotland Deep Littorina sediments. These species commonly occur in brackish-marine environments (Guillard and Kilham, 1978). The genus is typically epiphytic on seaweed but is a common constituent of the nearshore plankton (Round et al., 1990). In modern central Baltic assemblages, *Actinocyclus octonarius* is most abundant in late summer to early autumn (Hallfors et al., 1981).

3.9 TERRIGENOUS SEDIMENTATION

Although the ultimate source of the clay material found in Gotland Deep sediments is considered to be from terrestrial deposits, the main direct source of terrigenous clays to the Gotland Deep is from erosion and resuspension of coastal and shallow water sediments during storms (Gingele and Leipe, 1997), or by bottom erosion due to saline inflows (Sviridov et al., 1997; Emeis et al., 1998; Sivkov et al., 1998). Both storm erosion and saline inflows are distinctly seasonal and are maximised in winter (Matthäus and Schinke, 1994; Matthäus, 1995). Bergstrom and

Carlsson (1994) and Schinke and Matthäus (1998) also report that river runoff peaks in winter in many years, but river sediment input is generally small, is initially deposited only in shallow water, and is likely to go through several resuspension and deposition events before finally being deposited in the deep basins (Gingele and Leipe, 1997). The neritic diatom species *Actinocyclus* spp. that commonly occurs in clay-rich laminae are, therefore, inferred to be redeposited in the Gotland Deep simultaneously with this reworked terrigenous material.

3.10 Annual succession and varves

The couplet of diatomaceous mud and clay-rich mud commonly observed in the Gotland Deep sediment is typical of the annual biogenic-lithogenic sedimentation couplets or varves found in marine settings adjacent to land (e.g., Sancetta, 1996). The diatom component forms during the spring-summer growing season while the terrigenous sediment input is dominant in winter when biogenic production is minimal and storms redistribute sediment to the basin. The triplets and quadruplets, in which purer diatom ooze or mud "end-member" laminae may be identified, are also consistent with an annual sedimentation cycle (Figs. 3.4, 3.5 and 3.6).

Figures 3.4 and 3.5 show examples of six lamina sequences that form couplet or triplet varves. The sequences in Figures 3.4—1, 2, 3 and Figure 3.5—1 and 2, have a well-defined start and finish and an upward transition from a diatomaceous mud or ooze lamina to a clay-rich lamina. The diatomaceous laminae in each sequence contain diatom species typical of sedimentation following spring/summer blooms, such as *Thalassiosira* spp., *Thalassionema nitzschioides*, smaller *Chaetoceros* spp. resting spores, and chrysophyte cysts. The clay-rich lamina of each sequence contains only sparse assemblages of larger diatoms typical of autumnal production. Sequence 3 in Figure 3.5 also contains a two-lamina sequence with a diatom succession typical of annual production, however, the upper boundary is somewhat transitional.

The concentrations of Ca-rhodochrosite observed within lamina sequences only occur in the upper part of winter clay-rich mud laminae or just encroaching on spring diatomaceous mud laminae (e.g., Fig. 3.4, sequences 1-3), and therefore, in this context, represent an exclusively winter/early spring phenomenon.

3.11 SEDIMENTATION RATES

In previous Baltic Sea studies, the arguments in favour of the existence of varves have also been based on the relationship between laminae couplet thickness and radiochemical (Jonsson, 1992; Salonen et al., 1995) and bulk (Ignatius, 1958) sedimentation rates. If the depositional sequences do indeed represent varves, then this is problematic in terms of sedimentation rates with respect to the thickness of post-Ancylus sediments in core 20001-5. The post-Ancylus sediments in the Gotland Deep represent approximately 8100yrs. The measured varve thickness of approximately 0.7mm would imply approximately 5.7m of deposition during this time. Core 20001-5, however, only contains 2.29m of post-Ancylus sediments, implying a sedimentation rate of only 0.28mm per year. This discrepancy may be explained by either or both of the following:

1. The sedimentation rate indicated by varve thickness is not typical of the core as a whole, and varve sequences represent periods of more rapid sedimentation.
2. Core 20001-5 has been significantly eroded.

The post-Ancylus sediment thickness is asymmetrical from the NW to the SE across the Gotland Deep, and reported mean sedimentation rate varies from 0.23-0.75mm per year (Christiansen and Kunzendorf, 1998). This can be clearly seen in the three cores; 201301-5, 20001-5 and 201302-5, presented in Figure 2.2. The Ancylus-Littorina boundary is not observed in core 201302-5 before the core base at 6.82m, implying an average sedimentation rate in excess of 0.85mm per year. This asymmetry in sedimentation is attributed to bottom erosion by the periodic inflows of North Sea water into to the Baltic (Emeis et al., 1998; Sivkov et al., 1998). In addition, Sviridov et al., (1997) have observed erosional bottom features that indicate that inflowing water is forced by the bathymetry of the Gotland Deep to spiral anticlockwise into the deepest parts of the Gotland Deep. This produces regions of erosion in the north and west parts of the Gotland Deep, and regions of accumulation in the south and east (Emelyanov and Gritsenko, 1999). The cores 201301-5 and 20001-5, also show erosional features such as truncated laminae that are not observed in core 201302-5. It is, therefore, plausible that the measured varve thickness of 0.7mm represents the primary sedimentation rate in core 20001-5, but that erosion has significantly affected this core.

3.12 CONCLUSIONS

Several different diatomaceous and clay-rich laminae can be distinguished, and annual lamina sequences or varves are identified.

The identification of varves is a useful tool in delimiting seasonal depositional events such as the diagenetic Ca-rhodochrosite laminae which occur regularly in varves only as a winter/early spring deposit.

The development and/or preservation of identifiable varves in Gotland Deep sediments is patchy and much of the record is composed of intervals of indistinctly laminated or massive sediment, that may relate to interannual-decadal variability in the extent of bottom water renewal, basin oxidation, and the destruction of varves by bioturbation.

Figure 3.1 X-ray exposure of core 20001-5, 118-128cm (left), and low resolution x5 BSE image of typical laminated section (right). Box shows position of x75 BSE image shown in Figure 3.4a.

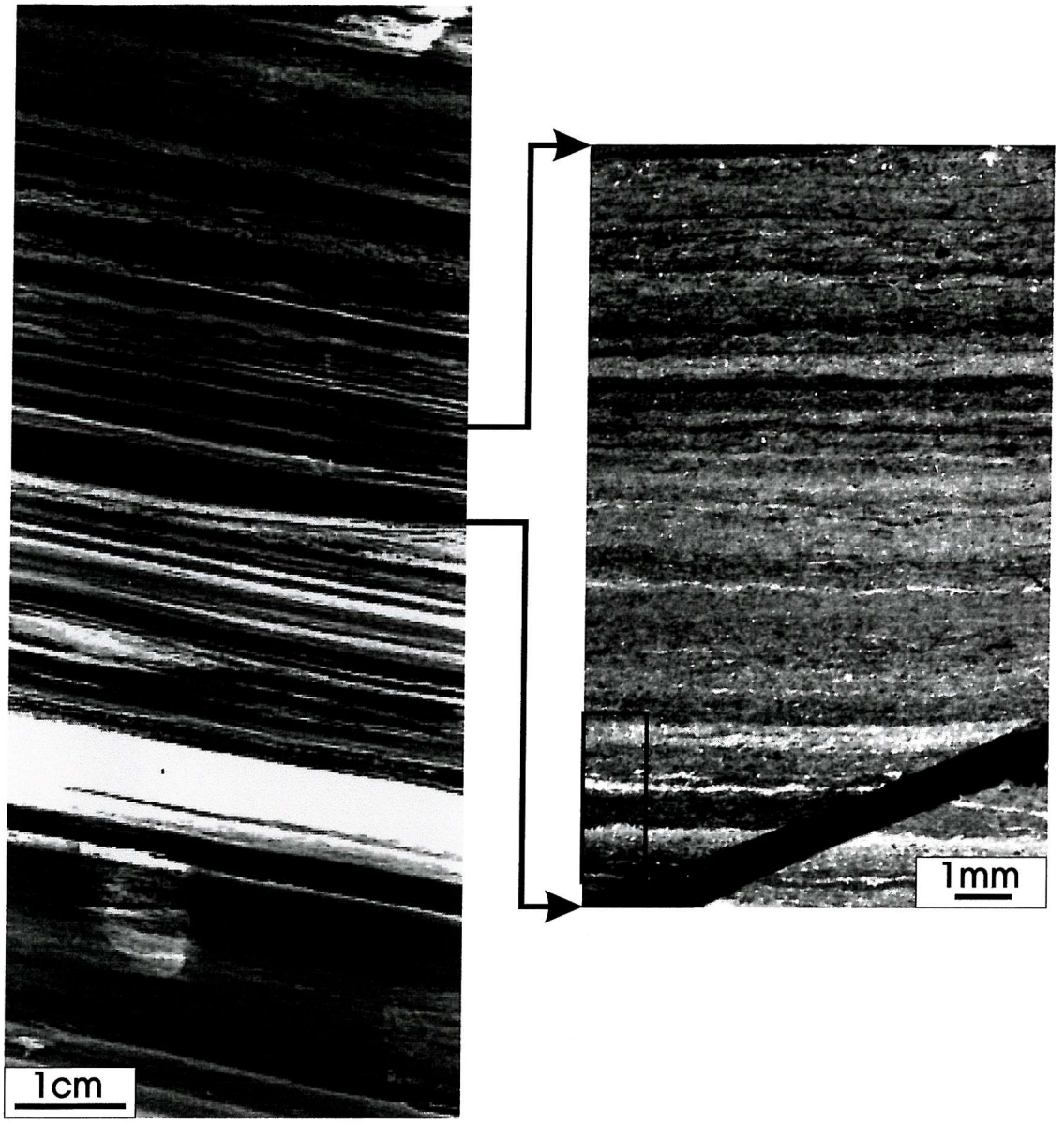

Figure 3.2. High magnification topographic BSE images. A. Aggregate of rhodochrosite crystals. B. Intact terminal processes of *Pseudosolenia calcar-avis*, with disjointed girdle bands. C. Chrysophyte cysts. D. Mixed assemblage ooze with, *Thalassionema nitzschioides*, *Chaetoceros lorenzianus,* and *C. diadema*. E. *Thalassiosira* spp. frustules. F. Diatomaceous mud with *Actinocyclus* spp. frustules.

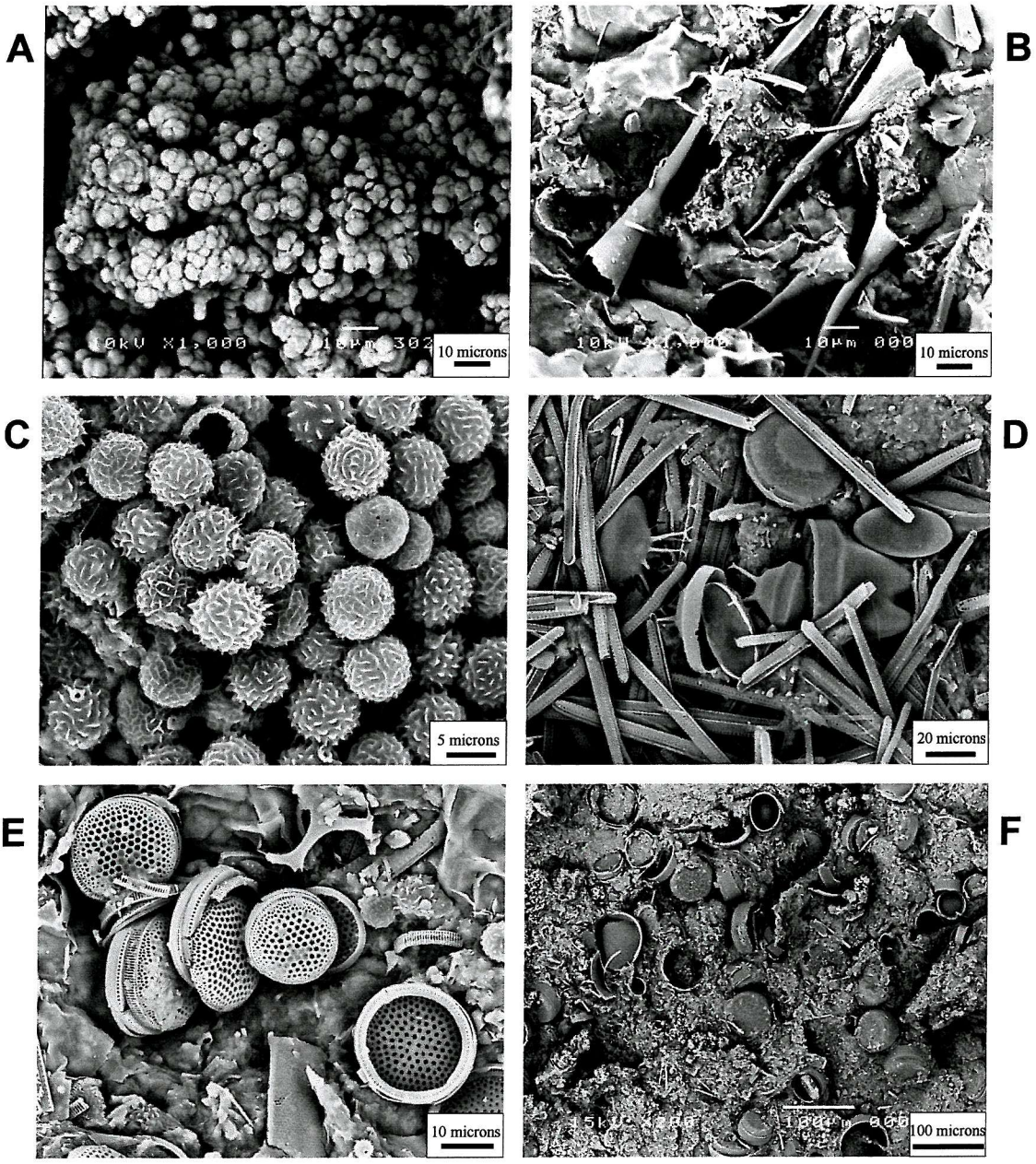

Figure 3.3 High magnification BSE images. A. Bright rhodochrosite lamina between Clay-rich mud and ooze lamina. Dolomite grain marked by white arrow. B. Pennate diatom ooze lamina, most likely to be *Thalassionema nitzschioides*. Framboidal Fe-sulphide grain marked by white arrow. C. Mixed *Chaetoceros* spp. mud lamina. D. Terrigenous mud lamina with large centrics. Quartz grain marked by white arrow.

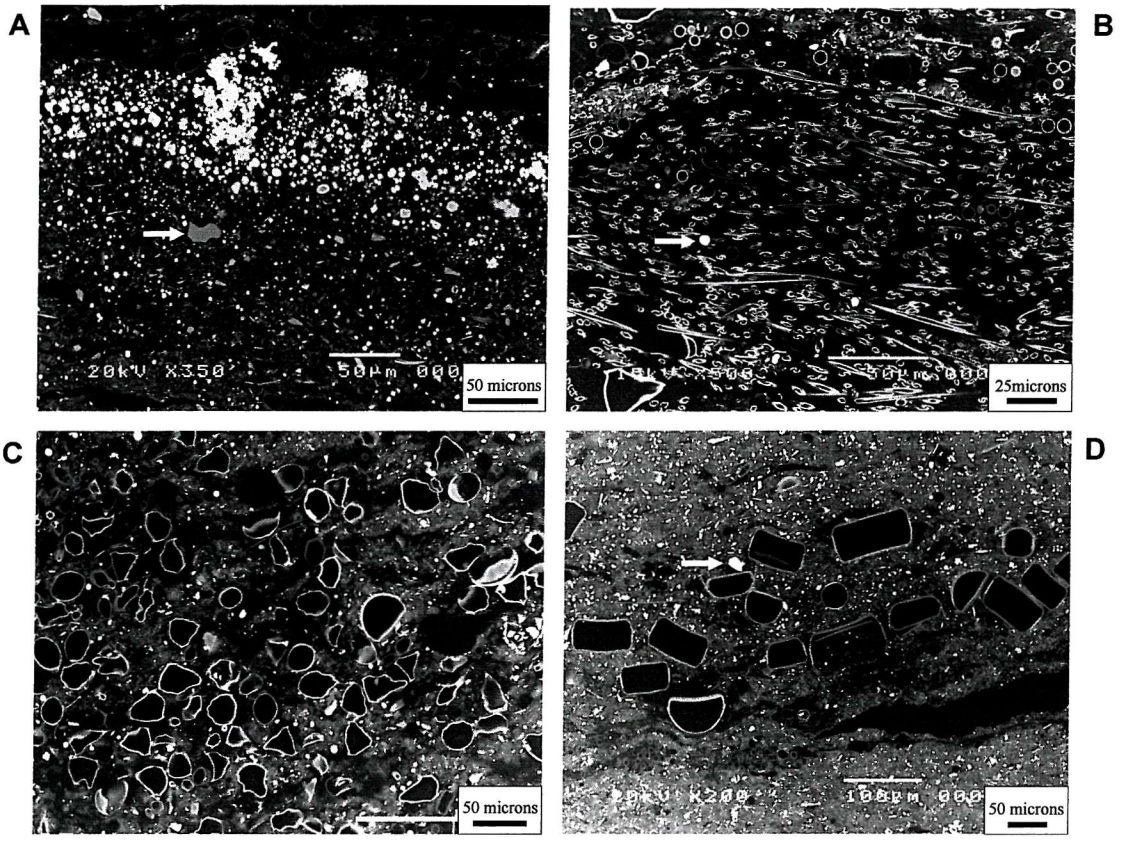

Figure 3.4 BSE image mosaic (x75) from Slab 6 (core depth 126cm) showing three depositional sequences (1-3) with descriptions of laminae composition. Although there is considerable variation in the precise lamina make-up between depositional sequences, these cycles are proposed to represent annual deposition, i.e., varves. LC-large centrics, Cht- *Chaetoceros* spp. resting spores, Cr-Chrysophyte cysts, Ths- *Thalassiosira* spp., Thn-*Thalassionema* spp., Rhz-rhizosolenids.

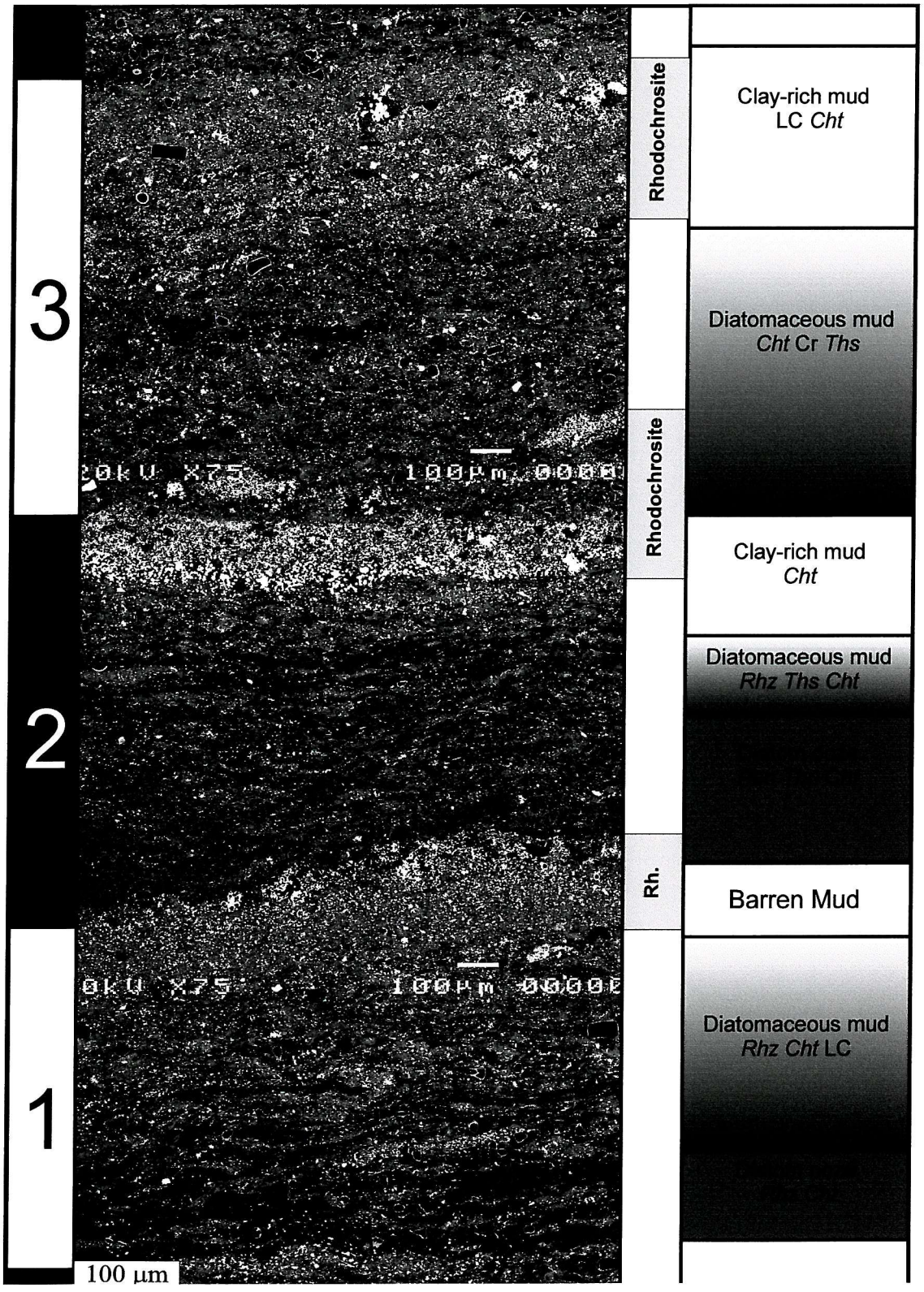

Figure 3.5 BSE image mosaic (x75) from Slab 4 (core depth 77cm) showing three depositional sequences (1-3) with descriptions of laminae composition. Although there is considerable variation in the precise lamina make-up between depositional sequences, these cycles are proposed to represent annual deposition, i.e., varves. LC-large centrics, Cht- *Chaetoceros* spp. resting spores, Cr-Chrysophyte cysts, Ths- *Thalassiosira* spp., Thn-*Thalassionema* spp., Rhz-rhizosolenids.

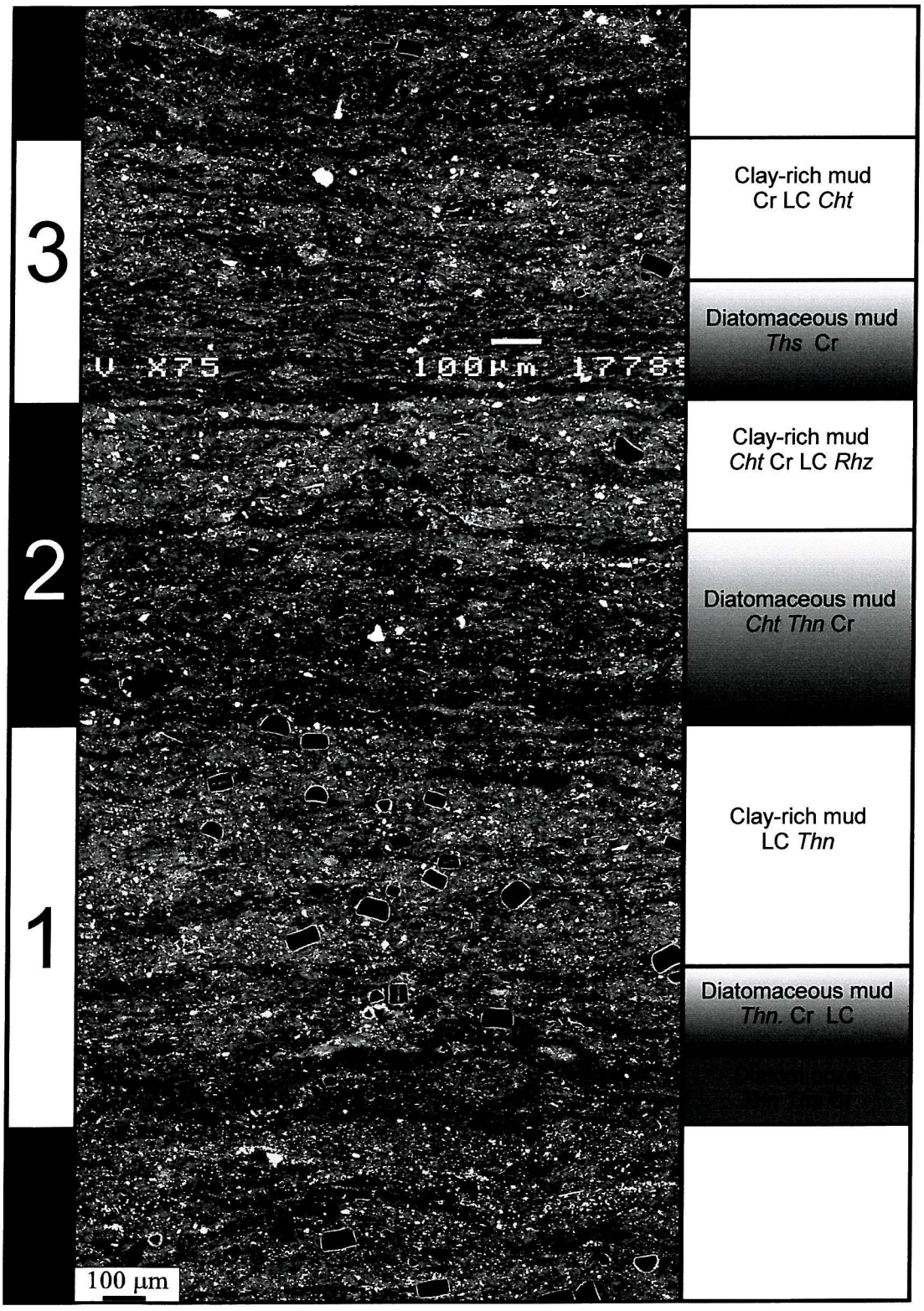

Figure 3.6 The different lamina sequences, or varves, found in Gotland Deep sediments, including numbers of occurrences. Observed position of Ca-rhodochrosite lamina in varves is also denoted.

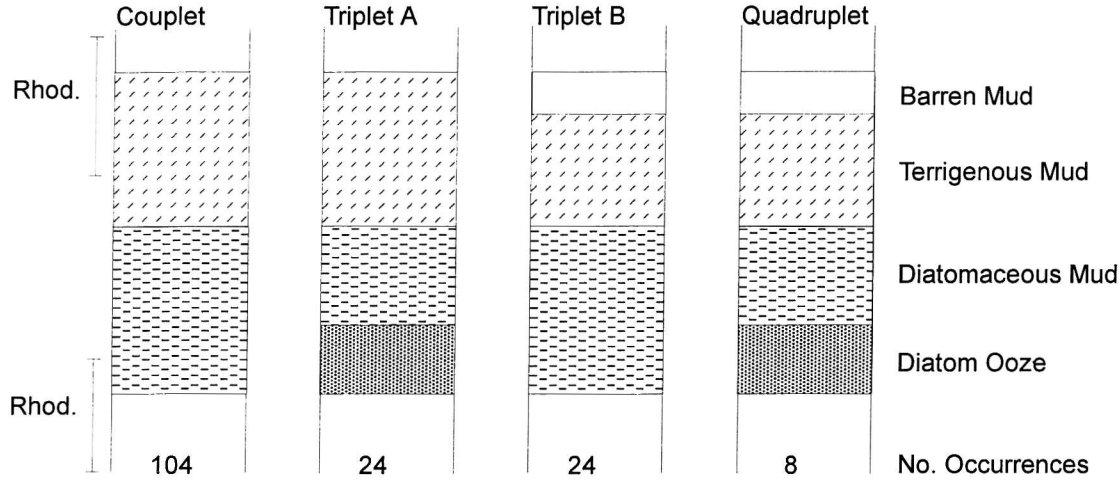

4 DEPOSITION OF Ca-RHODOCHROSITE LAMINAE AND FORMATION OF Mn-SULPHIDE

With 7 figures

4.1 INTRODUCTION

Manganese is very insoluble in ocean water with respect to solid Mn(VI)oxides, thus Mn has a very short oceanic residence time. The fate of Mn in the marine environment is therefore largely determined by the redox state of the sediments and bottom waters. Particulate Mn(IV)oxide is normally reduced to soluble Mn(II) as labile organic material is consumed by bacteria (Froelich et al., 1979; Berner, 1981). Because Mn(II) is very soluble and released into anoxic water, sediments in these settings would not normally be enriched in Mn (Thomson et al., 1986). However, Mn-carbonate laminae are commonly reported in many organic-rich laminated sediments (Suess, 1979; Hein and Koski, 1987; Okita et al., 1988; Xu et al., 1990; Jenkyns et al., 1991; Fan et al., 1992). Calvert and Pedersen (1993; 1996) proposed that the occurrence of Mn-carbonates in anoxic sediments indicates formation in sub-oxic conditions under an oxic water column. They have invoked a 'Mn-pump' in which Mn-oxide is supplied from oxic surface sediments and is reduced at depth, producing large *in situ* Mn^{2+} concentrations leading to pore-water conditions which are supersaturated with respect to Ca-rhodochrosite, $(Mn_x\ Ca_{1-x})CO_3$. Recent reports of Mn-carbonate in laminated anoxic sediments from Saanich Inlet, British Columbia (Calvert et al., 2001) have been linked to the occurrence of short-lived seasonal flushing events. Such linkage of Mn-carbonate formation to brief oxygenation events is supported by sedimentary and geochemical evidence from the organic carbon-rich Littorina and Modern Baltic sediments of the Gotland Deep (Sohlenius et al., 1996a), where the pervasive presence of discrete authigenic Ca-rhodochrosite laminae in these sediments is consistent with the formation of Ca-rhodochrosite in discrete, short-lived, depositional events (Huckriede and Meischner, 1996).

Recent models for Ca-rhodochrosite formation in the Gotland Deep (Huckriede and Meischner, 1996; Sohlenius et al., 1996a; Neumann et al., 1997; Sternbeck and Sohlenius, 1997), propose a link between the periodic major inflows of oxic saline North Sea water into the brackish Baltic Sea and Ca-rhodochrosite formation.

Normally there is a very strong salinity stratification in the Baltic Sea that effectively inhibits mixing of surface and deep waters (Matthäus, 1990) and the deep waters are prone to anoxia. Bacterially mediated Mn and Fe reduction should consume any Mn and Fe-oxides supplied to the deep as they sink into the anoxic zone (Froelich et al., 1979). In the anoxic zone there is then likely to be a decoupling of Mn and Fe deposition (Neumann et al., 1997). Mn^{2+} is soluble in sulphidic waters and can accumulate in the deep anoxic water column (Kremling, 1983; Dyrssen and Kremling, 1990), however, Fe^{2+} reacts quickly with excess free HS^- to form particulate Fe-sulphides, and may be stripped from the water column. Fe deposition is limited only by supply of Fe into the Gotland Deep (Boesen and Postma, 1988).

During an inflow event the Gotland Deep is flushed by saline water, which displaces the anoxic water column upward (Matthäus and Lass, 1995; Neumann et al., 1997). The inflowing water is oxic and rapidly re-oxidises the dissolved Mn^{2+} present, and large quantities of particulate Mn-oxide are deposited at the sediment water interface (Heiser et al., 2001). Upon the consumption of all the available oxygen, these Mn-oxides are then reduced once more producing high benthic Mn^{2+} concentrations. High benthic Mn^{2+} concentrations in combination with high benthic carbonate alkalinity, produced *in situ* by bacterial sulphate reduction, can lead to super-saturation with respect to a mixed Mn-Ca-Carbonate phase and the formation of Ca-rhodochrosite (Huckriede and Meischner, 1996; Sohlenius et al., 1996a; Neumann et al., 1997; Sternbeck and Sohlenius, 1997).

This is an elegant model consistent with much of the reported sedimentary evidence (Huckriede and Meischner, 1996; Sohlenius et al., 1996a; Neumann et al., 1997; Sternbeck and Sohlenius, 1997). The causes of saline inflows are becoming better understood with respect to North Atlantic atmospheric conditions (Matthäus and Schinke, 1994) and environmental variance (Schinke and Matthäus, 1998). If the causal link between major Baltic inflows and rhodochrosite laminae could be firmly established, then the use of Mn deposition as a proxy for past saline inflows and, by extension, past North Atlantic climatic conditions, would become possible. In order to understand the processes involved in the formation of Mn-carbonate rich laminae, scanning electron microscope (SEM) based techniques were used to study micro-fabric features and lamina scale elemental distributions that may be otherwise be overlooked (by e.g. bulk chemical analysis), (Brodie and Kemp, 1994; Kemp, 1996; Kemp et al., 1999; Pike and Kemp, 1999).

4.2 ANNUAL SUCCESSION OF LAMINAE

The Littorina sediments of the Baltic Sea contain intermittently well-laminated sequences alternating with indistinctly-laminated and bioturbated sequences. In well-laminated sequences distinct annual cycles of sedimentation, or varves, commonly occur. These varves contain a clear succession of laminae. Under back-scatter electron imagery the spring/summer laminae are represented by dark diatom ooze and/or diatomaceous muds containing the frustules of a succession of species characteristic of spring and summer. The late summer/winter deposit is represented by a grey lamina containing terrestrially derived mud, with very sparse microfossils (see chapter 3 for a full discussion of the laminated sediment structure and varve succession model). The presence of varves allows the placement of Ca-rhodochrosite laminae into a seasonal succession of laminae.

4.3 ENERGY DISPERSIVE X-RAY MICROANALYSIS (EDS) AND XRD MINERALOGY

XRD analysis was performed on 5 representative 1cm intervals from 116-143cm in order to determine general mineral composition. All XRD traces show peaks representing the clastic minerals; quartz, illite, plagioclase feldspar, and kaolinite, with smectite indicated in 3 samples. Ca-rhodochrosite was determined in 2 samples by comparison to XRD traces presented in Heiser et al. (2001).

Figures 4.1-4.3 show major element EDS data from a laminated sequence at a core depth of 122cm containing four distinct varves. Al is used here as a proxy for terrigenous clay and feldspar mineral distribution, as these minerals are the only major Al-bearing phases present. Other elements are shown in Figures 4.1-4.3 as X/Al ratios, to highlight any variance not due to clay mineral distribution. There is a good correlation between Al and other elements normally associated with clay phases, K (r, 0.97), Mg (r, 0.87), and this supports the use of X/Al ratios (Fig. 4.1). The annual cycle is reflected in the Al profiles, which have high values in the clay-rich winter deposits of varves 1, 3 and 4, and low values in the diatomaceous spring/summer laminae of varves 1 and 4.

The epoxy resin used to embed these sediments contains only C and Cl and O. Although C and O are both present in mineral phases, Cl is not present in any mineral phase present. As the resin contains approximately 2wt% Cl, and the resin is the only source of Cl in these sediments, Cl can be used here as an approximate proxy for porosity, with 2wt% Cl $\approx$ 100% porosity (Fig. 4.1). There is a general reduction in

porosity in the clay-rich winter deposit in varves 1, 2 and 3, and high porosity in the diatomaceous laminae in varves 1, 3 and 4, due to the open structure of diatom frustules in comparison to clay-rich laminae. Where the very large Mn/Al enrichment (>x10) occurs in Ca-rhodochrosite lamina C, there is also a marked reduction in porosity. Enrichments in Si/Al are due to the presence of siliceous diatoms in the Spring/Summer bloom laminae and are observed in all varves (Fig. 4.1).

Varves 1, 2 and 3 all contain bright Ca-rhodochrosite laminae. Large enrichments up to 2 orders in magnitude in both Mn/Al and Ca/Al occur within these laminae (Fig. 4.2). Mn and Ca have a very strong positive correlation (r, 0.97) demonstrating that both elements occur together in the same mineral phase, i.e., Ca-rhodochrosite. Mg/Al is modestly enriched in Ca-rhodochrosite laminae C (see Fig. 4.1), showing that small amounts of Mg are also sequestered in rhodochrosite. The Ca-rhodochrosite laminae occur in the winter terrigenous deposit or straddling the late winter deposit and the early spring diatomaceous deposit. Where Ca-rhodochrosite laminae occur in varves they uniquely occur as a winter/early spring deposit.

Fe/Al and S/Al also have a strong positive correlation (r, 0.89) suggesting that Fe is sequestered in these sediments in a sulphide phase (Fig. 4.3). Fe/Al shows relatively little variance when compared with that of Mn/Al; this illustrates the possible decoupling of Mn and Fe deposition in this setting. Neumann et al. (1997) proposed that Fe-oxides supplied to the Gotland deep are rapidly reduced and deposited as Fe-sulphides upon entering the anoxic zone, whereas reduced Mn accumulates in anoxic bottom water and is only deposited during discrete events. There are however minor enrichments in S/Al within Ca-rhodochrosite laminae A, B and D, and Fe/Al in Ca-rhodochrosite laminae A and D, which may be related to Mn deposition.

Table 4.1 shows the results of EDS spot analyses (excitation volume $2\mu m^3$) on 79 individual Ca-rhodochrosite crystallites. Although there is much variation in composition, the mean value gives a calculated Ca-rhodochrosite composition of $(Mn_{0.75}Ca_{0.22}Mg_{0.03}Fe_{0.00})CO_3$, which is in agreement with previous studies (Jakobsen and Postma, 1989; Huckriede and Meischner, 1996). In a stricter mineralogical context, this Ca-rhodochrosite composition has also been referred to as the mineral kutnahorite or pseudo-kutnahorite (Sternbeck, 1997; Böttcher, 1998). The large range in Cl (wt%) values indicates a very large range in porosity for individual grains. Strikingly, Ca-rhodochrosite is almost completely free of Fe but not S. The presence of S in Ca-rhodochrosite has not been previously reported (Calvert and Price, 1970;

Suess, 1979; Pedersen and Price, 1982; Jakobsen and Postma, 1989; Huckriede and Meischner, 1996; Lepland and Stevens, 1998). This S must be sequestered in a contaminant phase hitherto not described within the Ca-rhodochrosite phase. The compositional data in Table 4.1 does support a possible Mn-sulphide phase. Although with respect to the pore water conditions prevalent in Gotland Deep pore waters Mn-sulphide would not be expected (Kulik et al., 2000; Heiser et al., 2001), Aller (1980) report that due to the large range of values reported for the K_{sp} of Mn-sulphide, it is impossible to eliminate the possibility of forming or preserving Mn-sulphide on solubility calculations alone. Aller (1980) also report that for Long Island Sound sediments Mn^{2+} concentrations near the sediment-water interface can vary considerably on seasonal timescales, therefore, it is possible that some early Mn-sulphide forms in this setting, and is preserved by inclusion in the Ca-rhodochrosite lattice.

Table 4.1 Composition of rhodochrosite phase from EDS spot analysis

n=79	Mn	Ca	Mg	Fe	S	C	O	Cl	Total
Mean (wt%)	36.34	8.14	0.71	n.d.*	1.16	16.84	34.83	0.41	98.42
Standard Deviation	4.91	2.35	0.61	0.02	0.60	6.63	3.12	0.27	-
Minimum (wt%)	23.11	2.41	0.21	n.d.*	0.30	7.73	22.14	0.08	-
Maximum (wt%)	49.99	14.64	4.40	0.20	4.36	39.37	41.00	1.86	-

*n.d. – not detected.

4.4 Occurrence of Foraminifera

Sparse numbers of benthic and planktonic foraminifera tests were found in Littorina sediments; only 26 foramerifera tests were recovered from $6cm^3$ of sediment. The planktonic species include: *Globigerina bulloides* (d'Orbigny), *Globoturborotalia rubescens* (Hofker), *Turborotalita quinqueloba* (Natland), *Neogloboquadrina pachyderma* (Ehrenberg), *Globorotalia scitula* (Brady), and *Globigerinita glutinata* (Egger). The benthic species include: *Elphidium excavatum* (Terquem), *Elphidium albiumbilicatum* (Weiss), *Ammonia* sp., *Spiroloculina canaliculata* (d'Orbigny), and *Cassidulina* sp.

The benthic assemblage is typical of that found in the present Baltic Sea (Brodniewicz, 1965); however, any planktonic assemblage is unexpected in this

setting, because the basin is, shallow, brackish, and its waters are rich in suspended matter. The planktonic specimens are all rather small and delicate (~150μm) and are unbroken, which implies growth in the Baltic Sea. Nevertheless, a source from outside the Baltic or from erosion from older sediments cannot be excluded. If erosion of older sediments is the origin of foraminifera tests in this setting, then both benthic and planktonic foraminifera tests should be supplied simultaneously and not have any difference in occurrence; but there is an intriguing difference in the condition of the surface of planktonic and benthic tests. The tests of all 14 benthic specimens are heavily encrusted in Ca-rhodochrosite while all 12 planktonic specimens are free of Ca-rhodochrosite (e.g. Fig. 4.4a-d). The Ca-rhodochrosite occurs simultaneously on both the surface of the benthic foraminifera test and as fine inter-growths within the test itself (Fig. 4.4b). It was, therefore, impossible to sample the benthic foraminifera test composition by EDS spot analysis without Ca-rhodochrosite contamination.

The difference in Ca-rhodochrosite encrustation may be explained by invoking a process where benthic tests are present during Ca-rhodochrosite formation and planktonics tests are not. Benthic foraminifera can only live in oxygenated bottom waters. This implies a link between periodic oxic events, where benthic foraminifera re-colonise the formerly anoxic deeps, and the formation of Ca-rhodochrosite laminae, an association previously observed by Sohlenius et al. (1996b) and Huckriede and Meischner (1996).

As planktonic foraminifera tests are found free of Ca-rhodochrosite, they are almost certainly not present (with the benthic tests) during the Ca-rhodochrosite formation period, therefore an erosional original for planktonic tests seem unlikely. This suggests that during Littorina Times, when surface water conditions are reported to be more saline than present (Sohlenius et al., 1996a) planktonic foraminifera may have lived in the Baltic Sea. This observation also implies that the primary period of Ca-rhodochrosite formation is relatively short, otherwise planktonic foraminifera tests would be expected to become encrusted in Ca-rhodochrosite as they were buried in the sediments.

4.5 SEASONALITY OF OXIC INFLOWS

The only documented flushing of the Baltic deeps with oxygenated water occurs during episodic inflows of saline water called 'Major Baltic Inflows' (Matthäus and Franck, 1992). A lightboat stationed in the Darss Strait provided detailed data between

1880 and 1994 on the atmospheric conditions and hydrological conditions in the critical sill area (Matthäus, 1995). Matthäus and Franck (1992) used these data to hindcast the timing of major inflows of saline water into the Baltic Sea during the twentieth century. Figure 4.5a shows the extended winter season (August to April) when all major inflows occur. There is a normal distribution around a December maximum, but the very strongest inflows only occur from November to January. However, as it is only the strongest inflows that are likely to cause large changes in Gotland Deep conditions, the season where important inflows occur, in terms of Mn deposition, may be limited to the November to January period. In anoxic basins, Mn oxidation and deposition is believed to be very rapid (2-3 days) following initial flushing with oxygenated water (Emerson et al., 1982; Sternbeck and Sohlenius, 1997). It should therefore be the timing of first intrusion of saline water that controls Mn-oxide deposition.

Changes in Gotland Deep bottom water conditions from 1992-1996 (Fig. 4.5b) show the effects of oxic inflows occurring during that period. In January 1993 a Major Baltic Inflow occurred at the Darrs Sill, but inflowing water was not observed in the Gotland Deep until March/April 1993 (Matthäus and Lass, 1995), because the inflowing water must fill and overflow the smaller Arkona and Bornholm Basins (50 and 150km from Darrs Sill Area) before flowing over 400km along the Stolpe Channel to the Gotland Deep. In 1994, however, as the Bornholm basin was already filled with dense saline water from the 1993 event, two small inflow events occurred during December and March and flowed rapidly (in less than one month) to the Gotland Deep, causing bottom water with $[H_2S]$ >4cm^3/dm^3 to be replaced rapidly with inflowing waters with $[O_2]$ >3cm^3/dm^3 (Matthäus and Lass, 1995; Nehring et al., 1995a). In general, therefore, depending on variation in conditions in the approaches to the Gotland Deep, there is a variable delay of 1-4 months from the initial inflow at the Darss Sill, until a change in Gotland Deep water column conditions is measurable. Mn-oxide deposition is therefore likely to be seasonal, with deposition occurring between early February and late May, depending on the timing of the inflow event and the prevailing condition in the Baltic's Deep Basins.

A solid phase Mn-enrichment was observed in surface sediments sampled in 1994 equivalent to the amount of Mn^{2+} stored in anoxic bottom waters in 1992 before the 1993 inflow event (Brügmann et al., 1997; Heiser et al., 2001), showing that manganese deposition occurred as a result of this inflow event.

In both Chapter 3 and section 4.2 it is shown that Ca-rhodochrosite laminae occur as late winter-early spring deposits relative to varves. This timing information from varves is consistent with evidence of the timing of the first arrival of saline inflows in the Gotland Deep, which implies a direct causal link between the deposition of Mn-oxide laminae and major Baltic inflow occurrence.

4.6 Micro-fabric of Ca-rhodochrosite laminae

Under the SEM, the fine-scale structure of the Ca-rhodochrosite laminae may be discerned (Fig. 4.6a-d). Ca-rhodochrosite laminae commonly consist of aggregates of 2-10μm globular crystallites. In BSE images rhodochrosite laminae appear as a bright bands of crystallites, always occurring as parallel overprints to other clay-rich and diatomaceous laminae. In many cases a diffuse region of 2-3μm bright framboidal and/or cubic pyrite crystals occurs below the Ca-rhodochrosite laminae. The occurrence of cubic pyrite is limited only to areas associated with Ca-rhodochrosite laminae, but framboidal pyrite is commonly found elsewhere in Littorina sediments. In Landsort Deep sediments, Böttcher and Lepland (2000) associate single pyrite framboids with Fe-sulphide formation within the water column and clusters of framboidal pyrite, which include euhedral crystals, with Fe-sulphide formation within the sediments. In Jurassic mudstones, Taylor and Macquaker, (2000) attribute framboidal pyrite to early formation under highly sulphidic conditions and euhedral pyrite to slower formation under less reducing conditions. These pyrite sub-layers are, therefore, likely to have formed within the sediments, and possibly reflects a redox-dependent distribution of Fe during Ca-rhodochrosite formation.

Hexagonal Ca-rhodochrosite crystals (20-30μm) have been observed within or at the base of 12 (13%) of the 95 rhodochrosite laminae observed from 118-143cm. These crystals have a hollow core and are almost certainly pseudomorphs of hexagonal manganese sulphide, as they are consistent with the γ-Mn-sulphide crystal morphologies reported previously in Baltic sediments, both in the Landsort Deep (Baron and Debyser, 1957; Debyser, 1961; Suess, 1979; Lepland and Stevens, 1998) and in the Gotland Deep (Böttcher and Huckriede, 1997). A quite complex sequence of environmental conditions (see Fig. 4.7) is implied by the occurrence of these pseudomorphs.

A. Formation if Mn-sulphide

To form pseudomorphs as shown in Figure 4.6b, initially Mn-sulphide crystals must

have grown (Fig. 4.7a) following deposition of a Mn-oxide lamina. The precipitation of Mn-sulphide in preference to Mn-carbonate requires a very high excess of free sulphide relative to alkalinity and an environment completely depleted in Fe, which would otherwise preferentially react with sulphide to form Fe-sulphides (Böttcher and Huckriede, 1997). The site of maximum bacterial sulphate reduction rates in Gotland Deep sediments has been observed by Piker et al., (1998) at between 10-20cm below the sediment-water interface. High *in situ* H_2S and alkalinity concentrations should, therefore, be present below the Mn-oxide lamina. Large amounts of Mn^{2+} can be produced rapidly (Aller, 1980) by bacterial Mn-reduction (and possibly by direct chemical reduction) of the Mn-oxide lamina, hence, large concentrations of free Mn^{2+} will be present at the sediment-water interface. The likely site of Mn-sulphide precipitation is, therefore, at the base of the Mn-oxide lamina where high Mn^{2+} is met by high concentrations of H_2S diffusing upwards from the site of maximum bacterial sulphate reduction.

B. Formation of Mn-carbonate

Following initial Mn-sulphide growth, conditions must have altered sufficiently so that Ca-rhodochrosite overgrowths on the Mn-sulphide crystals were produced (Fig. 4.7b). Alkalinity is produced as a result of bacterial reduction of the Mn-oxide laminae, and simultaneously H_2S will be consumed by formation of Mn-sulphide. As a result, alkalinity can eventually become locally in excess relative to H_2S, and conditions may switch to favour Ca-rhodochrosite precipitation, both as an overgrowth on the hexagonal Mn-sulphide crystals and in separate Ca-rhodochrosite crystallites.

The banding evident in the pseudomorphs (Fig. 4.6b) suggests that the precise precipitation micro-habitat of the pseudomorphs may alternate between Mn-sulphide and rhodochrosite formation, depending on subtle lamina-scale variations in both the production and diffusion of H_2S and alkalinity.

C. *Dissolution of Mn-sulphide*

After all the Mn-oxide lamina has been consumed, the source of excess *in situ* Mn^{2+} will no longer be present, and no further rhodochrosite or Mn-sulphide can be formed due to this mechanism. In order to leave hollow Mn-sulphide pseudomorphs (Fig. 4.7c), therefore, the early-formed Mn-sulphide almost certainly will have become unstable and dissociated. As Mn-sulphide crystals have only been observed once previously in Gotland Deep sediments (Böttcher and Huckriede, 1997), it seems that Mn-sulphide preservation is not typical; indeed, the long-term sedimentary pore-water

conditions in the Gotland Deep have been commonly reported to be over-saturated (or meta-stable) with respect to Ca-rhodochrosite, but under-saturated with respect to Mn-sulphide (Kulik et al., 2000; Heiser et al., 2001). Mn-sulphide will, therefore, normally tend to dissociate and diffuse away into anoxic pore waters, leaving a Ca-rhodochrosite lamina containing Mn-sulphide pseudomorphs that record both the deposition of an ephemeral Mn-oxide lamina and the sensitive changes in geochemical conditions during Ca-rhodochrosite formation.

4.7 CONCLUSIONS

SEM images have revealed the occurrence of Ca-rhodochrosite overgrowth solely on benthic and not on planktonic foraminifera tests. This strongly implies a link between oxic bottom water conditions and rhodochrosite formation.

Energy dispersive microanalysis combined with back scatter electron imagery enables the placement of Ca-rhodochrosite laminae within an annual cycle of deposition, showing that Ca-rhodochrosite deposition is a rapid phenomenon occurring on seasonal time scales. The occurrence of Ca-rhodochrosite only as a winter/early spring deposit is in close agreement with the seasonality of flushing of the Gotland Deep as recorded in instrumental records. This finding provides supporting evidence for the assumed direct causal link between saline inflow events and Ca-rhodochrosite deposition, and suggests that this has been a regular feature of sedimentation throughout the Holocene sediments of the Gotland Deep.

The relatively common occurrence of Hexagonal γ Mn-sulphide pseudomorphs suggests that highly sulphidic conditions favouring the early formation of Mn-sulphide were reached much more commonly during Ca-rhodochrosite formation in the Gotland deep than previously reported.

Figure 4.1 High magnification (x20) back-scattered electron image showing four varves numbered 1-4 containing Ca-rhodochrosite laminae (core depth 126cm). Al (wt%), K/Al, Mg/Al, Cl (wt%) and Si/Al distributions shown from EDS line raster scan taken along extreme left hand side of BSE image. Ca-rhodochrosite laminae denoted by grey bands.

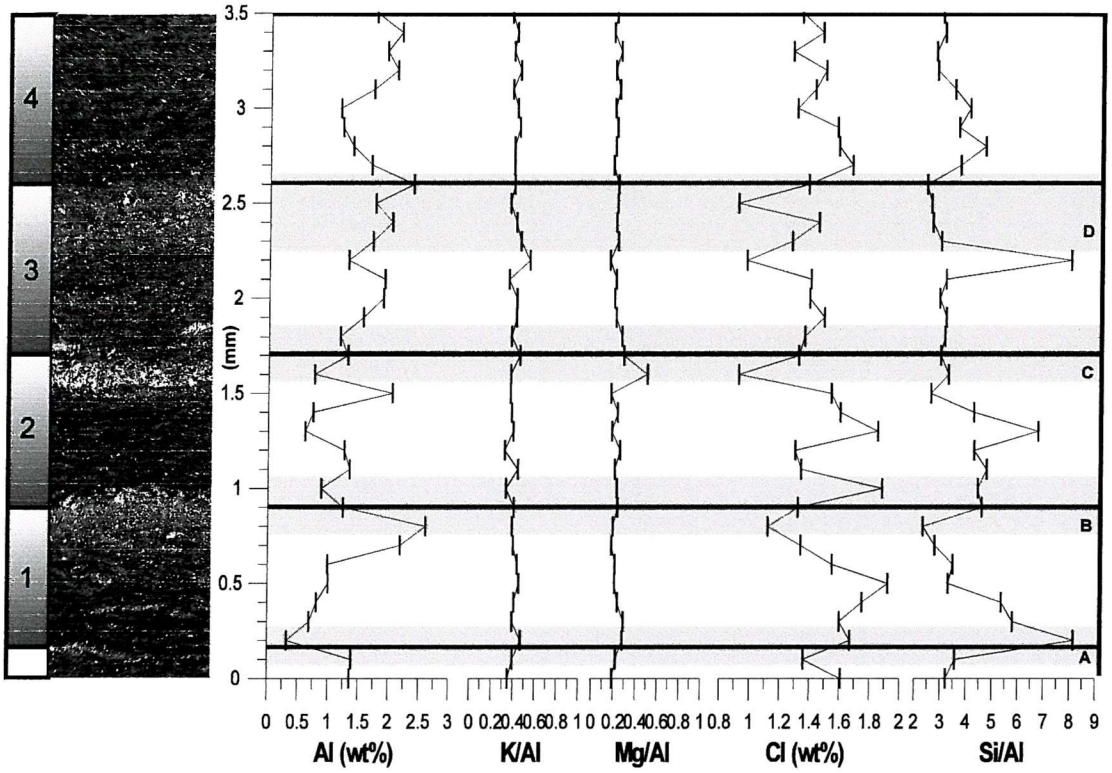

Figure 4.2 High magnification (x20) back-scattered electron image showing four varves numbered 1-4 containing Ca-rhodochrosite laminae (core depth 126cm). Mn/Al, Ca/Al distributions shown from EDS line raster scan taken along extreme left hand side of BSE image. Ca-rhodochrosite laminae denoted by grey bands.

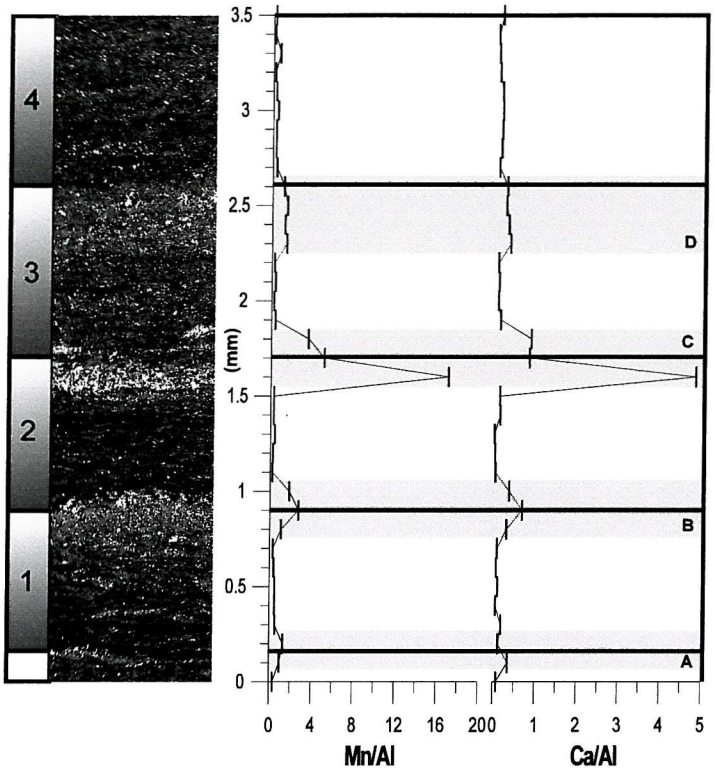

Figure 4.3 High magnification (x20) back-scattered electron image showing four varves numbered 1-4 containing Ca-rhodochrosite laminae (core depth 126cm). S/Al, Fe/Al distributions shown from EDS line raster scan taken along extreme left hand side of BSE image. Ca-rhodochrosite laminae denoted by grey bands.

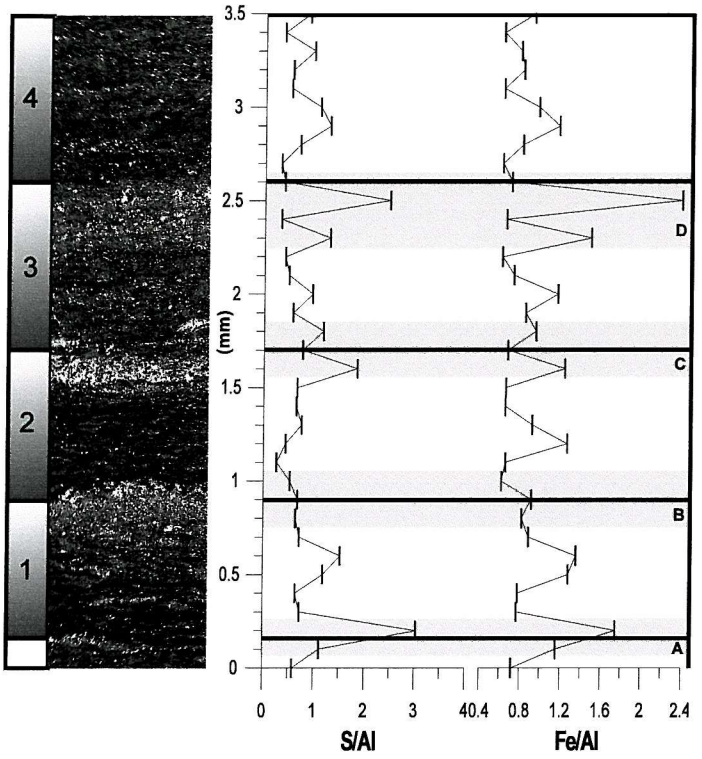

Figure 4.4 A: Benthic Foraminifera *Elphidium excavatum* heavily encrusted in Ca-rhodochrosite. B: back-scattered electron image cross-section of *E. excavatum*, bright outline is Ca-rhodochrosite overgrowth. Overgrowth extends along pores in *E. excavatum* foraminiferal test. C: Planktonic foraminifera *Globorotalia scitula*, surface ornamentation similar to *E. excavatum* in life. D: Right coiling planktonic foraminifera *Neogloboquadrina pachyderma.*

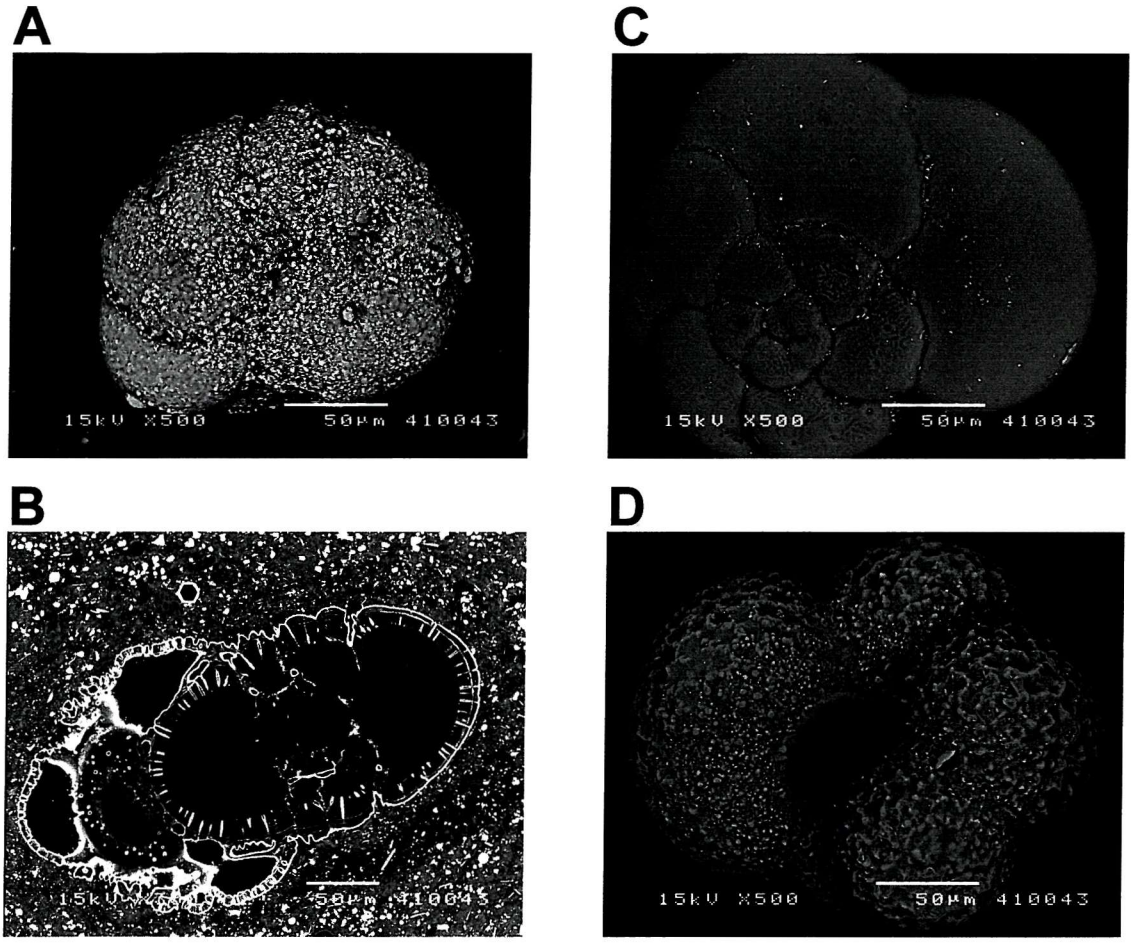

Figure 4.5. A. Seasonal distribution and intensity of Major Baltic Inflows, predicted from historical records (after Matthäus and Schinke, 1994). B. Variations in bottom water conditions (230-240m) in the Gotland Deep from 1992-96 (after Nehring et al., 1995b), and inflow events occurring at the Darrs Sill. H_2S concentrations plotted as negative O_2 concentrations.

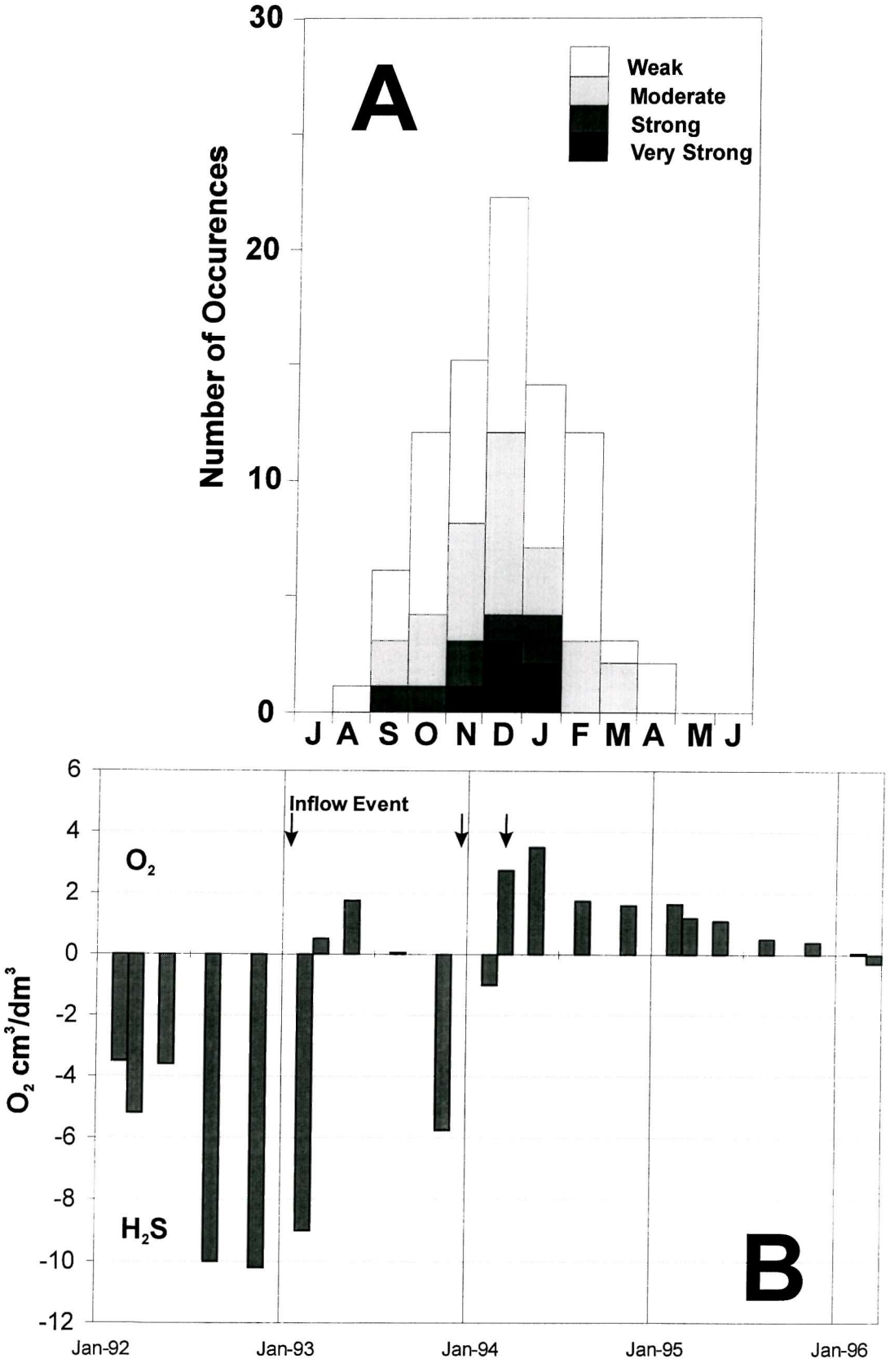

Figure 4.6. A: Topographical BSE image: aggregate of globular Ca-rhodochrosite crystallites. B: BSI image: Hexagonal Ca-rhodochrosite crystals (pseudomorphs of γ-Mn-sulphide) in ground-mass of globular crystallites. C: BSI image: Ca-rhodochrosite laminae show as bright band of crystallites. Zone of diffuse small (~1 μm) cubic pyrite crystallites beneath, shown in detail in D.

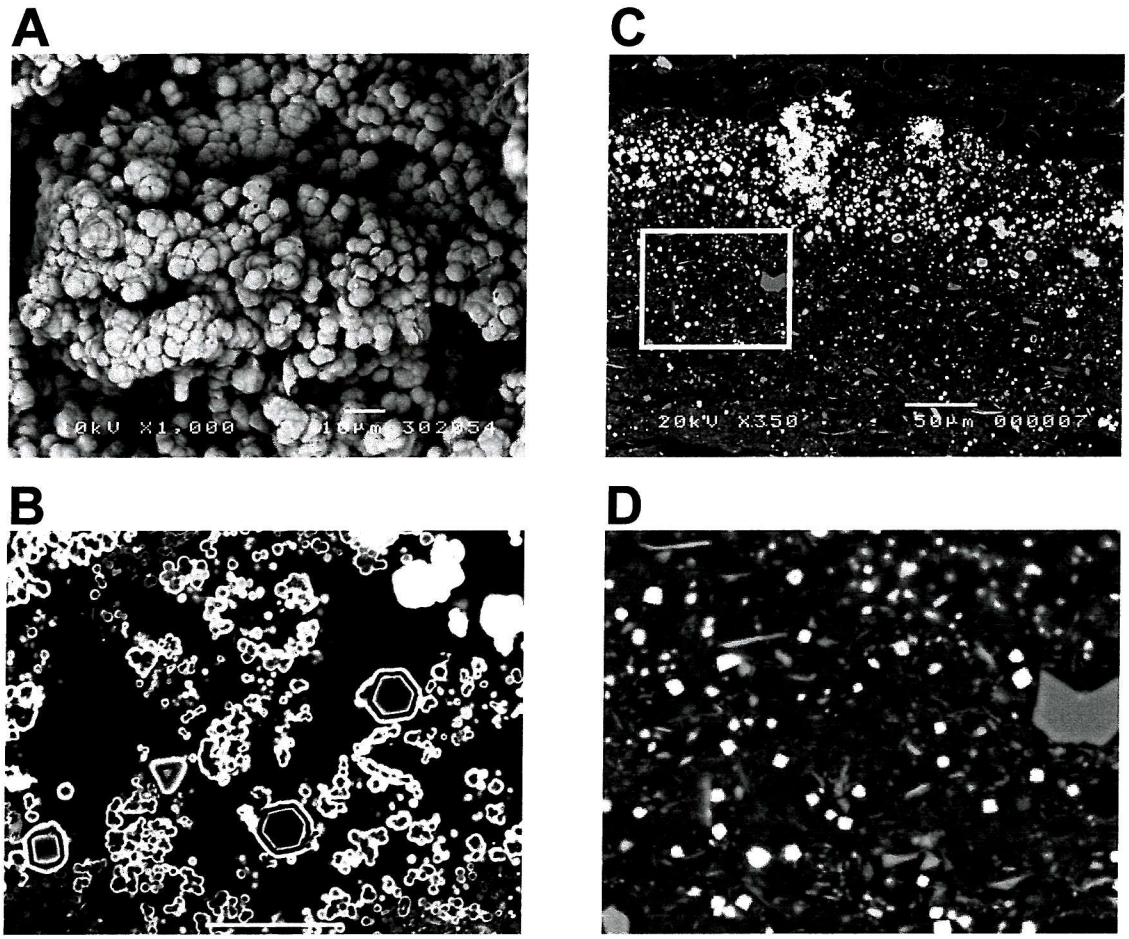

Figure 4.7 Mn-sulphide pseudomorph formation sequence.

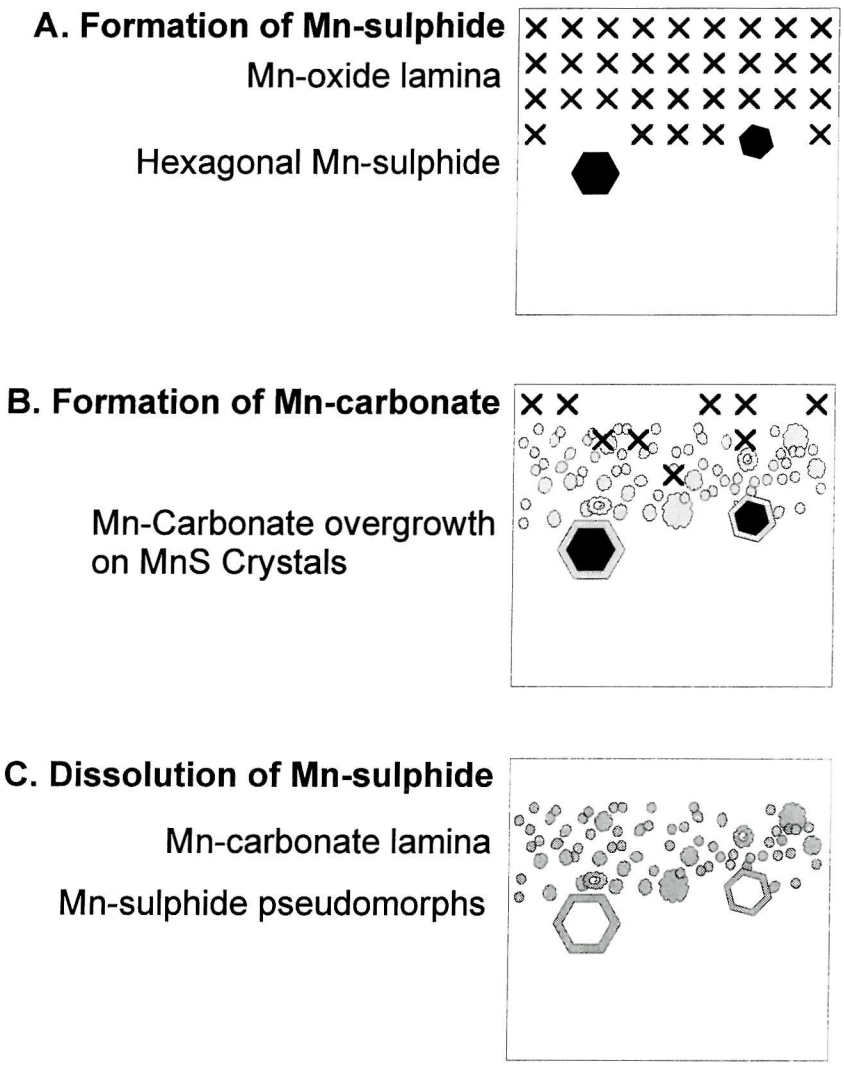

5 TRACE METAL DISTRIBUTION ASSOCIATED WITH Ca-RHODOCHROSITE LAMINAE

With 5 figures

5.1 INTRODUCTION

Many natural and anthropogenic processes lead to the release of redox sensitive metals in the marine environment. In the Baltic Sea the mean residence time for many metals; e.g., As (17yrs) Cd (5-6yrs) Cu (3-5yrs) Pb (0.3yrs) and Zn (2yrs), is considerably shorter than that of water (20-40yrs) (Brügmann et al., 1997; Sternbeck et al., 2000). The Baltic Sea, therefore, acts as an effective trap for many redox sensitive trace metals. Trace metals are generally enriched in anoxic settings (Calvert and Pedersen, 1993), and indeed many trace metals (Mn, Fe, Mo, U, V, Cd, Pb, Co, Ni, Cu, As and Zn) are reported to be enriched in the Gotland Deep sediments (Brügmann and Lange, 1990), supposedly fixed by the formation of both metal-sulphides and Mn-rich carbonates (Brügmann et al., 1998). This fixation could potentially immobilise toxic metals like Cd, Pb, Hg and Cu, removing them from the marine water column.

As all previous study have employed bulk sampling techniques and Ca-rhodochrosite and pyrite-rich laminae are observed to be finely interbedded on sub-millimetre scales (see chapter 4), there have been no previous studies of trace metal distributions associated with individual Ca-rhodochrosite laminae. Laser ablation ICP-MS allows the determination of trace metal concentration and distribution for many elements simultaneously at the lamina scale, allowing an assessment of the relative importance of Ca-rhodochrosite formation for the fate of trace metals in the Gotland Deep.

5.2 SAMPLE SECTIONS AND THE USE OF X/Al AND X/Ti RATIOS

Material analysed for this study was taken from selected intervals of organic-rich laminated muds of Littorina age at core depths between 0-229cm. Two sample areas, A and B, were chosen for laser ablation ICP-MS studies at a core depth of 126cm (A) and 197cm (B). Both A and B sample areas were within a varved sediment sequence, and contained prominent Ca-rhodochrosite laminae. High resolution SEM back-scattered electron images were taken for both areas to allow direct comparison of trace

element data to sediment fabric. Non-destructive major element energy dispersive X-ray micro-analysis (EDS) was carried out to allow direct comparison of major element and trace element data.

It is common practice to express geochemical data of this nature normalised to Al, i.e., as the X/Al ratio, so that the variations in 'excess' elemental abundance can be determined (i.e., not bound up in lithogenic clay minerals). (e.g. Calvert et al., 2001) Therefore EDS data are presented here in the X/Al form (Figs. 5.1-5.5). For the ICP-MS, however, this was not possible because Al data could not be collected for these samples. As there is some variation in the spot size produced by laser ablation (see Fig. 2.2), it is vital to express these data as an elemental ratio to account for spot size variation and, therefore, a substitute for Al data must be used. Following the approach of Sohlenius et al. (2001) Ti was used for normalisation for dilution by lithogenic minerals, therefore, ICP-MS trace element data are expressed here in the form of X/Ti. Although produced by different methods, the Ti and Al (wt%) profiles do show a good visual correlation (Fig. 5.1).

5.3 RESULTS

Figure 5.1 shows that there is a suite of elements (including Al and Ti) whose distribution coincides with that of lithogenic minerals. Cs/Ti, Rb/Ti, Zr/Ti, W/Ti, and K/Al all show no variation in their profiles, demonstrating that their distribution is also controlled by the distribution of lithogenic minerals. The variation shown by these elements is dependent on the balance between the deposition of organic-rich microfossil ooze laminae and the deposition of terrigenous clay throughout the varve sequence. There is also a significant dilution effect caused by the formation of Ca-rhodochrosite crystallites.

The bright winter Ca-rhodochrosite laminae can be seen clearly in BSE images (Fig. 5.1 – 5.5) of sample areas A and B. There laminae show large enrichments, of up to over 40 times background levels, in Mn/Al and Ca/Al in both sample areas A and B (Fig. 5.2); both Mg/Al and Sr/Ti also show significant but smaller enrichments (x3 and x10) within in the Ca-rhodochrosite laminae. There is an enrichment in Zn/Ti in both samples, however, there is a large difference in Zn/Ti enrichment levels between A and B. In sample A, Zn/Ti is enriched up to 140 times background levels, whereas B shows enrichments of just 3-5 times background levels.

S/Al shows peaks of between 3-4 times background levels in Ca-rhodochrosite laminae from both A and B (Figs. 5.3 and 5.4), which are not matched by similar levels of enrichment of Fe/Al. Many other chalcophile elements also have peaks (2-10 times background levels) within Ca-rhodochrosite laminae. Sample A (Fig. 5.3) has peaks in Pb/Ti, Cu/Ti, As/Ti, Co/Ti, Sn/Ti, and Ag/Ti within Ca-rhodochrosite laminae. Sample B (Fig 5.4), Ca-rhodochrosite laminae A, shows peaks in Cu/Ti, As/Ti, Co/Ti, Ni/Ti, and Ag/Ti. Sample B, Ca-rhodochrosite laminae B, shows peaks in Pb/Ti, As/Ti, Ni/Ti, and Sn/Ti. There are also peaks in chalcophile elements not associated with Ca-rhodochrosite laminae. In sample A, Cu/Ti, Ni/Ti, Co/Ti, Sn/Ti, and Ag/Ti, and in sample B, Pb/Ti, Cu/Ti, Ni/Ti, Co/Ti, As/Ti, Sn/Ti, and Ag/Ti are enriched outside Ca-rhodochrosite laminae, which relates to minor enrichments in Fe/Al.

Other redox sensitive elements (Fig. 5.5), Mo/Ti, U/Ti and V/Ti also show enrichments within Ca-rhodochrosite laminae and modest peaks where Fe/Al is elevated. The Ba/Ti profile, however, shows no peak in excess Ba within Ca-rhodochrosite laminae. Ba/Ti actually shows peak values corresponding to the dark microfossil-rich ooze laminae, where organic mater is potentially concentrated.

5.4 Trace metal enrichment in Gotland Deep sediments

The results show that, except for Al, Ti, Rb, Cs, Zn and W, almost every trace metal studied showed some enrichment within Ca-rhodochrosite laminae. Ca, Sr, Mg and Ba are expected theoretically to be incorporated into the carbonate solid-solution during Ca-rhodochrosite formation (Kulik et al., 2000). Ca, Sr, and Mg are indeed only enriched within Ca-rhodochrosite laminae. Ba, however, is not enriched in Ca-rhodochrosite laminae, but rather is enriched where there is a prominent ooze lamina. Ba is generally considered to be supplied to the sediments by the incorporation of Ba-sulphate onto organic matter/opaline silica (Bishop, 1988), therefore, Ba could act as a marker for organic matter preservation in these sediments as it does in other settings (e.g. Dymond et al., 1992; van Santvoort et al., 1996). The difference in distribution between the two sites for Zn is somewhat problematic. The massive enrichments of Zn within Ca-rhodochrosite laminae in sample A may be explained by the incorporation of Zn-carbonate into Ca-rhodochrosite. Although Zn can be incorporated into a solid-solution with Mn-carbonate (Böttcher, 1995), this has not been observed previously in marine sediments, and the formation of Zn-sulphide may

also explain the Zn enrichment; indeed the Zn/Ti profile in sample B is very similar to many other chalcophile elements.

The peaks in S observed within Ca-rhodochrosite laminae almost certainly relate to the S-bearing mineral detected as a contaminant in Ca-rhodochrosite crystallites in Chapter 4. As Fe is not incorporated in Ca-rhodochrosite, and Fe does not show large peaks within Ca-rhodochrosite laminae, this S is unlikely to relate to a Fe-sulphide enrichment. This S may relate to Mn-sulphide, which can form before or with Ca-rhodochrosite formation in the Gotland Deep (see Chapter 4) due to extreme Mn concentration exceeding saturation with respect to Mn-sulphide (Böttcher and Huckriede, 1997).

The distribution of the majority of other metals studied (Pb, Cu, Zn, As, Co, Ni, Sn, Ag, Mo, U, and V) is very similar to S, being enriched within Ca-rhodochrosite laminae and also where Fe is enriched. Two separate mechanisms may explain these enrichments.

Firstly, in the Gotland Deep, metals are scavenged from the anoxic water column by the formation of insoluble Fe-rich metal-sulphides (Kremling, 1983; Dyrssen and Kremling, 1990), while Mn is enhanced in anoxic waters (Brügmann et al., 1998). This would lead to the fixation in the sediments of trace elements prone to forming insoluble metal sulphides (i.e., Pb, Cu, Zn, As, Co, Ni, Sn, Ag, Mo) within Fe-sulphide-rich laminae. Although U and V do not form insoluble sulphides, they do form solid phases in anoxic settings (Calvert and Pedersen, 1993), and may also be scavenged to the sediments by particulate Fe-sulphide.

Secondly, following major Baltic inflow events, all metals are effectively scavenged by the formation of particulate Mn-oxides, including a second removal of elements already depleted by Fe-sulphide formation (Pohl and Hennings, 1999). Metals scavenged to the sediments in this way could then be sequestered in the sediments by formation of metal-sulphide phases in the sediments, producing enrichments in trace metals both within pyrite-rich and Ca-rhodochrosite laminae.

5.5 Conclusions

Trace metals are affected by seasonal-scale redox effects operating in the Gotland Deep, leading to enrichment in both Ca-rhodochrosite and Fe-rich laminae. The primary mechanism for sequestering trace metals to the sediments seems to be by scavenging these metals onto particulate Fe-sulphides in the water column. Secondary

scavenging of metals onto Mn-oxides following saline inflow events, also causes enrichment of trace metals within Ca-rhodochrosite laminae. As oxic conditions do not generally persist long after major inflow events, the potential for remobilization of trace metals may be limited and Gotland Deep sediments may act as an effective trap for many trace metals.

Figure 5.1 Al, Ti, Cs/Ti, Rb/Ti, Zr/Ti, W/Ti, and K/Al profiles. Heavy lines are 5pt. moving average. High magnification (x20) BSE images showing two varved sample intervals A and B (core depth 126cm and 197cm). Major element distribution from EDS line raster scan, and trace element profiles from laser ablation ICP-MS sampling. Rhodochrosite laminae denoted by grey bands.

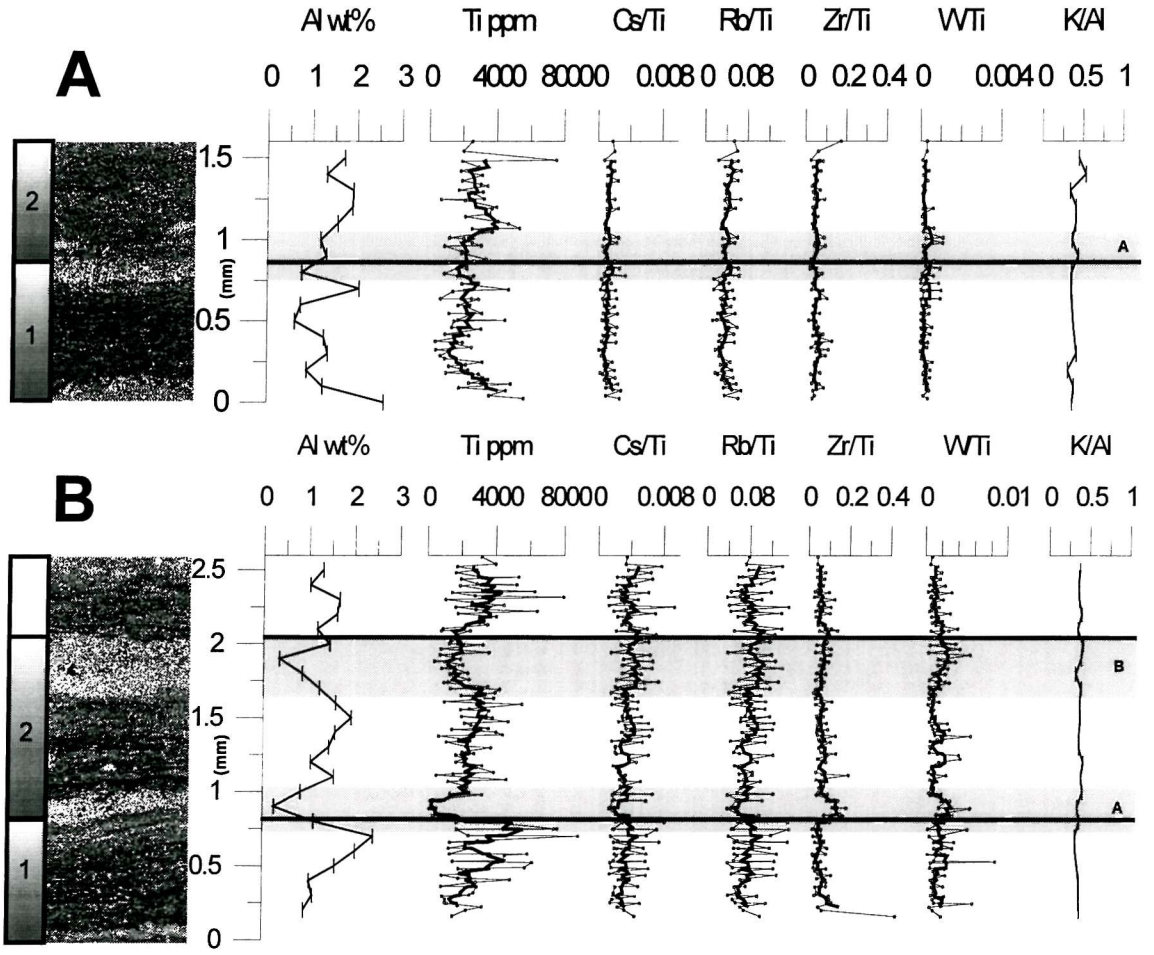

Figure 5.2 Mn/Al, Ca/Al, Mg/Al, Sr/Ti, and Zn/Ti profiles. Heavy lines are 5pt. moving average. High magnification (x20) BSE images showing two varved sample intervals A and B (core depth 126cm and 197cm). Major element distribution from EDS line raster scan, and trace element profiles from laser ablation ICP-MS sampling. Rhodochrosite laminae denoted by grey bands.

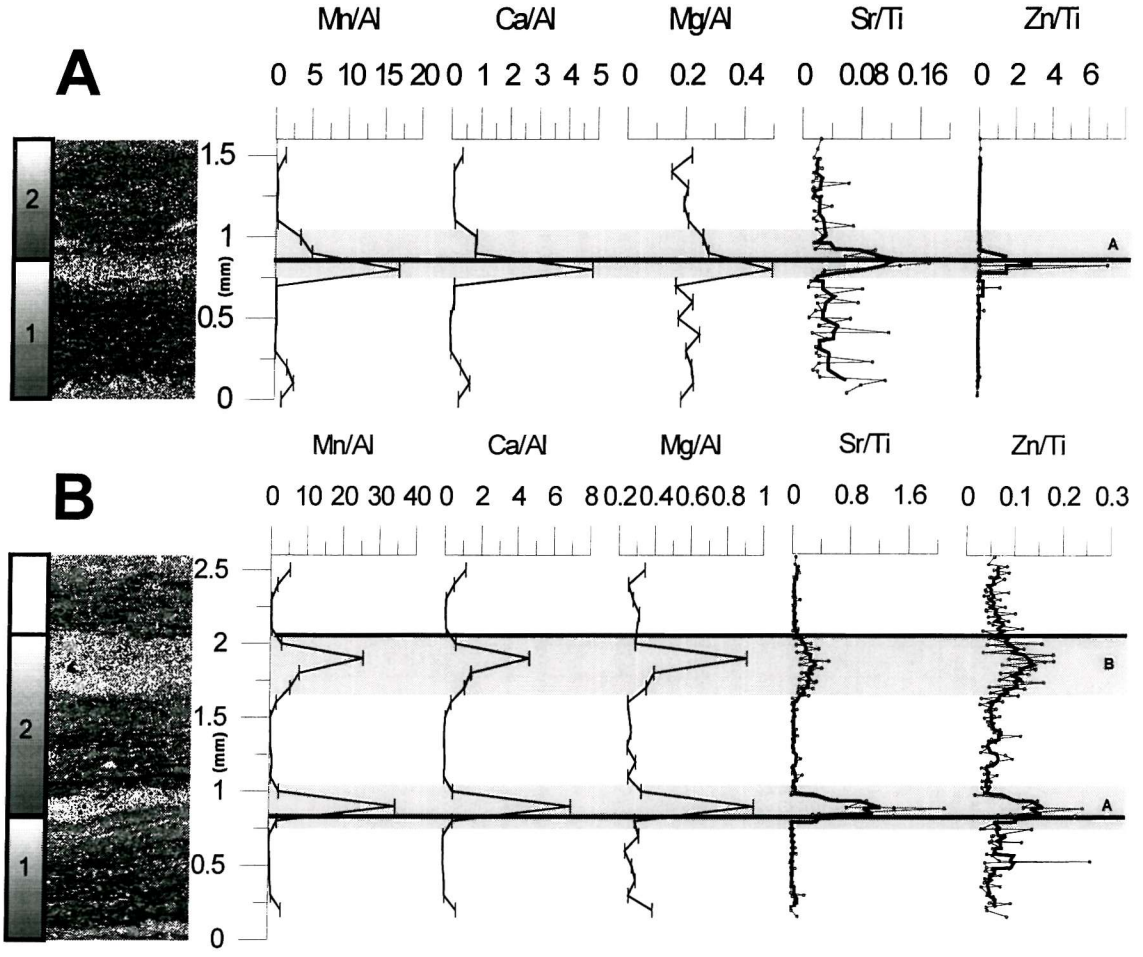

Figure 5.3 S/Al, Fe/Al, Pb/Ti, Cu/Ti, As/Ti, Co/Ti, Ni/Ti, Sn/Ti, and Ag/Ti profiles. Heavy lines are 5pt. moving average. High magnification (x20) BSE images showing varved sample A (core depth 126cm). Major element distribution from EDS line raster scan, and trace element profiles from laser ablation ICP-MS sampling. Rhodochrosite laminae denoted by grey bands.

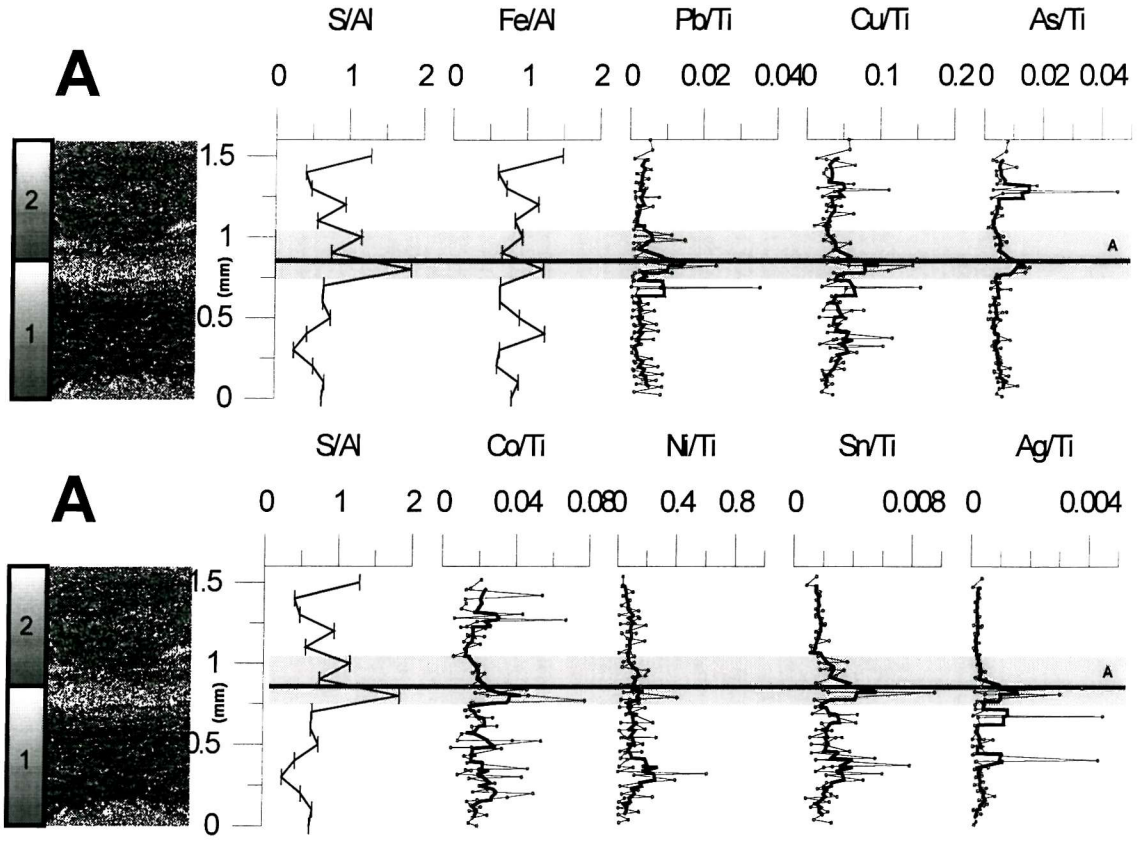

Figure 5.4 S/Al, Fe/Al, Pb/Ti, Cu/Ti, As/Ti, Co/Ti, Ni/Ti, Sn/Ti, and Ag/Ti profiles. Heavy lines are 5pt. moving average. High magnification (x20) BSE images showing varved sample B (core depth 197cm). Major element distribution from EDS line raster scan, and trace element profiles from laser ablation ICP-MS sampling. Rhodochrosite laminae denoted by grey bands.

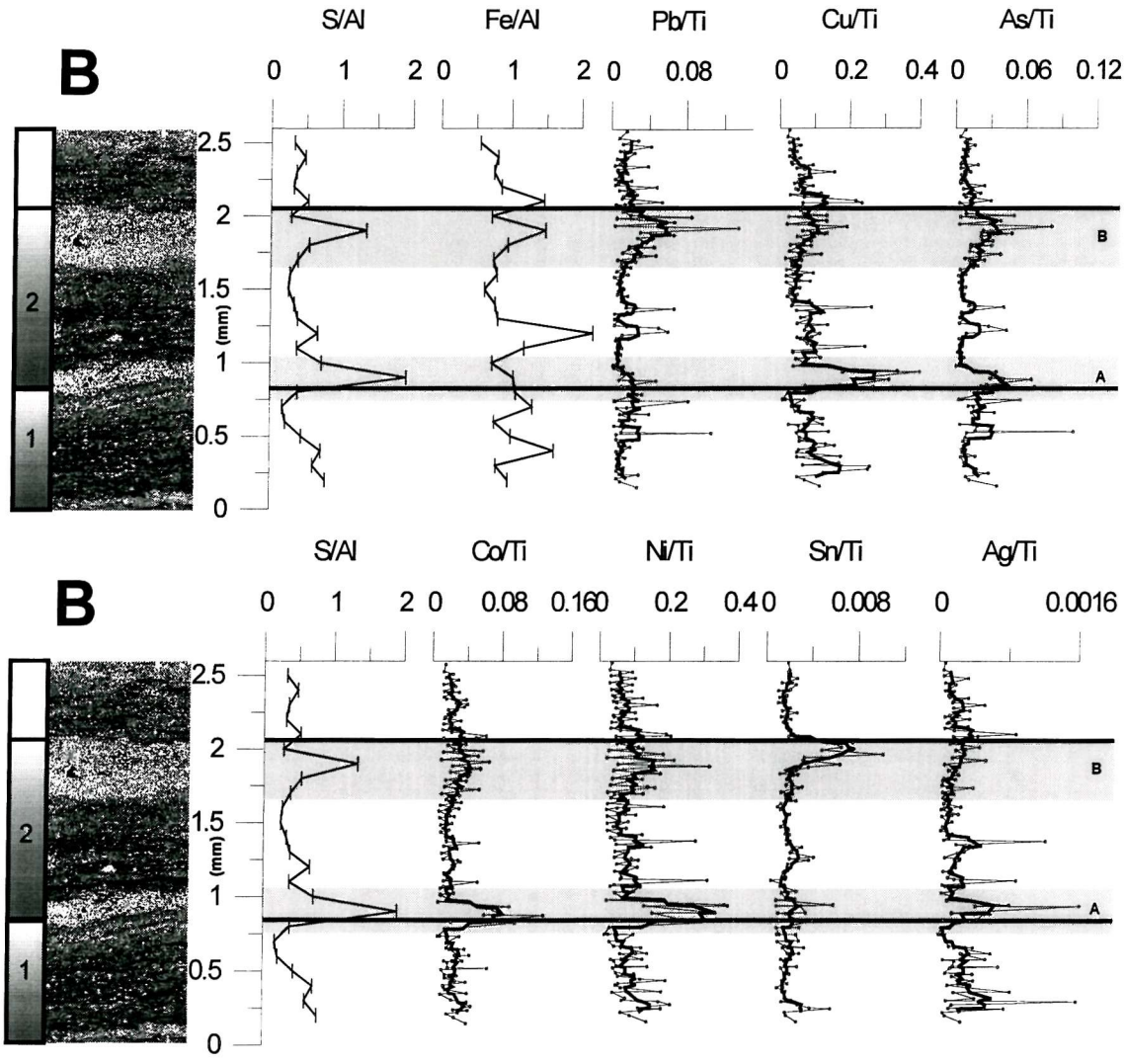

Figure 5.5 Mn/Al, Mo/Ti, U/Ti, Ba/Ti, and V/Ti profiles. Heavy lines are 5pt. moving average. High magnification (x20) BSE images showing two varved sample intervals A and B (core depth 126cm and 197cm). Major element distribution from EDS line raster scan, and trace element profiles from laser ablation ICP-MS sampling. Rhodochrosite laminae denoted by grey bands.

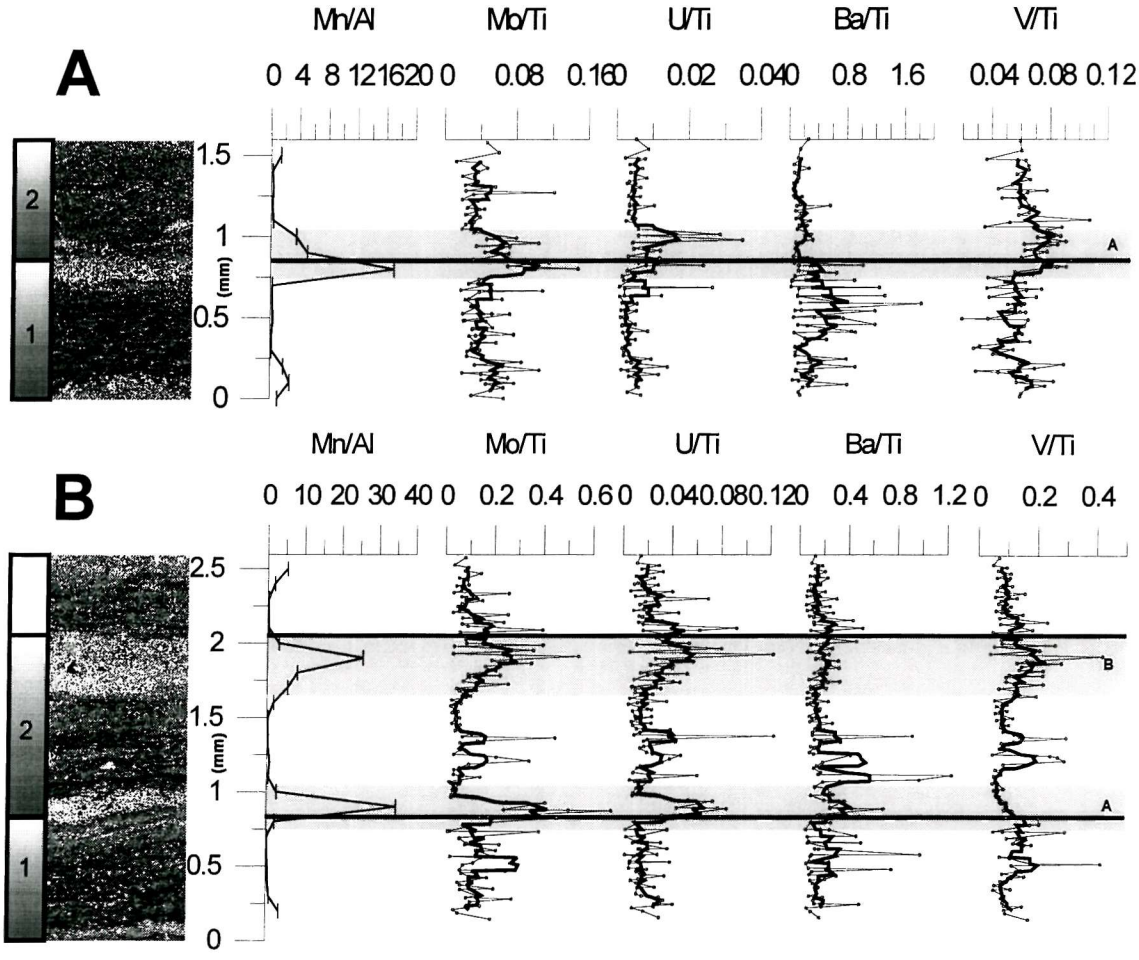

6 THE ROLE OF SULPHIDE DURING THE FORMATION OF Ca-RHODOCHROSITE

With 5 figures

6.1 INTRODUCTION

The distribution and fate of Mn and Fe in natural environments is controlled by the redox cycling of elements as labile organic matter is progressively oxidised by a succession of oxidising agents (Froelich et al., 1979; Berner, 1981; Burdige, 1993). Despite the similarity of diagenetic reactions involving Fe and Mn (Froelich et al., 1979), redox processes often result in their physical separation in sediments and pore waters (Burdige, 1993). This is because reduction of Mn-oxides produces a greater free energy yield relative to reduction of Fe-oxides, which leads to preferential microbial utilisation of Mn-oxides before Fe-oxides (Aller and Rude, 1988). The result in anoxic settings like the Gotland Deep, however, where the supply of labile organic matter is high and exchange of bottom water is limited, is to consume all available oxidising agents thus producing sulphidic bottom waters enriched in Fe^{2+} and Mn^{2+}, and laminated sediments (Manheim, 1961). The post-Ancylus sediments of the Gotland Deep are enriched in both Fe and Mn due to the separate formation of Fe-sulphides in an anoxic water column (Boesen and Postma, 1988) and Ca-rhodochrosite formation following major Baltic inflow events (see section 6.2). Formation of Mn-sulphide is not usually considered to be an important sink of Mn due to its rare occurrence, and previous reports have found that Gotland Deep pore-water conditions are normally under-saturated with respect to Mn-sulphide (Kulik et al., 2000; Heiser et al., 2001). Only one study (Böttcher and Huckriede, 1997) has hitherto directly reported Mn-sulphide in Gotland Deep sediments; and abundant Mn-sulphides only occur in restricted intervals in Landsort Deep sediments (Lepland and Stevens, 1998), where Mn-sulphide formation has been ascribed to super-stagnant hyper-anoxic water column events, leading to super-saturation with respect to Mn-sulphide, and precipitation within the water column. In Chapter 4, however, it was observed that Mn-sulphide pseudomorphs in Gotland Deep sediments occur associated with many Ca-rhodochrosite laminae, and that sulphur is a major contaminant (up to 4wt%) in all rhodochrosite crystallites. This suggests that there may be an interplay between Mn-

sulphide and Ca-rhodochrosite formation. The Littorina sediments are intermittently laminated reflecting fluctuating periods of oxic and anoxic conditions, suggesting that variations in benthic redox conditions may control the diagenetic processes occurring in the Gotland Deep.

In order to test these suppositions, detailed observations of phase compositions, fabric relations and lamina scale elemental distributions were produced using a combination of scanning electron microscope (SEM) and energy dispersive X-ray micro-analysis (EDS) techniques. This chapter aims to discern the composition and distribution of diagenetic carbonate and sulphide phases within Gotland Deep sediments, in order to elucidate: 1. The mechanisms of formation and composition of these diagenetic phases, and; 2. The perturbation of these processes in relation to interannual-scale variation in benthic redox conditions.

6.2 Formation of Ca-rhodochrosite

In the Baltic Sea deposition and formation of Ca-rhodochrosite laminae has been widely investigated and debated (Suess, 1979; Jakobsen and Postma, 1989; Huckriede and Meischner, 1996; Neumann et al., 1997; Sternbeck and Sohlenius, 1997; Lepland and Stevens, 1998). In the Gotland Deep, Ca-rhodochrosite formation has been linked to the periodic renewal of the stagnant deep water (Matthäus, 1995), the subsequent oxidation and precipitation of dissolved Mn^{2+} and Fe^{2+} as particulate oxy-hydroxides in the water column, and settlement of the resultant particulate matter to the sediment surface (Heiser et al., 2001). Ca-rhodochrosite precipitation is then driven kinetically by large pore-water Mn^{2+} concentrations resulting from rapid microbial reduction of the Mn-oxide lamina (Aller and Rude, 1988; Böttcher, 1998). Kulik et al. (2000) have shown theoretically that precipitation of Ca-rhodochrosite requires simply an excess of readily reducible Mn and does not require high alkalinity conditions produced by bacterial sulphate reduction. This has been affirmed by experimental results (Sternbeck, 1997) and also by reports of Ca-rhodochrosite $\delta^{13}C$ values from the Panama Basin close to normal seawater carbonate (Pedersen and Price, 1982). Ca-rhodochrosite $\delta^{13}C$ values from the Gotland Deep, however, are typically isotopically light from -6 to -14‰ (Suess, 1979; Huckriede and Meischner, 1996) indicating that, in this setting, diagenetically produced alkalinity is incorporated into Ca-rhodochrosite. The precipitation of Ca-rhodochrosite is thought to occur rapidly following Mn-oxide deposition (Sternbeck and Sohlenius, 1997). The co-precipitation

of Mn with calcite (Mucci, 1988; Pingitore et al., 1988) occurs much more rapidly than precipitation of pure $MnCO_3$ (Sternbeck, 1997) and leads to the rapid fixing of free Mn in a mixed Mn-Ca-CO_3 phase, which forms within the sediments (Morad and Al-aasm, 1997) at or below the sediment-water interface (Kulik et al., 2000). The resulting Ca-rhodochrosite produced is metastable with respect to pore water Mn and Ca concentrations (Böttcher, 1998).

6.3 Energy dispersive X-ray microanalysis (EDS) profiles

Figures 6.1 and 6.2 show high resolution major element profiles plotted against fabric bioturbation index for a 50cm section of Littorina sediments (core depth 165-216cm). The use of major elements profiles to delimit the distribution of different mineral phases is discussed in detail in Chapter 4. Al (wt%) is used as a proxy for clay mineral distribution; Ca/Al and Mn/Al for Ca-rhodochrosite; S/Al and Fe/Al for Fe-sulphide; Si/Al for biogenic silica (diatoms); and Cl (wt%) for porosity. Application of the bioturbation index (BI), that records changes between laminated anoxic conditions and homogeneous oxic periods (after Behl and Kennett, 1996), allows delineation of 4 anoxic and 3 oxic intervals through the 50cm record (labelled A1-4 and O1-3 respectively). There is very good agreement between the BI and the inverted Al (wt%) record, showing depletion in anoxic intervals and enrichment during oxic intervals. In the anoxic intervals, there is also an enrichment in Si/Al, Fe/Al, S/Al, and Cl (wt%) (Fig. 6.2) indicating that biogenic silica, Fe-sulphide, and porosity are enriched in these intervals. By applying the commonly reported relationship between pyrite-S and organic carbon it is therefore also likely that organic carbon preservation is also enriched in these anoxic intervals (Berner and Raiswell, 1983), however, the C/S ratios reported for Littorina sediments are lower (~1.55) than other anoxic Holocene sediments (Sohlenius et al., 1996a; Sternbeck and Sohlenius, 1997). On the simplest interpretation, therefore, it appears that the observed Al (wt%) record is the product of a closed-sum effect, and Al (wt%) variation records a residual enrichment in clay minerals during oxic intervals, which are diluted by organic matter, biogenic silica, and sulphide minerals during anoxic intervals. As the BI record is produced by visual logging subject to visual interpretation, an independent gauge of anoxic-oxic boundaries was fixed by establishing an arbitrary reference level of 2.3wt% Al, below which anoxic condition are assumed.

The matching Mn/Al and Ca/Al profiles (Fig. 6.1) represent Ca-rhodochrosite laminae, and show that Ca-rhodochrosite does not seem to be limited in occurrence or magnitude to either oxic or anoxic intervals, but rather can occur regularly throughout the 165-216cm interval. The implication of regular Ca-rhodochrosite formation is that anoxic periods are regularly interrupted by oxic inflow events. Oxic conditions, however, must only be sustained for relatively short periods (1-2 months or less) so that re-colonisation by benthic organisms and bioturbation does not occur. Conversely, bioturbated oxic intervals must have included intermittent anoxic periods when the water column could be charged with Mn^{2+}, which is a basic requirement for the accepted Ca-rhodochrosite formation model (see section 6.2). The anoxic-oxic intervals, therefore, represent the long-term mean Gotland Deep conditions that are affected by short-term seasonal/interannual variations in benthic oxygenation. The Ca/Al record (Fig. 6.1) is in very close agreement with Mn/Al, except for interval A4. In A4 very prominent Mn/Al enrichments, are not matched by similar Ca/Al peaks. There are also very large peaks in S/Al, that are not matched by Fe/Al. These Mn/Al peaks in A4 represent Mn-sulphide laminae. SEM imaging revealed three separate intervals containing Mn-sulphide laminae in the A4 interval.

Unlike Ca-rhodochrosite (see Chapter 3), the Mn-sulphide does not generally form thin distinct laminae, except for one incidence where a leaf structure (Fig 6.3a, b) has been preserved by Mn-sulphide, showing the remarkable degree of preservation of organic material and structures in interval A4. The Mn-sulphide normally occurs as 5-30μm crystallites dispersed over up to 3mm in diatom ooze laminae (Fig. 6.3c, d), no Ca-rhodochrosite crystallites are evident. The Mn-sulphide crystallites shown (Fig. 6.3d) have two distinctly different forms; irregular spheroids and euhedral rhombs. Both morphologies, however, have similar compositions and are not treated separately in Table 6.1. Hexagonal Mn-sulphide crystals and pseudomorphs that have been previously observed (see Chapter 4 and reference therein) were not observed. Mn-sulphide crystals are reported to oxidise rapidly during sampling (Suess, 1979), it is possible that the Mn-sulphide crystals shown in Figure 6 have been affected by oxidation during, or prior to, resin imbedding.

The molar composition of the sulphide phase formed is quite sulphur-rich at $Mn_{0.69}S$. The Mn-sulphides are completely free of Fe, as expected, since Fe would otherwise preferentially react with sulphide to produce Fe-sulphides (Böttcher and Huckriede, 1997). The origin of the Mg and Na contamination remain unexplained,

but may relate to oxidation of Mn-sulphide during sampling. The sediment embedding process uses epoxy resin containing C and O, and is the only source of Cl remaining in the sediments (sea water is replaced by resin during embedding). Thus the presence of C, O and Cl in the Mn-sulphide phase shows only that there is considerable variation in porosity within the matrix of these Mn-sulphides, although the high oxygen content may also point to oxidation and Mn-oxide formation prior to, or during, resin embedding.

Table 6.1 Composition of Mn-sulphide phase from EDS spot analysis

n=51	Mn	S	Fe	Ca	Mg	Na	C	Cl	O	Total
Mean (wt%)	23.02	19.59	n.d.*	0.04	2.21	5.66	5.94	0.46	42.60	99.52
Standard Deviation	6.13	3.54	n.d.*	0.04	2.69	4.34	7.96	0.29	8.35	-
Minimum (wt%)	12.79	10.82	n.d.*	n.d.*	0.10	0.22	n.d.*	0.10	10.63	-
Maximum (wt%)	44.43	30.58	n.d.*	0.24	11.12	14.82	39.84	1.14	52.26	-

*n. d. – not detected

The occurrence of Mn-sulphide laminae in A4 may reflect a continuance of the Mn-deposition throughout the 165-216cm section. This probably relates to the occurrence of regular inflow events, and the resultant deposition of a Mn-oxide lamina to the sediments; however, the diagenetic response has been to produce Mn-sulphide in A4, and Ca-rhodochrosite at most other times. The A4 interval contains the highest Si/Al, Cl (wt%) and S/Al levels recorded in the 165-216cm section, and, therefore, as the sediments are likely to be enriched in organic matter, this is also likely to represent a sustained period of highly sulphidic conditions. These localised, highly sulphidic conditions may lead to the production of Mn-sulphide at the expense of Ca-rhodochrosite following an inflow event, and also create conditions where Mn-sulphide is stable within the sediments.

In contrast to the Mn-sulphides found in interval A4, Fe-sulphides are found plentifully in other intervals, with a composition shown in Table 6.2. The molar composition is $Fe_{0.0.91}Mn_{0.09}S_{1.70}$. The Fe-sulphide contains ~9% Mn, indicating an environment of formation that was rich in Mn^{2+} that can easily substitute into the Fe-sulphide phase (Sternbeck et al., 2000). This is consistent with the model for Fe-

Sulphide formation in anoxic Gotland Deep conditions where large amounts of Mn^{2+} commonly build up (Boesen and Postma, 1988; Neumann et al., 1997).

Table 6.2 Composition of Fe-sulphide phase from EDS spot analysis

n=5	S	Fe	Mn	Ca	Cl	C	O	Total
Mean (wt%)	37.38	34.71	3.29	0.05	0.18	8.73	14.66	99.01
Standard Deviation	6.92	5.11	1.17	0.02	0.11	3.05	6.56	-
Minimum (wt%)	45.94	42.89	4.15	0.07	0.32	11.52	22.24	-
Maximum (wt%)	30.29	30.14	1.25	0.03	0.06	5.25	8.41	-

6.4 VARIATION IN Ca-RHODOCHROSITE Mn/Ca RATIO

The cross-plot of Mn (wt%) against S (wt%) (Fig. 6.4a) for the whole 165-216cm interval shows that the lowest Mn distribution is limited by a Mn-sulphide phase, whose composition is enriched in S compared to MnS. The large scatter of Mn (wt%) values above the MnS composition are due to the presence of Ca-rhodochrosite. A Mn (wt%) v S (wt%) cross-plot for just the Mn-sulphide containing A4 interval (Fig. 6.4b) shows that Mn and S correlate very well (r^2=0.98) and that little or no Ca-rhodochrosite is formed in interval A4. The Mn-sulphide molar composition ($Mn_{0.75}S$) deduced by this technique is consistent with that deduced by EDS spot analysis.

A cross-plot of Ca (wt%) against Mn (wt%) for the whole 165-216cm interval (Fig 6.4c) shows that the observed rhodochrosite phase has a Mn/Ca wt% ratio of 4.88, consistent with the EDS spot analysis (Table 6.3). The Mn/Ca wt% ratio (Fig 6.1) also seems to vary systematically throughout the 165-216cm interval, with S/Al. In anoxic intervals Mn/Ca tends to higher values, perhaps due to the greater incorporation of Mn-sulphide into Ca-rhodochrosite in these intervals. There is considerable variation in observed composition of Ca-rhodochrosite (Table 6.3) in terms of mean Mn/Ca ratio, ranging from 2.47 (Sternbeck and Sohlenius, 1997) to 6.67 (this study). The average Mn/Ca ratio of 6.67 recorded in this study is very high compared to rhodochrosite compositions previously recorded by a variety of different techniques (Table 6.3). This is almost certainly due to the inclusion of data from Mn-sulphide rich laminae with Mn/Ca ratios over 100. Nevertheless, Mn/Ca values of up to 4.9 are commonly recorded in studies of Ca-rhodochrosite composition (Table 6.3). The cross-plot of Mn/Ca against S/Al (Fig. 6.4d) shows a reasonable degree of correlation,

r^2=0.76. The Y-axis intercept indicates a Mn/Ca ratio of just 3.30, where excess S/Al is not present, close to the bottom end of the Ca-rhodochrosite compositional range and the model predictions of Kulik et al. (2000). A baseline Mn/Ca value of 3.30 has been added to Figure 6.1, showing that the Mn/Ca ratio only approaches this low value in some oxic intervals, where the ability to form Mn-sulphide may be reduced.

Table 6.3 Mean Composition of Ca-rhodochrosite in terms of Mn/Ca and Mg/Ca

Method of Determination	Mn/Ca (wt%)	Mg/Ca (wt%)
Leaching		
HM,96	4.62	0.113
SS, 97	2.47	nd
K, 2000	3.70	0.180
SEM-EDS/Microprobe spot analysis		
JP, 89	3.41	0.130
LS, 98#	4.81	0.045
Chapter 4	4.69	0.136
Mn v Ca regression plot		
section 6.4	4.88	-
Line Raster Profile Average Mn/Ca		
section 6.4	6.67	-
Y-intercept, Mn/Ca v S/Al regression plot		
section 6.4	3.30	-
Solid-Solution, Aqueous-Solution Model		
K, 2000	3.75	0.115

References—HM,96 - Huckriede and Meischner, 1996; SS, 97 - Sternbeck and Sohlenius, 1997; K,2000 - Kulik et al., 2000; JP - Jakobsen and Postma, 1989; LS, 98 - Lepland and Stevens, 1998.

Notes—Nd - not determined, #Landsort Deep study.

The systematic variance in Mn/Ca ratios with S/Al, therefore, simply may be due to increasing amounts of Mn-sulphide precipitation during more sulphidic anoxic intervals, and the composition of Ca-rhodochrosite produced may be relatively constant. If the composition of Ca-rhodochrosite is constant, then one might expect the Mg/Ca ratio of Ca-rhodochrosite to be constant, as only Mn incorporation will be affected by formation of Mn-sulphide. As Ca-rhodochrosite formation conditions may be substantially different in Landsort Deep, it might be plausible to discount the very low Mg/Ca ratio found there for Ca-rhodochrosite (Lepland and Stevens, 1998). Table 6.3, however, shows that there is still considerable variation in Mg/Ca ratios in Ca-rhodochrosite from 0.113-0.180. Another method of testing whether the Mn/Ca ratio is controlled by Mn-sulphide variation is mathematically to subtract the Mn co-precipitated as Mn-sulphide, producing the residual Mn/Ca ratio of the Ca-

rhodochrosite phase. The average Ca-rhodochrosite composition from EDS spot analysis is 36.39wt% Mn, 8.10wt% Ca, giving a Mn/Ca ratio of 4.69; this Ca-rhodochrosite also contains on average 1.16wt% S (see Chapter 4). If one assumes a molar composition of $Mn_{0.75}S$, then 1.49wt% Mn is on average sequestered as Mn-sulphide. The Mn/Ca ratio of the residual Ca-rhodochrosite can then be reduced to 4.29. This is still fairly high compared to the range of Mn/Ca reported (Table 6.3). The composition of Ca-rhodochrosite, therefore, may also systematically tend to higher Mn/Ca ratios in anoxic intervals, where more sulphidic pore-waters may more rapidly reduce Mn-oxide, producing greater *in situ* Mn^{2+} concentrations and Ca-rhodochrosite compositions richer in Mn.

6.5 Conceptual model for Ca-rhodochrosite formation

A criticism that can be made of the established model for Ca-rhodochrosite formation in the Gotland Deep (see section 6.2, and references therein) is that, while it elegantly explains how Mn-oxide can be concentrated at the sediment-water interface, it fails to explain the geochemical process that converts a Mn-oxide lamina to the Ca-rhodochrosite lamina observed in the sediments. Observations from SEM studies (Chapter 4; Section 6.2, 6.3), however, have provided new insights on the composition and distribution of diagenetic phases, which potentially may help to define the Ca-rhodochrosite formation process. A five-stage conceptual model (Fig. 6.5), while not exhaustive in terms of chemical species, has been constructed to produce a formation mechanism that attempts to explain all the observed features associated with Ca-rhodochrosite laminae:

1. Normal anoxic conditions (and build up of Mn^{2+})

The normal salinity stratification within the Baltic Sea leads to stagnation and build up of sulphidic conditions in deep water of the Gotland Deep. Anoxic conditions may persist for several years or more (Matthäus, 1995) allowing Mn^{2+} and Fe^{2+} concentrations in the anoxic deep water to build up to over 500 times and 50 times surface water concentrations respectively (Brügmann et al., 1998). Concentrations of Mn^{2+} is much greater than Fe^{2+} because the formation of Fe-sulphide in the water column limits dissolved Fe concentrations (Boesen and Postma, 1988; Neumann et al., 1997). Thus the initial conditions, prior to the inflow event, are high Mn^{2+} concentrations increasing with depth, with relatively reduced Fe^{2+} concentrations.

High bacterial sulphate reduction (BSR) rates within the anoxic sediments (Piker et al., 1998) also lead to high HS^- and alkalinity concentrations.

2. Oxygen renewal (and deposition of Fe-Mn-oxide)

The normal anoxic benthic conditions are greatly perturbed following the intrusion of oxic water from the North Sea. Diffusive oxygen penetration will form a new redoxcline at a very shallow depth within the sediments (Brügmann et al., 1997), but highly sulphidic conditions will still be present in the pore-waters at depth. Both free sulphide and oxygen will be consumed at the redoxcline and the exact depth of oxygen penetration will be controlled by the balance between rates of sulphide and oxygen diffusion. BSR will still produce alkalinity (and sulphide) at depth and alkalinity will have a diffusive contact with the oxic water column. Free Mn^{2+} and Fe^{2+} will only occur at depth due to oxygen penetration from the water column, and will also be oxidised at the redoxcline as they diffuse upwards; this may result in the formation of Fe and Mn-oxide 'sub-lamina' in the sediments just above the redoxcline (Burdige and Gieskes, 1983; Thomson et al., 1986). The oxygen-penetration stage could potentially last several months or more (Nehring et al., 1995b), which may provide an opportunity for benthic re-colonisation by benthic foraminifera (e.g., *Elphidium excavatum*) that is observed associated with Ca-rhodochrosite laminae (Fig. 4.4; Sohlenius et al., 1996b). Most importantly, the dissolved Mn^{2+} and Fe^{2+} that had built up in the anoxic water column will be oxidised and settle to the sediment forming a solid Mn and Fe oxy-hydroxide lamina. Emerson et al. (1982) reported that for Saanich Inlet, British Columbia, the process of Mn-oxidation and sedimentation following deep water renewal was extremely rapid and was completed in just a few days.

3. Ca-rhodochrosite and Mn-sulphide formation

The Fe-Mn-oxide lamina will be stable until the available oxygen in the bottom waters is consumed and the redoxcline within the sediments starts to rise. As the redoxcline intercepts the Fe-Mn-oxide laminae, bacterially mediated reduction will rapidly start to reduce the mixed oxy-hydroxide lamina, which may contain as much as 20wt% Fe-oxide (Brügmann et al., 1998). As the Ca-rhodochrosite is always found to contain very little or no Fe (Chapter 4; Huckriede and Meischner, 1996) and Mn-sulphide can only form in an environment free of Fe (Böttcher and Huckriede, 1997), a mechanism must be invoked to separate Mn selectively from the mixed oxide lamina prior to formation of Mn-phases. Following the 1994 inflow event, Brügmann et al. (1997) found that a Fe-rich layer was found directly beneath a Ca-rhodochrosite lamina, and

indeed pyrite-rich laminae are commonly found at the base of rhodochrosite laminae (Chapter 4). Brügmann et al. (1997) suggest that this is possible due to more rapid settling of Fe-rich oxy-hydroxides, but it seems unlikely that there would be any substantial difference in the flocculation and settling velocity of Mn and Fe oxy-hydroxides, such that two separate laminae could be formed. It is more likely that redox processes relating the reduction of a single, mixed Fe-Mn-oxide lamina produce separate Mn-rich, Fe-free phases and Fe-rich phases.

Mn oxy-hydroxides are normally considered more readily reducible than Fe oxy-hydroxides (Froelich et al., 1979; Burdige, 1993), and Aller and Rude (1988) showed by experiment that in bacterially mediated reduction of mixed Mn-Fe-oxides, Mn-oxides, especially those of Mn^{4+}, are far more reducible than Fe-oxides. As the mixed oxy-hydroxide lamina starts to decompose, almost certainly Mn-oxides will be reduced first producing large amounts of Mn^{2+} but no Fe^{2+}. Reduced Fe^{2+} present in the pore-waters at depth will also be inhibited for upward diffusion by a displacement reaction with Mn-oxides producing Fe-oxides and Mn^{2+} (Postma and Appelo, 2000). Thus high Mn^{2+} concentrations will be produced in the presence of upward diffusing alkalinity, and ample Ca^{2+} from pore-waters and the water column. Ca-rhodochrosite can therefore most likely begin to form at the oxy-hydroxide lamina.

Mn^{2+} diffusing into the region of sulphidic conditions at depth will encounter free sulphide, and if concentrations of Mn are high enough, formation of Mn-sulphide becomes possible. Both alkalinity and sulphide will be consumed by the formation of mineral phases and the exact proportions of Mn-sulphide and Ca-rhodochrosite formation may be controlled by subtle variations in the production and upward diffusion rates of free sulphide and alkalinity. Mn-sulphide pseudomorphs occasionally show banded structures (Fig. 4.6), which may relate to alternating conditions in the formation micro-habitat, from Mn-sulphide to Ca-rhodochrosite formation. As Ca-rhodochrosite laminae are by far more common than Mn-sulphide laminae, in most cases formation of Ca-rhodochrosite must dominate. In very sulphidic conditions, however, such as interval A4 (Figs., 6.1-6.2), sulphide formation may dominate. Another effect of more sulphidic conditions may be that reduction of oxy-hydroxide laminae occurs more rapidly, producing greater *in situ* Mn^{2+} concentrations and more rapid Ca-rhodochrosite production. Under such conditions diffusion of Ca^{2+} to the region of Ca-rhodochrosite formation may be limiting, producing Ca-rhodochrosite with higher Mn/Ca ratios.

4. Fe-sulphide formation

As the available Mn-oxide is consumed the very high Mn^{2+} concentrations required for formation of Mn-rich phases will no longer be present. The remaining Fe-oxide portion of the mixed oxy-hydroxide lamina (and sub-lamina) may then start to be reduced producing *in situ* Fe^{2+} enrichments. In marine settings, Fe-carbonate cannot form in the presence of sulphate (Carman and Rahm, 1997; Glasby and Schulz, 1999), indeed, no Fe-carbonate phase has ever been observed in Gotland Deep sediments. Nevertheless, downward diffusing Fe^{2+} will encounter upward diffusing sulphide where formation of Fe-sulphide can occur, providing a possible origin for the Fe-sulphide lamina observed below many Ca-rhodochrosite laminae (Brügmann et al., 1997; Chapter 4). An alternative origin for these Fe-sulphides may come from the reduction of the Fe-Mn-oxides which may have built up below the sediment-water interface due to oxidation of pore-water Fe^{2+} and Mn^{2+}. It is unlikely that enough Mn-oxide will be present in the sub-lamina to generate sufficient Mn^{2+} concentrations such that Ca-rhodochrosite precipitates, however, in a Fe-limited setting such as the Gotland Deep (Boesen and Postma, 1988), any excess Fe^{2+} produced should be converted to Fe-sulphide.

5. Return to anoxic conditions

From thermodynamic (Sternbeck and Sohlenius, 1997) and experimental (Aller and Rude, 1988) perspectives, the whole process of reduction of the oxy-hydroxide laminae and production of authigenic phases is believed to occur very rapidly, perhaps over only a few days. After the oxy-hydroxide lamina has been consumed, there will be a relaxation back to anoxic conditions similar to the initial state before the oxic inflow. Under normal Gotland Deep pore water conditions Ca-rhodochrosite and Fe-sulphide are stable or meta-stable, but the normal pore-water conditions are under-saturated with respect to Mn-sulphide (Kulik et al., 2000; Heiser et al., 2001). Mn-sulphide is only preserved in a few rare organic-rich intervals, where more sulphidic pore-water conditions may occur, and elsewhere only Mn-sulphide pseudomorphs remain as evidence of earlier Mn-sulphide formation. Much of the Mn^{2+} initially sequestered as Mn-sulphide may therefore be released back into the anoxic pore waters and water column. Jakobsen and Postma (1989) showed that dissolution textures are common for Ca-rhodochrosite crystallites, which may relate to Mn-sulphide dissolution. Nevertheless all Ca-rhodochrosite crystallites contain significant

contamination by sulphur, which may represent Mn-sulphide protected from dissolution by inclusion in Ca-rhodochrosite crystallites.

6.6 CONCLUSIONS

A sediment fabric bioturbation index based on back-scattered electron images was able to define long-term anoxic-oxic intervals, representing periods of different short-term oxic renewal frequency. This was in good agreement with the inverse Al (wt%) record, showing that a simple measure of Al (wt%) could prove a useful tool in determining variance in benthic oxidation levels in this setting.

There is evidence for regular Mn-deposition as a direct result of oxic inflow events, as evidenced by Ca-rhodochrosite and Mn-sulphide laminae throughout a 50cm section of Early Littorina sediments. These laminae may provide a useful record of major Baltic Inflow events throughout the Holocene.

Mn-sulphide laminae were observed to occur in the single most anoxic interval A4 which has the lowest Al (wt%). The formation of Mn-sulphide seems to be the result of an inflow event occurring during a period of extremely sulphidic pore-water conditions, leading to the formation of Mn-sulphide at the expense of Ca-rhodochrosite. Variation in the initial benthic concentrations of free sulphide at the time of an inflow event may affect the amount of Mn-sulphide produced and the Mn/Ca ratio of Ca-rhodochrosite. Both will tend towards higher values under more sulphidic formation conditions.

Ca-rhodochrosite, Mn-sulphide, and Fe-sulphide may be produced following a major Baltic inflow event as a result of the progressive rapid microbial reduction of mixed Mn-Fe-oxy-hydroxide laminae.

Figure 6.1 Major element EDS line raster profiles of 51cm interval (165-216cm), showing profiles of Al (wt%), Mn/Al, Ca/Al, Mn/Ca and S/Al plotted against fabric bioturbation index. Heavy lines are 7pt. moving average. MnS laminae denoted by grey bands.

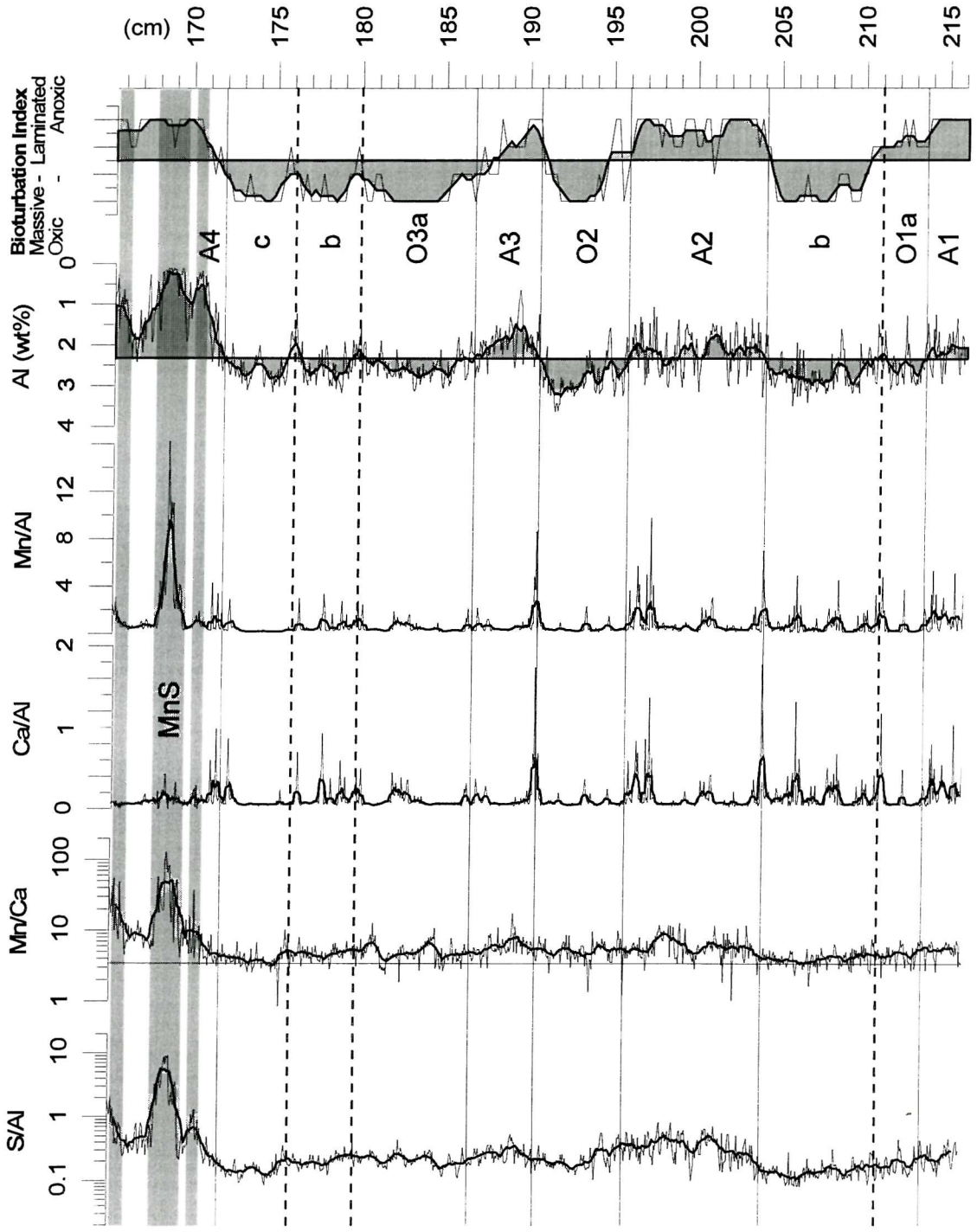

Figure 6.2 Major element EDS line raster profiles of 51cm interval (165-216cm), showing profiles of Al (wt%), Cl (wt%) S/Al, Fe/Al, and Si/Al plotted against fabric bioturbation index. Heavy lines are 7pt. moving average. MnS laminae denoted by grey bands.

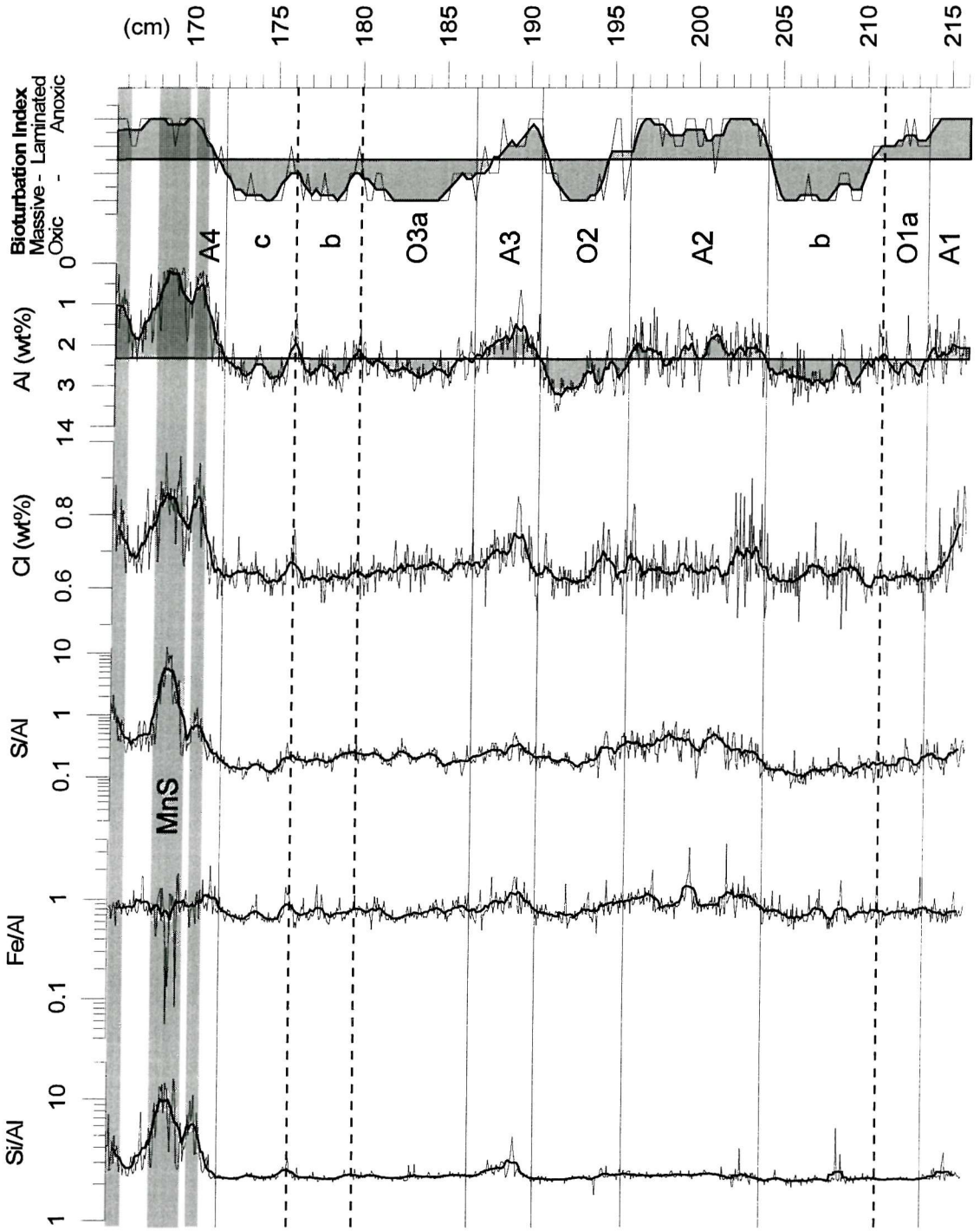

Figure 6.3 Back-scattered electron images of Mn-sulphide rich laminae.

A. Fossil leaf structure preserved by Mn-sulphide, shown in detail in B.

C. Diatom ooze with abundant Mn-sulphide crystallites typical of Mn-sulphide rich laminae, shown in detail in D.

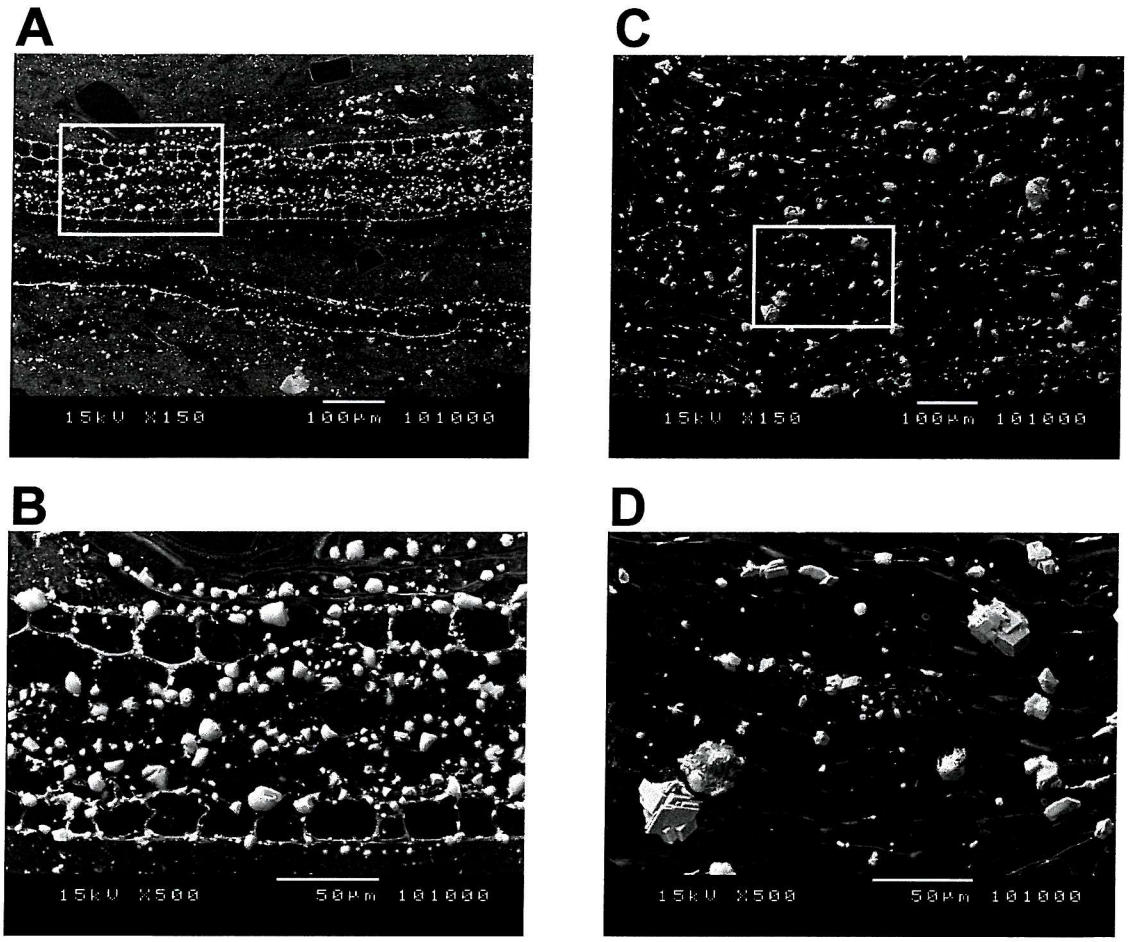

Figure 6.4 A. Cross-plot of Mn (wt%) v S (wt%) for whole interval 165-216cm.

B. Cross-plot of (wt%) v S (wt%) for Mn-sulphide rich interval A4, 165-172cm.

C. Cross-plot of Ca (wt%) v Mn (wt%) for whole interval 165-216cm.

D. Cross-plot of Mn/Ca v S/Al for whole interval 165-216cm.

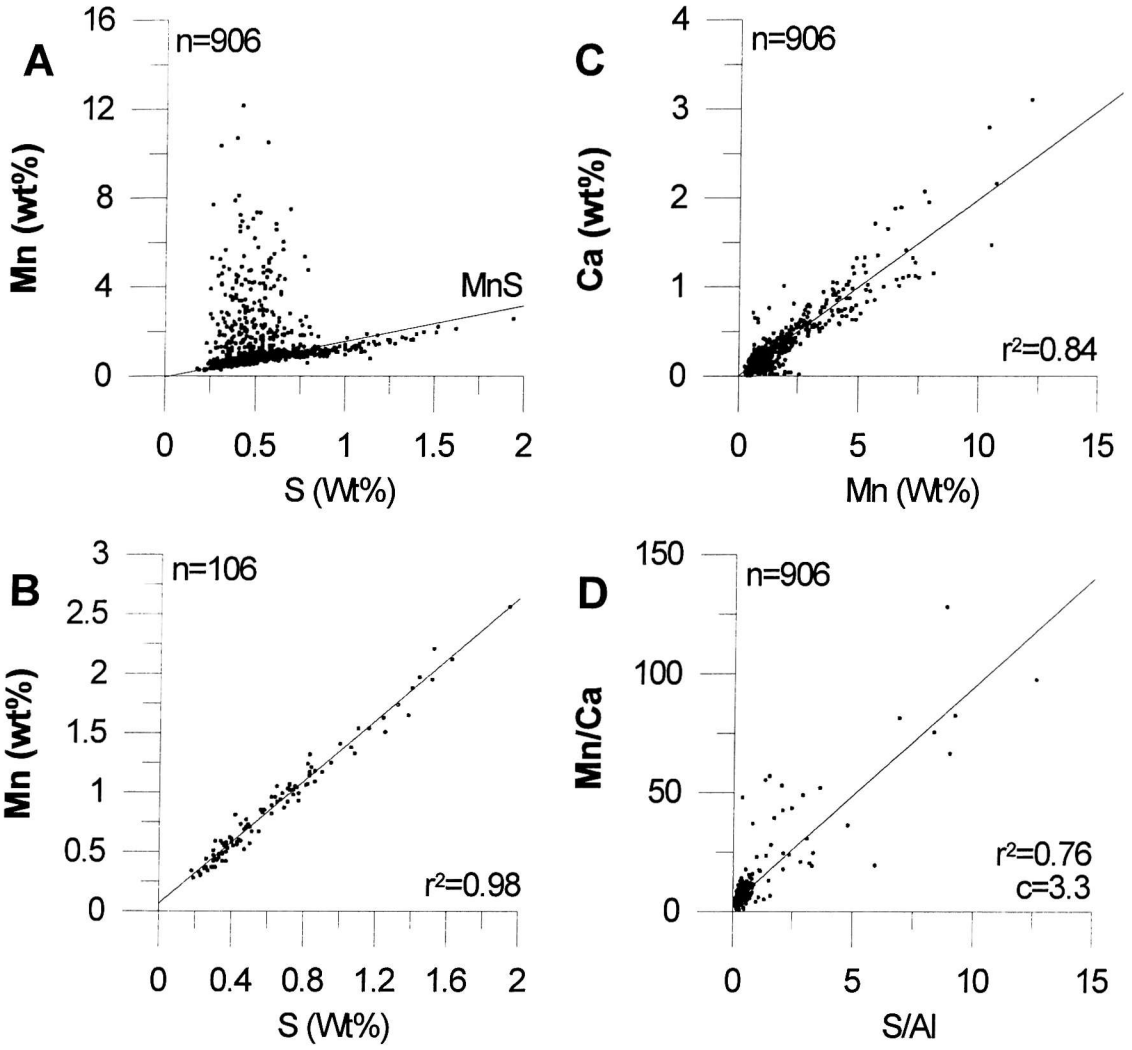

Figure 6.5 Conceptual model for Ca-rhodochrosite formation.

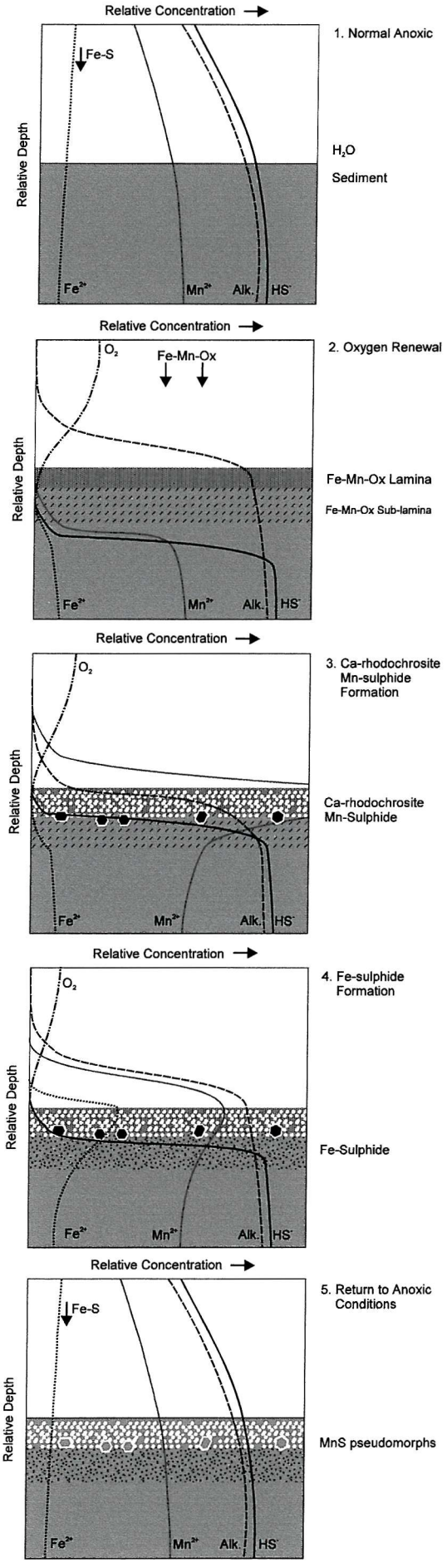

7 AN EARLY HOLOCENE GEOCHEMICAL RECORD OF SALINE INFLOW

With 5 figures

7.1 INTRODUCTION

Major Baltic inflows have occurred regularly throughout the 20th century (Matthäus, 1995) and have been regarded as causing the presence of Mn-enrichment in Gotland Deep sediments in the form of diagenetic Ca-rhodochrosite laminae in many studies (Huckriede and Meischner, 1996; Neumann et al., 1997; Sohlenius et al., 1996b; Sternbeck and Sohlenius, 1997; Chapters 4, 6). These saline inflow events are the product of North Atlantic atmospheric processes that culminate in overflows of highly saline water to the Baltic Sea at the Darss Sill. Saline inflows occur solely in winter, when westward wind systems, associated with blocking high pressure areas over the Baltic Sea, force water out of the Baltic Sea into the Danish straits causing a drop in Baltic Sea level (Matthäus and Schinke, 1994). This set-up period is then followed by the main inflow period itself, when a switch to eastward winds, associated with cyclonic activity, causes saline Belt Sea water to flow back into the Baltic Sea (Matthäus and Schinke, 1994). Schinke and Matthäus (1998) report that saline inflow occurrence is significantly greater in years with low surface runoff, which causes higher salinity in the Belt Sea, and overall lower cyclonic activity, which allows set-up periods to occur.

The North Atlantic Oscillation (NAO) was first described as variation in the zonal circulation by Walker and Bliss (1932), and is now commonly defined as the difference in the mean winter sea level pressure between the Azores High and the Icelandic Low (Hurrell, 1995). Variation in the NAO is reported to be the most important factor controlling the interannual climate variability observed in the North Atlantic region (Marshall et al., 1997). Conditions favourable for saline inflow are associated with negative NAO index winters when lower cyclonic activity, reduced precipitation, and more blocking highs occur in the Baltic region (Rogers, 1997; Nesterov, 1998). Börngen et al. (1990) reported that there is some coherence between records of saline inflow occurrence and the North Atlantic meridional circulation. The NAO has also been implicated in observed variations in the frequency of bottom water

renewal in Swedish fjords (Nordberg et al., 2000; Nordberg et al., in review) and the Baltic Sea itself (Hänninen and Vuorinen, 2000).

Sedimentary Mn-enrichments were used as a proxy for saline inflows occurring in the past 250yr by Neumann et al. (1997), however, no studies as yet have investigated this relationship in Early Holocene sediments predating historical records. Energy dispersive spectrometry (EDS) techniques, used under the SEM, produce records in which the Mn-enrichment due to individual Ca-rhodochrosite laminae can be delimited, representing higher resolution than previous studies. This Chapter, therefore, aims to assess the processes which affect Mn-enrichment in Early Holocene Gotland Deep sediments and to determine the suitability of Mn-enrichments as proxy records of interannual and decadal-scale variance in saline inflow events.

7.2 Mean sedimentation rate in core 20001-5

The position of core 20001-5 in the Gotland Deep is prone to erosion by bottom currents (Sivkov et al., 1998) and the upper part of core 20001-5 contains much evidence for erosion, in the form of truncated laminae on both macro (Fig. 2.2) and micro (SEM) scales. Thus it is likely that the apparent bulk sedimentation rate for this core of approximately 0.28mm/yr. (Christiansen and Kunzendorf, 1998; Chapter 3) is not representative of the actual pre-erosion sedimentation rate. These erosional features were, however, not observed in lower parts of core 20001-5, and this interval may, therefore, represent a coherent and continuous record of sedimentation. On this basis, a 51cm interval from 165-216cm was chosen for detailed study. Palaeomagnetic stratigraphy has not been able to produce a reliable age model for the post-Ancylus sediments in core 20001-5 (A. Roberts, pers. com.), and only one ^{14}C-AMS date has been obtained from this core (U. Struck, pers. com.). The varve thickness data are, therefore, the only available measurement of the annual sedimentation rate. The mean sedimentation rate measured from 160 varves in upper sections of the core (Chapter 3) is 0.7mm/yr., which is at the upper end of the normal range of sedimentation rates reported in Gotland Deep cores (0.23-0.75mm/yr. (Christiansen and Kunzendorf, 1998). Only 45 varves, however, were observed in the 165-216cm interval and indicate a mean sedimentation rate of 0.99mm/yr ±36% (±1σ), similar to the highest sedimentation rate ever reported for a consolidated Gotland Deep core of 1mm/yr. (Ignatius, 1958). This sedimentation rate would imply a time period of 501yr. ±36% for the whole 165-216cm interval. The main problem encountered when applying the

mean varve thickness as an estimate of sedimentation rate, is that varves are not continuous throughout the 165-216cm interval. In fact, only 9% of the interval is comprised of varves, therefore, the mean varve thickness may not be representative of these sediments as a whole. This chapter will, consequently, generally concentrate on the 165-216cm Mn-record in terms of depth-scale relationships, and the 0.99mm/yr. varve sedimentation rate will only be applied tentatively where appropriate.

7.3 VARIATION IN SEDIMENTARY Mn-ENRICHMENT FOLLOWING SALINE INFLOWS

If Mn-enrichment records (Fig. 7.1) are to be used as a proxy of inflow events, a linkage between deep water renewal (volume of water transported into the Baltic Sea) and the formation of sedimentary Mn-enrichment (wt% Mn) must be established. The observed chain of events leading to storage of Mn in the sediments, therefore, will now be considered in detail to provide the theoretical context in which this proxy can be used.

1. Accumulation of Mn in the Gotland Deep

Mixing of oxygenated waters across the primary Baltic halocline is so restricted (Matthäus, 1990) that renewal by saline inflow is considered to be the only process in which significant changes in Gotland Deep redox conditions can occur (Matthäus, 1995). Between inflow events, the basin will quickly stagnate as the supply of organic matter is high (Sohlenius, 1996) and oxygen is rapidly consumed in the deep waters (Matthäus and Lass, 1995; Nehring et al., 1995a; Nehring et al., 1995b; Matthäus et al., 1996). This typically produces sulphidic bottom waters where Mn^{2+} can start to accumulate (Manheim, 1961). The main source of Mn for the Gotland Deep is as Mn-oxides in terrigenous sediments which are supplied by resuspension of coastal and shallow water sediments during storms (Gingele and Leipe, 1997). Thus the primary control on the amount of Mn accumulated in anoxic Gotland Deep bottom waters may simply be related to atmospheric conditions (storm activity) during each stagnation period.

There is, however, a second possible source of Mn on the upper slopes of the Gotland Deep above the redoxcline. Mn-oxide builds up on the upper slopes of anoxic basins (Manheim, 1961) due to the recycling of dissolved Mn^{2+} and solid Mn-oxide at the redoxcline (Boström and Ingri, 1988). Following the 1994 saline inflow event, the redoxcline depth was elevated to 130m, more than 20m above the former redoxcline depth (Matthäus, 1995). Under such circumstances, Mn-oxide deposited on the rim of

the Gotland Deep may be prone to remobilization through contact with sulphidic waters. Mn could eventually be cycled, via oxidation by the inflowing waters, to the Mn-oxide lamina in the deepest parts of the Gotland Deep, until all sulphidic waters are oxidised. This mechanism could alleviate the problem of Mn supply, where Ca-rhodochrosite laminae are observed in successive varves (Chapters 3, 4). The formation of Ca-rhodochrosite requires large amounts of free Mn^{2+}, and it is not known if enough Mn can be supplied to the deep basin by normal sedimentation in one year or less. If the Mn-oxide on the slopes, however, can be harvested by uplifted anoxic waters during inflow events, then formation of Ca-rhodochrosite laminae after successive inflows becomes possible.

2. Initial titration of Mn^{2+} (and HS^-, Fe^{2+} etc...) by oxygen

Hypothetically if the reduced Mn-pool in the Gotland Deep was infinite, then the amount of Mn sequestered in the sediments might relate directly to the amount of oxygen introduced during a saline inflow event. The 1993-94 saline inflow marked the end of the longest stagnation period (11yr.) ever recorded in the Gotland Deep (Matthäus and Lass, 1995). Prior to this saline inflow, the bottom waters also contained the highest concentration of HS^-, Mn^{2+} and Fe^{2+} ever recorded (Brügmann et al., 1997; Heiser et al., 2001). The magnitude of the 1993-94 saline inflow was in the moderate range of Matthäus and Franck's (1992) intensity index, and due to mixing in the Baltic's deep basins, the oxygen content of the saline inflow was significantly reduced (Matthäus and Lass, 1995) before entering the Gotland Deep. Nevertheless, in May 1994, Gotland Deep bottom waters were oxic (Nehring et al., 1995a), and all of the free Mn^{2+} and Fe^{2+} was oxidised and deposited as a Mn-Fe-oxide lamina (Brügmann et al., 1997). Evidence from the 1993-94 inflow event, therefore, seems to indicate that the supply of oxygen by saline inflows is usually sufficient, even after long stagnation periods, to oxidise all the reduced species accumulated in Gotland Deep bottom waters. One apparent problem of this effect (in terms of Mn-enrichment) is the case where two inflows occur so close together that no anoxic stagnation period occurs; because all the Mn will already be oxidised, the second inflow event cannot then be recorded by a separate Mn-enrichment.

3. Sequestering of the Mn-oxide lamina

Mn-oxides are not stable under reducing conditions (Froelich et al., 1979) and, therefore, to produce sedimentary Mn-enrichments, the conversion to early diagenetic minerals, such as Ca-rhodochrosite (Huckriede and Meischner, 1996; Sohlenius, 1996;

Neumann et al., 1997; Sternbeck and Sohlenius, 1997; Chapter 4) and/or Mn-sulphide (Böttcher and Huckriede, 1997; Chapter 6), must occur. The precise proportions of Ca-rhodochrosite and Mn-sulphide formed may vary according to the pore-water redox conditions at time of formation (Chapter 6). Lepland and Stevens (1998) argue convincingly that some Mn^{2+} will be lost at this stage by simply diffusing away into the bottom waters. The overall proportion of the Mn-oxide lamina converted to diagenetic minerals is most likely to depend on the rate of Mn-reduction. More rapid Mn-reduction will cause greater *in situ* Mn^{2+} concentrations and more rapid diagenetic mineral formation and will limit the amount of Mn^{2+} which is lost back into the bottom waters. Again this is likely to be determined by the precise pore-water redox conditions at the time of mineral formation.

4. Dissolution and resuspension of Mn-lamina

Once sedimentary Mn-enrichments are sequestered they are then subject to burial and the possibility of later diagenesis at depth that may lead to the dissolution of early formed Mn-rich minerals. Gotland Deep pore-waters are often reported to be over-saturated with respect to Ca-rhodochrosite and under-saturated with respect to Mn-sulphide (Kulik et al., 2000; Heiser et al., 2001). Any early formed Mn-sulphide will, therefore, be expected to dissociate into the pore-waters, and not be retained in the record. Jakobsen and Postma (1989) have observed that Ca-rhodochrosite crystallites are heavily affected by dissolution textures. This indicates that, at depth, there is also some dissolution of Ca-rhodochrosite.

Gotland Deep sediments are also prone to erosion caused by the inflow events themselves (Sviridov et al., 1997; Emeis et al., 1998; Sivkov et al., 1998). Heiser et al. (2001) reported the effects of erosion on the sedimentary Mn-enrichment that formed at shallow depths within Gotland Deep sediments following the 1993/94 inflow event. Two small inflows that subsequently occurred in 1994/95 resulted in the resuspension of the shallow sediments containing this Mn-enrichment. No trace of the Mn-enrichment observed in 1994, remained after the 1994/95 inflow events (Heiser et al., 2001), and presumably the Mn itself was re-dispersed back into the Gotland Deep bottom waters. Thus, even if Mn-enrichments are sequestered in Gotland Deep sediments, subsequent inflow events can result in the resuspension of Mn and removal of evidence of these events from the record.

One other factor that must be borne in mind is the possible loss by laboratory handling. Suess (1979) report (also reported in Chapter 6) that Mn-sulphide crystals

can be affected by oxidation when sampled. Also in Chapter 2 a whole sediment slab is reported to have no Ca-rhodochrosite laminae present after exposure to oxygen in transit. Every effort must be made to minimise the exposure of Gotland Deep sediment samples to oxygen in order to limit this problem.

7.4 Conceptual treatment of Mn-record: Analysis of a series of events

The many factors affecting the sedimentary Mn-enrichment are summarised in Figure 7.2. The only two independent parameters listed, atmospheric conditions and organic-carbon supply, may both even be influenced by a single external forcing mechanism, such as the NAO (Hänninen and Vuorinen, 2000). A simple relationship between a few forcing mechanisms and the Mn-record might therefore be expected; however, there are many different processes (outlined in Section 7.3) that affect the amount of Mn (wt%) actually measured in the sediments. It is unknown if these processes will result in a systematic or predictable variation in Mn-enrichment being preserved, and the observed variation in individual Mn-enrichments may be effectively independent from any actual variation in saline inflows. Nevertheless, the presence of Mn-rich laminae does record the occurrence of past saline inflow events, and to help determine the presence of long-term order, the Mn-record (Fig. 7.1) will now be interpreted in terms of a series of events.

Converting the record to a binary signal (0,1,0,...,n) based on the presence or absence of a Ca-rhodochrosite lamina will disregard the effects of Mn (wt%) variation and allow analysis of the distribution of Mn-enrichments as a series of discrete events (Cox and Lewis, 1966). The Mn-record was re-sampled every millimetre by two different techniques to produce the two slightly different 'barcode' type records as shown in Figure 7.1. The Mn-event (EDS) record was produced by subtracting the mean Mn (wt%) level from the Mn (wt%) record and designating each millimetre with a remaining positive enrichment as a Mn-event (1); negative enrichments were designated as not Mn-events (0). The second Mn-event (Visual Log) record was produced by considering each millimetre in x5 BSE images and designating those with visible Ca-rhodochrosite laminae as Mn-events (1) and those without as not Mn-events (0). The section where Mn-sulphide laminae occur (165-171cm; see Chapter 6, Fig. 6.1) was excluded from these records as Mn-sulphide laminae are much thicker (~3mm) than Ca-rhodochrosite laminae (~0.5mm), and therefore, may relate to more than one saline inflow event.

The EDS and Visual Log records (Fig. 7.1), ideally should be identical but in fact differences occur due to the different way each type of log samples Mn-events. EDS logs will tend to over-estimate the total number of events due to Ca-rhodochrosite laminae straddling sample intervals being recorded as two separate events. The Visual Log, in contrast, will tend to under-estimate the number of events where Ca-rhodochrosite crystallites occur as indistinct concentrations and not as clearly visible laminae. Figure 7.3a shows a cumulative log of Mn-events, where each step represents a single Mn-event, and the slope of the graph is related to the rate of Mn-event occurrence. The EDS log records 134 Mn-events, as compared to 115 Mn-events which occur in the Visual Log. The actual number of Mn-events is, therefore, likely to be between the EDS and Visual Log estimates. Figure 7.3b shows that there is actually little difference between the EDS and Visual logs in terms of the distribution of Mn-events occurring in successive 20mm intervals. Both Figures 7.3a and 7.3b clearly show a long-term trend in the data with relatively fewer events occurring towards the top of the 171-219cm interval.

The Al (wt%) record (Fig. 7.1) can be used in this setting as a proxy of the mean redox state of specific intervals (Chapter 6). Each 20mm interval can, therefore, be defined in terms of either an oxic or anoxic mean redox state (Fig. 7.3b), allowing the examination of the distribution of Mn-events in terms of the mean redox state in the Gotland Deep, as shown in Table 7.1. In both EDS and Visual Logs there are slightly more (~11-20%) Mn-events/cm recorded in the anoxic intervals. This is most likely to be due to variations in prevailing Gotland Deep conditions when individual inflow events occur. In anoxic intervals the prevailing conditions will actually more often be sulphidic with bottom water enriched in Mn^{2+}, the vital precursor for sedimentary Mn-enrichment following saline inflow events. The opposite will occur in oxic intervals, thus the number of saline inflows will be more completely recorded in anoxic intervals and less so in oxic intervals. The difference in numbers of Mn-events/cm that occur, between anoxic and oxic intervals, is actually quite small (~11-20%). This indicates that relatively small differences in the frequency of bottom water renewal has led to the quite large changes observed in the Al (wt%) record and subsequent classification of intervals as either anoxic or oxic.

Table 7.1 Distribution of Mn-events between oxic-anoxic intervals

	No. Mn-events	Total depth of intervals (cm)	Mn-events/cm	Range (as % of total)
EDS Log				
Oxic Int.	75	28	2.7	
Anoxic Int.	59	18	3.3	
Total Int.	*134*	*46*	*2.9*	20.6%
Visual Log				
Oxic Int.	68	28	2.4	
Anoxic Int.	49	18	2.7	
Total Int.	*117*	*46*	*2.5*	11.5%

The distribution of the intervals between successive Mn-events (i.e. the recurrence interval) will now be considered in comparison to a random distribution of events. Figure 7.4 summarises the distribution of Mn-event recurrence intervals, logged by both EDS and Visual techniques, as probability density (i.e., the percentage of recurrences at any given interval). Also plotted on Figure 7.4 is a probability distribution given by the Poisson function. The Poisson function was derived by the French mathematician S. D. Poisson in 1837, and was first applied in the statistical description of deaths caused by horse kicking in the Prussian army (Bortkiewicz, 1898). The Poisson distribution has since been applied to describe many other random processes, such as faults in machines, number of telephone calls received at exchanges, and radioactive decay (Cox and Lewis, 1966). For events that occur randomly and independently, with a number of successes (x), with a constant rate (μ) per unit time or region, the probability distribution $f(x)$, is given by the equation:

$$f(x) = p(x; \mu) = \frac{e^{-\mu}\mu^{x}}{x!}$$

($x = 0, 1, 2 \ldots n.$)

The Poisson distribution provides a good approximation of Binomial distribution (and Normal distribution at high μ) but has the advantage of being set by just one external variable μ (Kreyszic, 1999). In the specific case of Mn-event recurrence intervals considered here; if x = the actual recurrence interval, then, μ = average number of successes in a given time or region, i.e. the mean recurrence interval. The mean recurrence interval for Mn-events is 3.43mm (EDS) and 3.93mm (Visual) respectively, therefore, an intermediate μ-value of 3.75mm has been used to set the

Poisson distribution in figure 7.4. Error limits have also been added at 2σ above and below the ideal Poisson distribution. Derivation of 2σ is from observations of 100 random data sets of 120 events produced by a Poisson function embedded in an internet Java-applet (www.math.uah.edu/stat/applets /PoissonExperiment.html). If the Mn-event recurrence interval probability density distribution were also observed to be within these 2σ error limits, then it would be very likely that the occurrence of Mn-events is simply a random stochastic process, with no long range-order. It is quite clear from figure 7.4, however, that this is not the case. Both Mn-event distributions are highly skewed towards short recurrence intervals with over 0.6 (60%) of the recurrence intervals at 1 or 2mm. There are conversely low numbers of recurrence intervals of between 3-8mm, but also a long tail of recurrence intervals over 10mm. The Mn-event records are, therefore, characterised by groups of successive Mn-events interrupted by longer intervals without Mn-events. It is also likely that this distribution of Mn-events (and the inflow-events that cause them) is, therefore, not random and indeed may be forced by an external mechanism, producing periods of high Mn-events and interim periods of low Mn-event occurrence.

7.5 SPECTRAL ANALYSIS

As discussed above (Sections 7.3, 7.4), interannual-scale variability in Gotland Deep conditions can lead to large variations in the amount of Mn sequestered in the sediments on millimetre scales. Despite this variation there is possibly longer term order with respect to the presence or absence of groups of inflows. Sufficient smoothing of the raw Mn wt% data (Fig. 7.1) will, therefore, produce a depth averaged record in which groups of saline inflows should lead to broad intervals of Mn-enrichment, suitable for analysis in terms of centimetre (possibly decadal) scale variance. In preparation for spectral analysis, a smoothed Mn-series (Fig. 7.1) was produced by application of a 5mm gaussian K-smooth filter.

The linear trend, and the data mean, were removed from the Mn-series prior to spectral analysis, and two different techniques were then applied to the smoothed Mn-series in order to produce spectral estimates, using AnalySeries v1.2 (Paillard et al., 1996). Figure 7.5a shows a spectral estimate produced by the Blackman-Tukey Method (BTM), (first introduced by Blackman and Tukey (1958) and developed by Jenkins and Watts (1968)) by application 362 lags of a single Tukey window. Figure 7.5b shows a spectral estimate produced by the Multi-Taper Method (MTM)

(Thomson, 1982), by application of 3 eigentapers. Background spectra were added to both spectral estimates by applying a second order polynomial quadratic least squares fit to estimate the background 'red noise' spectrum found in many natural time series (Thomson, 1990; Ghil and Yiou, 1995). Upper significance intervals were then added to the polynomial fits by application of a chi-squared distribution with 2 (BTM) and 6 (MTM) degrees of freedom (DOF) respectively (Dettinger et al. (1995) states that the number of DOF = 2K; where K = number of spectral windows/tapers applied). BTM produces spectral estimates with moderate spectral resolution and significance intervals. Whereas MTM, produces better spectral resolution, but with poorer significance intervals. Whilst Thomson (1990) argues that only the MTM produces reliable spectral estimates, Paillard et al. (1996) advises a common-sense approach where spectra from more than one technique are considered when interpreting significant frequencies. The BTM spectrum shows a significant peak at 34.8mm, which is resolved as two sub-peaks at 33 and 35.5mm in the MTM spectrum. There is therefore very likely to be at least one significant periodicity present between 33-35.5mm in the smoothed Mn-records.

Although the sedimentation rate in this 51cm section is not well constrained (see Section 7.2), applying the range of measured varve thickness for this section (0.99mm ±36%) does indicate a plausible range for this discrete decadal periodicity, placing it somewhere between 25-55yr. Neumann et al. (1997) also have reported sedimentary Mn-enrichments in a well dated (^{210}Pb) Gotland Deep core with maxima every 30-60yr. that are consistent with historical clusters of saline inflows. Although there seems to be some consistency between the Mn-records discussed in this study and in Neumann et al. (1997), this consistency does not extend to the periodicities reported for the instrumental NAO index records, which have weak (not statistically significant) frequency maxima at 2, 7-8, 20 and 70yrs (Hurrell and Van Loon, 1997), quite neatly missing out the periodicity range indicated by both Mn-records. Thus there appears to be an inconsistency between the reports that indicate that North Atlantic climate variations (NAO) ultimately drive the variations in saline inflow to the Baltic Sea (see Section 7.1) and the records of Mn-events from Gotland Deep sediments which record these same inflows events.

This inconsistency is a common problem for all reported proxy-records of North Atlantic climate. Spectral analysis of ice accumulation rates in Greenland ice-cores have revealed a prominent 90yr. periodicity (Appenzeller et al., 1998), and comparison

of ice-core, tree-ring, and instrumental records of NAO (see Schmutz et al. (2000) and references therein) have shown that proxy-records have only modest reconstructive skill at decadal time scales, and no skill at interannual time scales. Schmutz et al. (2000) do indicate, however, that in future studies a combination of different proxy-records, such as that reported by Cullen et al. (2001), could significantly improve reconstructive ability. Further Mn-records from well-dated Holocene Gotland Deep cores are, therefore, now needed to confirm the natural variation present in Gotland Deep sediments, both to improve understanding of Baltic Sea processes and to provide much needed records which may aid in the understanding North Atlantic climate processes.

7.6 Conclusions

Many complex factors affect the variability in Mn-enrichment following individual saline inflows, and these are likely to produce effectively random variations in Mn-enrichments on interannual time scales. Mn-records are, therefore, unlikely to provide valid records of short-term variation in saline inflows.

On decadal time scales, however, suitably smoothed Mn-enrichment time series do provide a good record of the longer-term variance in saline inflows, in terms of the presence or absence of groups of inflows.

A significant spectral peak has been observed in the smoothed Mn-record at between 33-35.5mm, which may relate to periodic variance in saline inflow occurrence during the Early Holocene on multi-decadal time scales.

Figure 7.1 Mn-Records. EDS line raster profiles of 51cm interval (165-216cm), showing profiles of Al (wt%), and Mn (wt%), plotted with binary 'barcode' logs of Mn-events from both EDS and visual logging techniques, and a smoothed Mn (wt%) record. Heavy line is 7pt. moving average of Al (wt%).

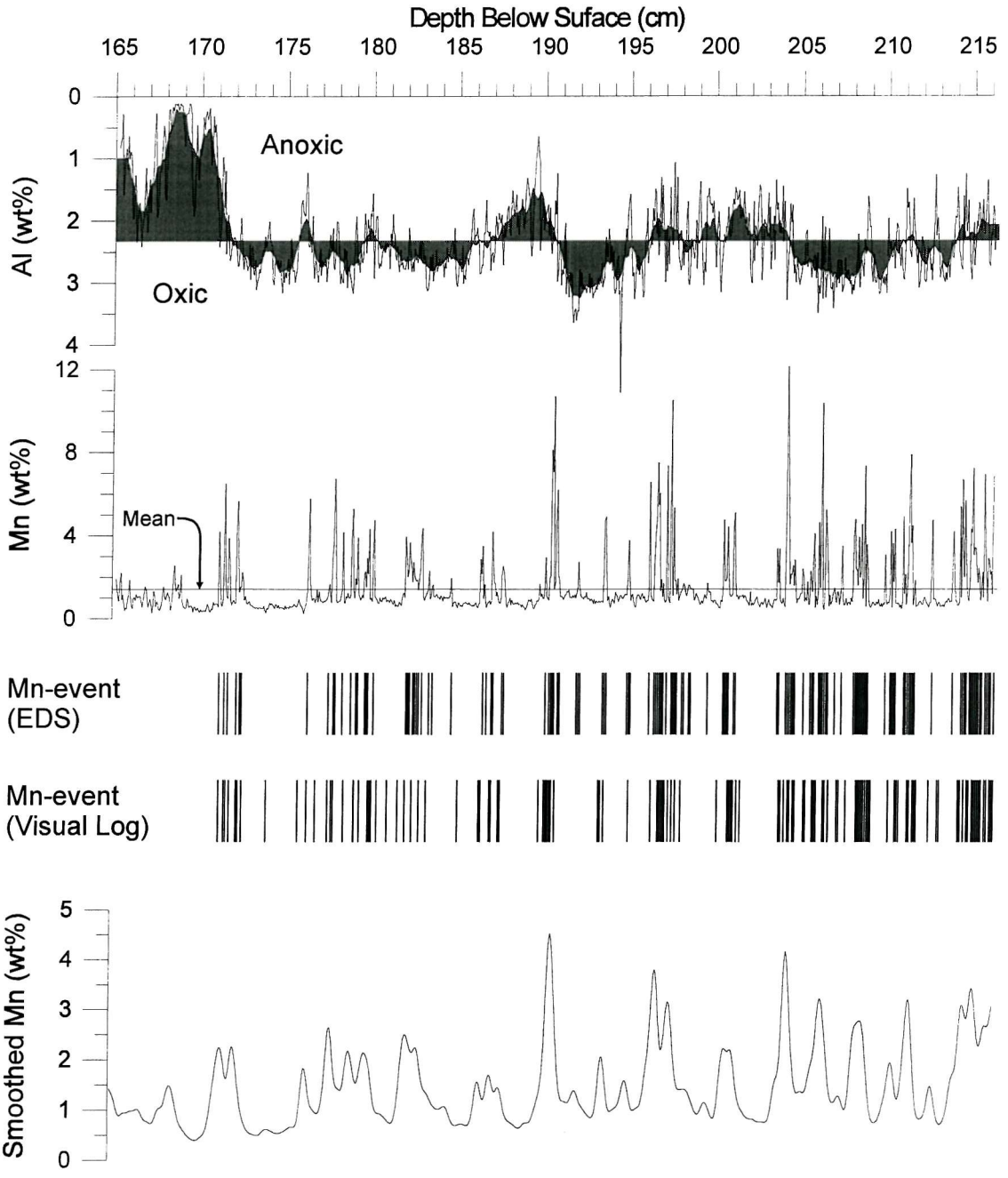

Figure 7.2 Factors affecting Mn-enrichment in Gotland Deep sediments.

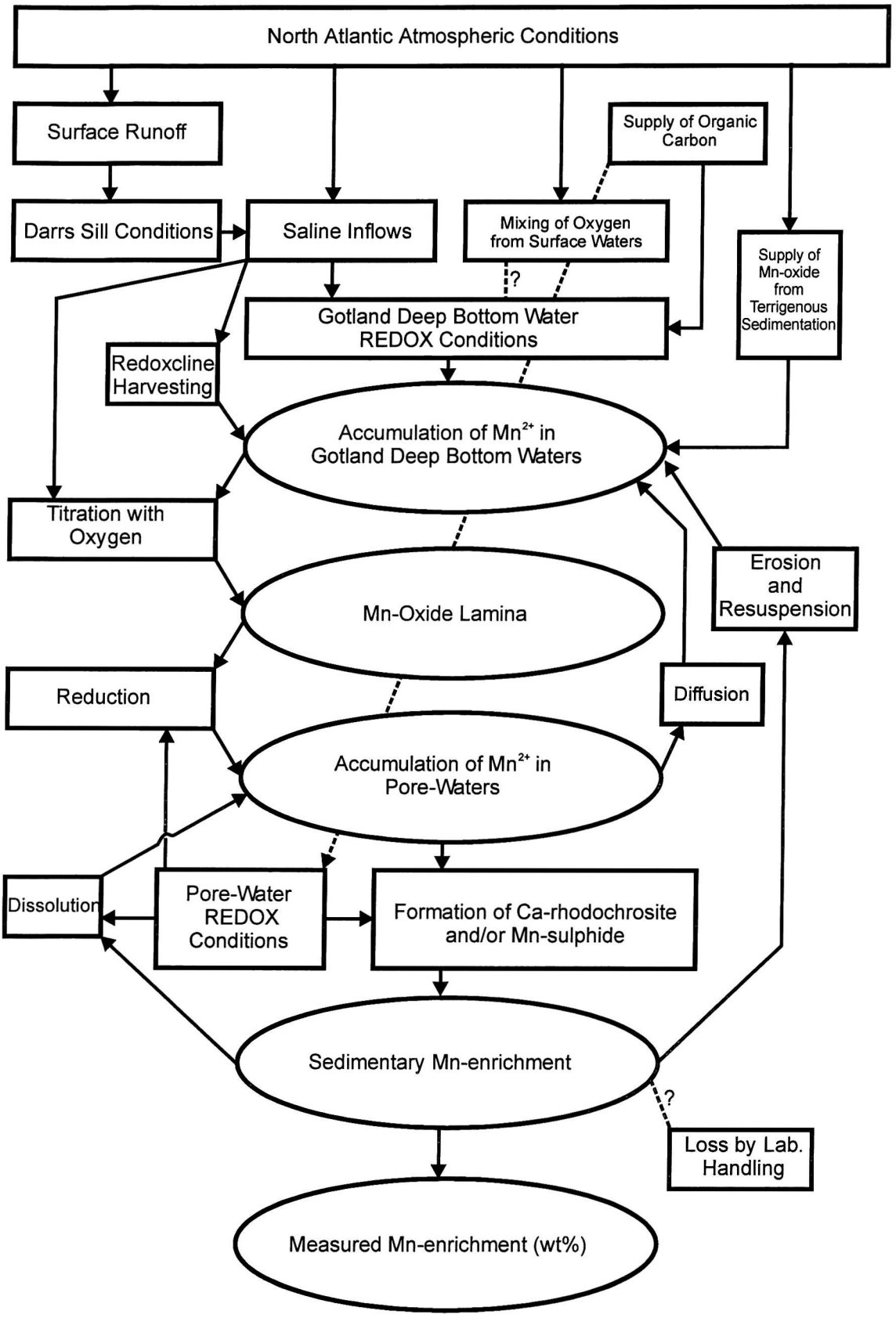

Figure 7.3 A. Plot of cumulative Mn-events with depth.

B. Bar chart of number of Mn-events in successive 20mm intervals.

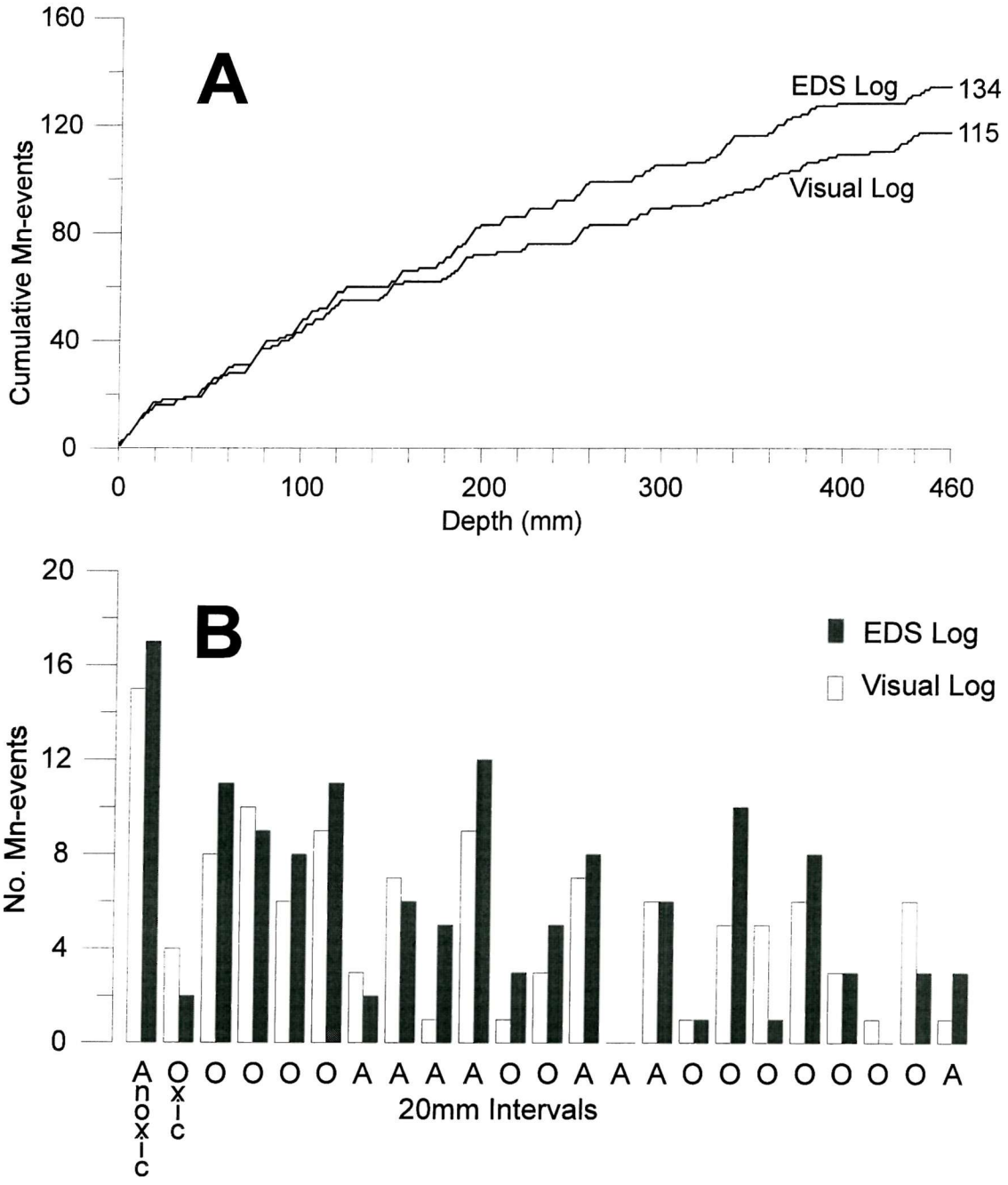

Figure 7.4 Bar chart of probability density of Mn-event recurrence intervals, with a line plot of a Poisson distribution (mean=3.75, $\pm 2\sigma$ error limits).

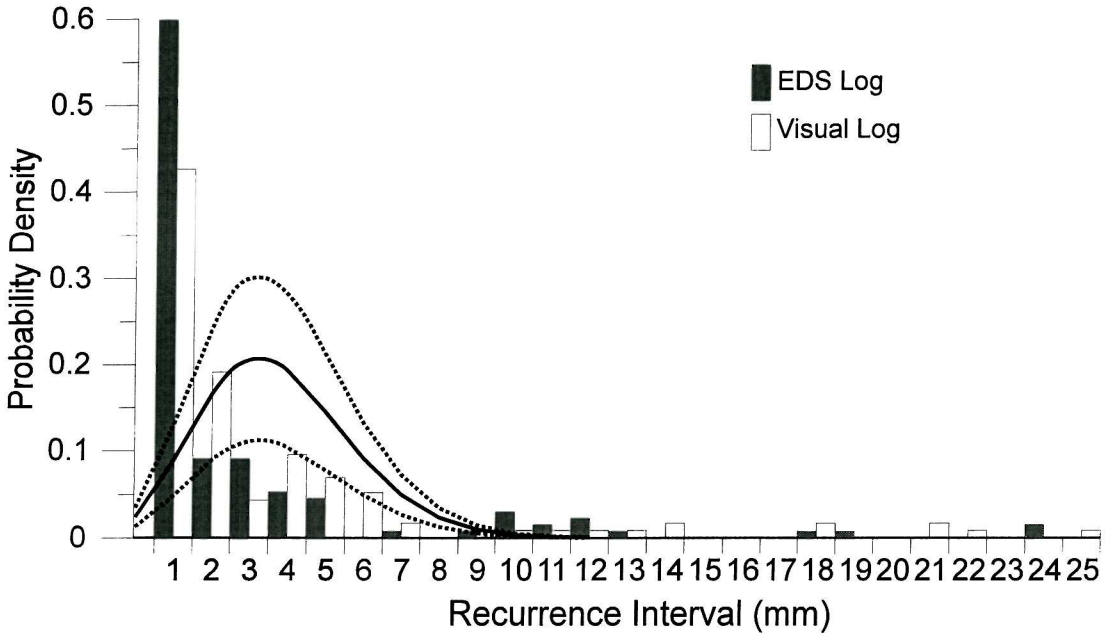

Figure 7.5 A. Spectral estimate of smoothed Mn (wt%) series from Blackman-Tukey Method. B. Spectral estimate of smoothed Mn (wt%) series from Multi-Taper Method.

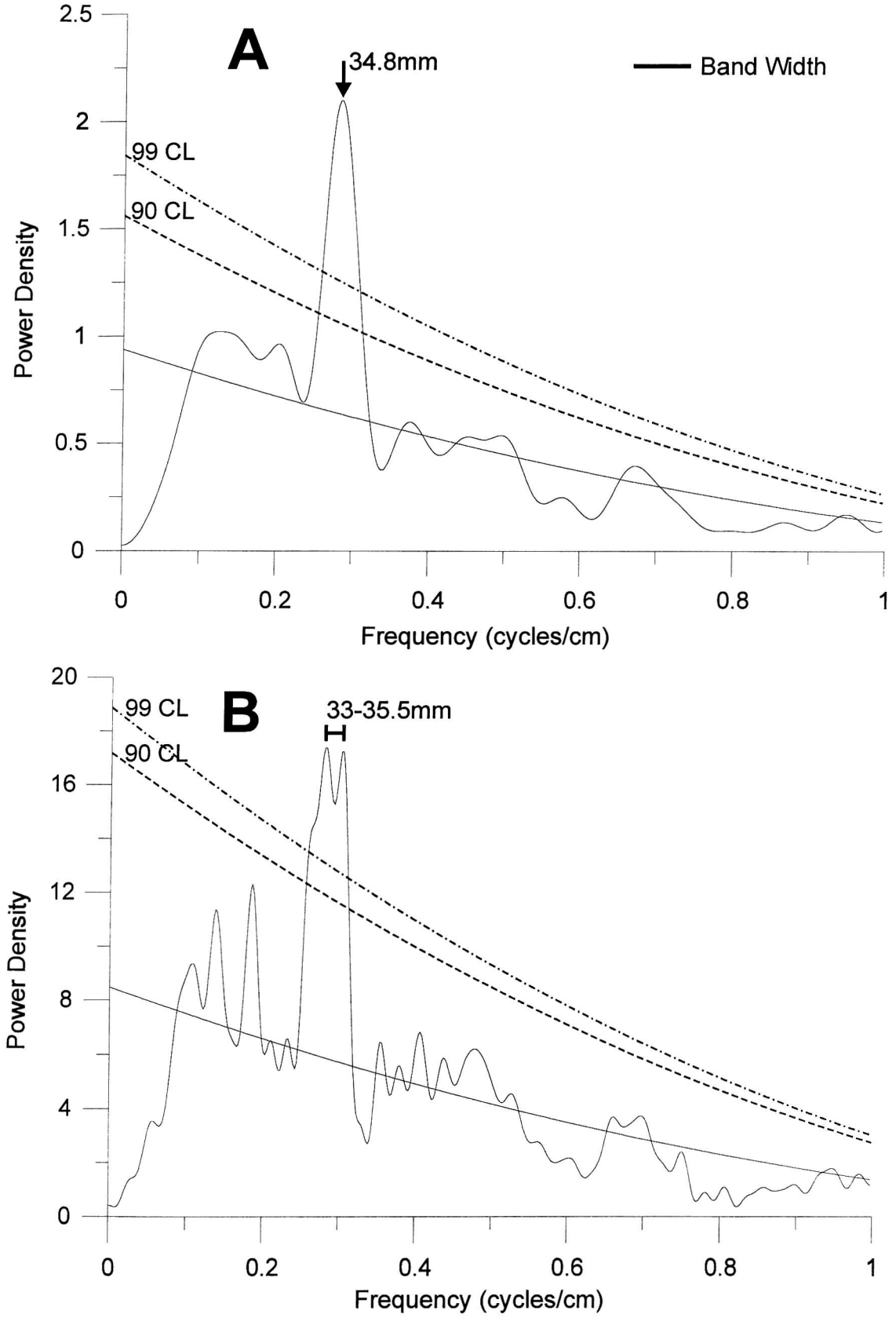

8 SUMMARY

Scanning electron microscope and geochemical techniques have been used to examine lamina-scale fabric and geochemical relationships recorded in sediments from the Gotland Deep and relate these to ocean-climate processes in the Baltic Sea. In Chapter 3 the nature and origin of biogenic and lithogenic laminae were discussed. Several different diatomaceous and clay-rich laminae were distinguished and were then related to annual lamina sequences, i.e. varves. Although the development and/or preservation of identifiable varves in Gotland Deep sediments is patchy and much of the record is taken up by intervals of indistinctly laminated or massive sediment, the identification of varves is a useful tool in delimiting seasonal depositional events, such as the diagenetic Ca-rhodochrosite laminae which occur regularly in varves only as a winter/early spring deposit.

This relationship was further explored in Chapter 4 where energy dispersive microanalysis combined with back-scatter electron imagery enabled the placement of Ca-rhodochrosite laminae within an annual cycle of deposition, showing that Ca-rhodochrosite deposition is a rapid phenomenon occurring on seasonal time scales. The occurrence of Ca-rhodochrosite is in close agreement with the seasonality of flushing of the Gotland Deep as recorded in instrumental records. This finding provides supporting evidence for the assumed direct causal link between saline inflow events and Ca-rhodochrosite deposition. The occurrence of Ca-rhodochrosite overgrowth solely on benthic, and not on planktonic foraminifera tests, also strongly implies a link between oxic bottom water conditions and Ca-rhodochrosite formation.

The relatively common occurrence of Hexagonal γ Mn-sulphide pseudomorphs is reported for the first time, and suggests that highly sulphidic conditions favouring the early formation of Mn-sulphide were reached much more commonly during Ca-rhodochrosite formation in the Gotland deep than previously reported.

In Chapter 5 ICP-MS techniques were used, in addition to SEM techniques, to elucidate the distribution of trace metals on the laminae scale. Although no systematic enrichment was observed, many trace metals are seen to be enriched within both Ca-rhodochrosite and Fe-rich laminae, implying that trace metals are affected by seasonal scale redox effects operating in the Gotland Deep. The main mechanism for

sequestering trace metals to the sediments seems to be by being scavenged onto particulate Fe-sulphide and Mn-oxides.

The role of sulphide in the sequestering of Mn in Gotland Deep sediments was discussed in detail in Chapter 6. Mn-sulphide lamina were observed to occur in a single anoxic interval A4, which has a high sulphur content and is presumed to be organic-carbon rich. The formation of Mn-sulphide seems to be the result of an inflow event occurring during a period of extremely sulphidic pore-water conditions, leading to the formation of Mn-sulphide at the expense of Ca-rhodochrosite. Variation in the initial benthic concentrations of free sulphide at the time of an inflow event may control the amount of Mn-sulphide produced and the Mn/Ca ratio of Ca-rhodochrosite; both will tend towards higher values under more sulphidic conditions. This regular Mn-deposition is inferred to be a direct result of periodic oxic saline inflow events. Ca-rhodochrosite, Mn-sulphide, and Fe-sulphide may be produced following a major Baltic inflow event as a result of the progressive rapid microbial reduction of mixed Mn-Fe-oxy-hydroxide laminae.

A sediment fabric bioturbation index based on back-scattered electron images was able to define anoxic-oxic intervals, representing periods of different oxic renewal frequency. This was in good agreement with the inverse Al (wt%) record, showing that a simple measure of Al (wt%) could prove a useful tool in determining variance in benthic oxidation levels in this setting.

Chapter 7 contains a critical assessment of the use of Mn-enrichment in Gotland Deep sediments as a proxy of saline inflow throughout the Holocene. Many complex factors affect the variability in Mn-enrichment following individual saline inflows, and these are likely to produce effectively random variations in Mn-enrichments on interannual time scales. Mn-records are, therefore, unlikely to provide valid records of interannual variation in saline inflows. On decadal time scales, however, suitably smoothed Mn-enrichment time series do provide a good record of the longer-term variance in saline inflows, in terms of the presence or absence of groups of inflows. A significant spectral peak has been observed in the smoothed Mn spectra, which may relate to periodic variance in saline inflow occurrence during the Early Holocene on multi-decadal time scales.

9 DIRECTIONS FOR FURTHER WORK

9.1 SALINE INFLOW RECORD FROM GOTLAND DEEP CORE 201302-5.

Sub-millimetre scale EDS analysis of the Littorina sediments from the Gotland Deep has been shown in this study to produce valuable records of both environmental change and saline inflows. Neumann et al (1997) successfully demonstrated that sedimentary Mn-enrichments could be used as a proxy record for periods of high saline inflows. This record has, however, yet to be systematically extended back into the Holocene beyond the realm of historical data (except for the ~50cm section of Core 20001 studied in Chapter 7). To do this, one needs to find suitable Gotland Deep core material. The relatively short (2.29m) Littorina section in core 20001 shows ample evidence of erosion and is therefore unlikely to yield the coherent continuous record that is required.

In contrast, core 201302-5 has over 6.82m of Littorina sediments and shows little evidence of macro-scale erosion. Although earlier pre-Littorina sediments are not evident, core 201301-5 may contain a relatively continuous record of Littorina sedimentation. Geochemical (SEM-EDS, XRF, TOC, ICP-AES) analyses of core 201302 at a sufficiently high resolution (<1cm) could, therefore, potentially provide a record of decadal and centennial scale variations in saline inflow that may be related to unknown variations in NAO patterns. In order to make use of these geochemical records, a reliable age model for the core will have to be established. Varve thickness records and correlation of lithological and geophysical parameters could all be used, but a range of ^{14}C-AMS dates would be the ideal tool for constraining any age model. Core 201302-5 is available for use and is in cold storage at the Institute of Baltic Sea Research at Warnemuende, Germany.

9.2 OTHER HOLOCENE SEDIMENTS

Organic-rich laminated Holocene sediments, containing abundant Ca-rhodochrosite laminae, are also found in the Landsort Deep, Baltic Sea. These sediments provide a very useful comparison to Gotland Deep sediments. Lepland and Stevens (1998) argue that Ca-rhodochrosite formation in the Landsort Deep is not related to the periodic flushing of the Baltic Sea due to the long inflow path from the Darrs Sill. Matthäus et al. (1999), however, has reported historical records of

simultaneous bottom water temperature variations in all Baltic Sea deep basins. These temperature variations are due to the balance of slow mixing of cold surface waters to the deep basin, and the rapid renewal by saline inflow of warmer waters (Matthäus, 1990). It is therefore likely that a similar Ca-rhodochrosite formation mechanism occurs in both the Landsort and Gotland Deep. Dr. Ian Croudace (University of Southampton) has already produced XRF data for Landsort Deep core GC-56, sampling at 1cm resolution over the whole core. Richard Pearce (University of Southampton) has also performed a pilot micro-fabric study of selected intervals of this core. If SEM and EDS study can be used to verify that Ca-rhodochrosite formation in the Landsort deep is similar to the Gotland Deep, then there is an opportunity to use these existing XRF data as a proxy record of saline inflow to the Landsort Deep.

Saanich Inlet, British Columbia, is also affected by periodic seasonal flushing (Anderson and Devol, 1973). During the periodic flushing of Saanich Inlet, bottom water Mn^{2+} levels are rapidly depleted (Emerson et al., 1982), and particulate Mn-oxide is reported to be deposited at the sediment water interface, but Ca-rhodochrosite laminae have hitherto not been observed in Saanich Inlet sediments. Calvert et al. (2001), however, have recently reported concurrent sedimentary enrichments in both Mn and inorganic carbon which they relate to the presence of Mn-carbonate. Thus it is possible that a Ca-rhodochrosite formation process similar to the Baltic Sea is in operation in Saanich Inlet. Again detailed SEM and EDS based studies could be used to confirm the presence of Ca-rhodochrosite, and to validate use of Mn as a proxy of past oxic inflows in this setting. A large number of polished thin sections from varved Saanich Inlet sediments are currently held at the University of Southampton, which may be suitable for just such a study.

A recent report (Bahk et al., 2001) of laminated Early Holocene sediments from the Sea of Japan containing Mn-carbonate laminae, has sited redox overturns caused by intermittent flushing with oxic bottom waters as a possible formation mechanism for these laminae. It is possible that further SEM study may reveal that Mn-carbonate formation in the Sea of Japan is also analogous to processes occurring in Baltic Sea.

9.3 Ancient Mn-rich shales

There are many ancient examples of laminated manganiferous shales, which may have an analogous depositional environment to the modern Baltic Sea, including:

1. Jurassic Toarcian shales of Central Europe (Jenkyns, 1988; Jenkyns et al., 1991)
2. Lower Carboniferous Manganese ores of Central Europe (Huckriede and Meischner, 1996).
3. Proterozoic (Xu et al., 1990) to Triassic (Fan et al., 1992) super-gene manganese deposits of Southern China.
4. Neoproterozoic stratiform manganese formations of Central India (Gutzmer and Beukes, 1998).
5. Paleozoic-Mesozoic shales and cherts of Central Japan (Sugisaki et al., 1991).
6. Franciscan Complex laminated chert-hosted manganese deposits of Northern California (Hein and Koski, 1987).
7. Jurassic stratiform manganese carbonate ores of Central Mexico (Okita et al., 1988; Maynard et al., 1990).
8. Cambrian manganese-rich shales of the Harlech Dome, North Wales (Matley and Wilson, 1946).

Sub-millimetre scale sediment fabric and geochemical analysis of these shales could potentially be used to assess the similarity of relic micro-fabric and elemental associations in these sediments to those found in Holocene sediments. It is possible that a common Ca-rhodochrosite formation mechanism may be delineated in the depositional environments of some these ancient sediments.

REFERENCES

Alldredge, A.L. and Gotschalk, C.C., 1989. Direct observation of the mass flocculation of diatom blooms: characteristics, settling velocities and formation of diatom aggregates. Deep Sea Res., 36: 159-171.

Aller, R.C., 1980. Diagenetic processes near the sediment-water interface of Long Island Sound, II, Fe and Mn. Ad. Geophys., 22: 351-415.

Aller, R.C. and Rude, P.D., 1988. Complete oxidation of solid phase sulfides by manganese and bacteria in anoxic marine sediments. Geochim. Cosmochim. Acta, 52: 751-765.

Anderson, J.J. and Devol, A.H., 1973. Deep water renewal in Saanich Inlet, an intermittently anoxic basin. Est. Coast. Mar. Sci., 1: 1-10.

Appenzeller, C., Stocker, T.F. and Anklin, m., 1998. North Atlantic Oscillation dynamics recorded in Greenland ice cores. Science, 282: 446-449.

Bahk, J.J., Chough, S.K., Jeong, K.S. and Han, S.J., 2001. Sedimentary records of paleoenvironmental changes during the last deglaciation in the Ulleung Interplain Gap, East Sea (Sea of Japan). Glob. Planet. Change, 28: 241-253.

Baron, G. and Debyser, J., 1957. Sur la presence dans les vases organiques de la mer Baltique du sulfure manganeux b hexagonal. C. R. Acad. Sci. Paris, 245: 1148-1150.

Behl, R.J. and Kennett, J.P., 1996. Brief interstadial events in the Santa Barbara basin, NE Pacific, during the past 60 kyr. Nature, 379(6562): 243-246.

Bergstrom, S. and Carlsson, B., 1994. River runoff to the Baltic Sea, 1959-1990. Ambio, 23(4-5): 280-287.

Berner, R.A., 1981. A New Geochemical Classification Of Sedimentary Environments. J. Sediment. Petrol., 51(2): 0359-0365.

Berner, R.A. and Raiswell, R., 1983. Burial of organic carbon and pyrite sulfur in sediments over Phanerozoic time: a new theory. Geochim. Cosmochim. Acta, 47: 855-862.

Bishop, J.K.B., 1988. The barite-opal-organic carbon association in oceanic particulate matter. Nature, 332: 341-343.

Björck, S., 1995. A review of the history of the Baltic Sea. Quat. Int., 27: 19-40.

Björck, S., Kromer, B., Johnsen, S., Bennike, O., Hammarlund, D., Lemdahl, G., Possnert, G., Rasmussen, T.L., Wohlfarth, B., Hammer, C.U. and Spurk, M., 1996. Atmospheric deglacial records around the North Atlantic. Science, 274: 1155-1160.

Blackman, R.B. and Tukey, J.W., 1958. The measurement of power spectra from the point of view of communication engineering. Dover Publications, New York, 190 pp.

Boesen, C. and Postma, D., 1988. Pyrite formation in anoxic environments of the Baltic. Am. J. Sci., 288: 575-603.

Börngen, M., Hupfer, P. and Olberg, M., 1990. Occurrence and absence of strong salt influxes into the Baltic Sea. Beitr. Meereskd., 61: 11-19.

Bortkiewicz, L.v., 1898. Das Gesetz Der Kleinen Zahlen. Teubner, Leipzig.

Boström, K. and Ingri, J., 1988. Origin of iron-manganese-rich suspended matter in the Landsort Deep, NW Baltic Sea. Mar. Chem., 24: 93-98.

Böttcher, M., 1995. The formation of rhodochrosite-smithsonite ($MnCO_3$-$ZnCO_3$) solid-solutions at 5°C. Mineral. Mag., 59: 481-488.

Böttcher, M.E., 1998. Manganese(II) partitioning during experimental precipitation of rhodochrosite-calcite solid solutions from aqueous solutions. Mar. Chem., 62: 287-297.

Böttcher, M.E. and Huckriede, H., 1997. First occurrence and stable isotope composition of authigenic g-MnS in the central Gotland Deep (Baltic Sea). Mar. Geol., 137: 201-205.

Böttcher, M.E. and Lepland, A., 2000. Biogeochemistry of sulfur in a sediment core from the west-central Baltic Sea: Evidence from stable isotopes and pyrite textures. J. Marine Syst., 25: 299-312.

Brodie, I. and Kemp, A.E.S., 1994. Variation in Biogenic and Detrital Fluxes and Formation of Laminae in Late Quaternary Sediments from the Peruvian Coastal Upwelling Zone. Mar. Geol., 116(3-4): 385-398.

Brodniewicz, I., 1965. Recent and some Holocene foraminifera of the Southern Baltic Sea. Acta Palaeontol. Pol., 10(2): 131-233.

Brügmann, L., Halberg, R., Larsson, C. and Löffler, A., 1997. Changing redox conditions in the Baltic Sea deep basins: Impacts of concentration and speciation of trace metals. Ambio, 26(2): 107-112.

Brügmann, L., Halberg, R., Larsson, C. and Löffler, A., 1998. Trace metal speciation in sea and pore water of the Gotland Deep, Baltic Sea, 1994. Appl. Geochem., 13(359-368).

Brügmann, L. and Lange, D., 1990. Metal distribution in sediments of the Baltic Sea. Limnol. (Berlin), 20(1): 15-28.

Bull, D. and Kemp, A.E.S., 1995. Composition and origins of laminae in late Quaternary and Holocene sediments from the Santa Barbara basin. In: J.P. Kennett and J.G. Baldauf (Editors), Proc. ODP, Sci. Res., 146: 77-87.

Burdige, D.J., 1993. The biogeochemistry of manganese and iron reduction in marine sediments. Earth Sci. Rev., 35: 249-284.

Burdige, D.J. and Gieskes, J.M., 1983. A pore water/solid solution diagenetic model for manganese in marine sediments. Am. J. Sci., 283: 29-47.

Calvert, S.E. and Pedersen, T.F., 1993. Geochemistry of recent oxic and anoxic marine sediments: implications for the geological record. Mar. Geol., 113: 67-88.

Calvert, S.E. and Pedersen, T.F., 1996. Sedimentary geochemistry of manganese: implications for the environment of formation of manganiferous black shales. Econ. Geol., 91: 36-47.

Calvert, S.E., Pedersen, T.F. and Karlin, R.E., 2001. Geochemical and isotopic evidence for post-glacial palaeoceanographic changes in Saanich Inlet, British Columbia. Mar. Geol., 174: 287-305.

Calvert, S.E. and Price, N.B., 1970. Composition of manganese nodules and manganese carbonates from Loch Fyne, Scotland. Contr. Mineral. and Petrol., 29: 215-233.

Carman, R. and Rahm, L., 1997. Early diagenesis and chemical characteristics of interstitial water and sediments in the deep deposition bottoms of the Baltic proper. J. Sea Res., 37(1-2): 25-47.

Christiansen, C. and Kunzendorf, H., 1998. Datings and sedimentation rate estimations during GOBEX - a summary. In: K.C. Emeis and U. Struck (Editors), Gotland Deep Experiment (GOBEX). Status report on investigations concerning benthic processes, sediment formation and accumulation. Meereswiss. Ber., Warnemünde, **34**, pp. 55-76.

Cox, D.R. and Lewis, P.A.W., 1966. The statistical analysis of series of events. Methuen's monographs on applied probability and statistics. Meuthuen & Co. Ltd., London.

Cullen, H.M., D'Arrigo, D., Cook, E.R. and Mann, M.E., 2001. Multiproxy reconstructions of the North Atlantic Oscillation. Paleoceanogr., 16(1): 27-39.

Danyushevskaya, A.I., 1992. Geochemistry of organic matter in bottom sediments of the Baltic Sea. Oceanol., 32: 469-475.

Dean, J.M., Kemp, A.E.S., Bull, D., Pike, J., Patterson, G. and Zolitschka, B., 1999. Taking varves to bits: Scanning electron microscopy in the study of laminated sediments and varves. J. Paleolimnol., 22(2): 121-136.

Debyser, J., 1961. Contribution à l'étude géochimique des vases marine. Soc. Editions Technip, Paris, 249 pp.

Dettinger, M.D., Ghil, M., Strong, C.M., Weibel, W. and Yiou, P., 1995. Software expedites singular-spectrum analysis of noisy time series. Eos Trans. Am. Geophys. Union, 76(2): 12,14, 21.

Dymond, J., Suess, E. and Lyle, M., 1992. Barium in deep-sea sediment: a geochemical proxy for paleoproductivity. paleoceanogr., 7: 163-181.

Dyrssen, D. and Kremling, K., 1990. Increasing hydrogen sulphide concentration and trace metal behaviour in the anoxic Baltic waters. Mar. Chem., 30: 193-204.

Emeis, K.C., Neumann, T., Endler, R., Struck, U., Kunzendorf, H. and Christiansen, C., 1998. Geochemical records of sediments in the Eastern Gotland Basin-products of sediment dynamics in a not-so-stagnant basin? Appl. Geochem., 13: 349-358.

Emeis, K.C. and Struck, U., 1998. Gotland Deep Experiment (GOBEX). Status report on investigations concerning benthic processes, sediment formation and accumulation. Meereswiss. Ber., Warnemünde, 34.

Emelyanov, E.M. and Gritsenko, V.A., 1999. On the role of near-bottom currents in the formation of bottom sediments in the Gotland Basin, the Baltic Sea. Oceanol., 39(5): 709-718.

Emerson, S., Kalhorn, S., Jacobs, L., Tebo, B.M., Nealson, K.H. and Rosson, R.A., 1982. Environmental oxidation rate of manganese(II): Bacterial Catalysis. Geochim. Cosmochim. Acta, 46(1073-1079).

Fan, D., Lui, T. and Ye, J., 1992. The process of formation of manganese carbonate deposits hosted in black shale series. Econ. Geol., 87: 65-67.

Froelich, P.N., Klinkhammer, G.P., Bender, M.L., Luedtke, N.A., Heath, G.R., Cullen, D., Dauphin, P., Hammond, D., Hartman, B. and Maynard, V., 1979. Early

Oxidation of Organic Matter in Pelagic Sediments of the Eastern Equatorial Atlantic: Suboxic Diagenesis. Geochim. Cosmochim. Acta, 43: 1075-1090.

Ghil, M. and Yiou, P., 1995. Spectral methods: What they can and cannot do for climatic times series. In: D.L.T. Anderson and J. Willebrand (Editors), Decadal Climate Variability. Spinger, Berlin.

Gingele, F.X. and Leipe, T., 1997. Clay mineral assemblages in the western Baltic Sea: recent distribution and relation to sedimentary units. Mar. Geol., 140: 97-115.

Glasby, G.P. and Schulz, H.D., 1999. E_H, pH diagrams for Mn, Fe, Co, Ni, Cu, and As under seawater conditions: Application of two new types of E_H, pH diagrams to the study of specific problems in marine geochemistry. Aquatic Geochemistry, 5: 227-248.

Grimm, K.A., 1992. High-resolution imaging of laminated diatomaceous sediments and their paleoceanographic significance (Quaternary, ODP Site 798, Japan Sea). Proc. ODP Sci. Res., 128(547-557).

Grimm, K.A., Lange, C.B. and Gill, A.S., 1996. Biological forcing of hemipelagic sedimentary laminae: Evidence from ODP Site 893, Santa Barbara Basin, California. Journal of Sedimentary Research, 66(3): 613-624.

Guillard, R.R.L. and Kilham, P., 1978. Ecology of marine planktonic diatoms. In: D. Werner (Editor), The Biology of Diatoms. Univ. Calif. Press, Berkely, Bot. Mon., pp. 470-483.

Gutzmer, J. and Beukes, N.J., 1998. The manganese formation of the Neoproterozoic Penganga Group, India-revision of an enigma. Econ. Geol., 93: 1091-1102.

Hallfors, G., Niemi, A., Ackefors, H. and Lassig, J., 1981. Biological oceanography. In: A. Viopio (Editor), The Baltic Sea. Elsevier Sci. Publ. Co., Amsterdam.

Hänninen, J. and Vuorinen, I., 2000. Climate factors in the Atlantic control of the oceanographic and ecological changes in the Baltic Sea. Limnol. Oceanogr., 45(3): 703-710.

Hein, J.R. and Koski, R.A., 1987. Bacterially mediated diagenetic origin for chert-hosted manganese deposits in the Franciscan Complex, California Coast Ranges. Geology, 15: 722-726.

Heiser, U., Neumann, T., Scholten, J. and Stüben, D., 2001. Recycling of manganese from anoxic sediments in stagnant deeps by seawater inflow: A study of surface sediments from the Gotland Basin, Baltic Sea. Mar. Geol., 177: 151-166.

Heiskanen, A.S. and Kononen, K., 1994. Sedimentation of Vernal and Late Summer Phytoplankton Communities in the Coastal Baltic Sea. Archiv Fur Hydrobiologie, 131(2): 175-198.

Huckriede, H. and Meischner, D., 1996. Origin and environment of manganese-rich sediments within black shale deeps. Geochim. Cosmochim. Acta, 60(1399-1413.).

Hurrell, J.W., 1995. Decadal trends in the North Atlantic Oscillation: regional temperatures and precipitation. Science, 269: 676-679.

Ignatius, H., 1958. On the rate of sedimentation in the Baltic Sea. Bull. Comm. Geol. Finl., 180: 135-145.

Ignatius, H., Axberg, S., Niemistö, L. and Winterhalter, B., 1981. Quaternary geology of the Baltic Sea. In: A. Voipio (Editor), The Baltic Sea. Elsevier Sci. Publ. Co., Amsterdam, pp. 54-104.

Jakobsen, R. and Postma, D., 1989. Formation and solid solution behaviour of Ca-rhodochrosites in marine muds of the Baltic Deeps. Geochim. Cosmochim. Acta, 53: 2639-2648.

Jansson, B.O., 1989. The Baltic Sea. In: L. Rey and V. Alexander (Editors), 13-15 May 1995. Proceedings of the sixth conference of the Comite Arctique International.

Jenkins, G.M. and Watts, D.G., 1968. Spectral analysis and its applications. Holden-Day, San Francisco.

Jenkyns, H.C., 1988. The Early Toarcian (Jurassic) anoxic event: stratigraphic, sedimentary and geochemical evidence. Am. J. Sci., 288: 101-151.

Jenkyns, H.C., Géczy, B. and Marshall, J.D., 1991. Jurassic manganese carbonates of central Europe and the early Toarcian anoxic event. J. Geol., 99(2): 137-149.

Jonsson, P., 1992. Large-scale changes of contaminants in Baltic Sea sediments during the twentieth century. Acta Uni. Uppsala, 407: 52 pp.

Kabailiené, M., 1995. The Baltic Ice Lake and Yoldia Sea Stages, Based on Data from Diatom analysis in the Central, South-Eastern and Eastern Baltic. Quat. Int., 27: 69-72.

Kemp, A.E.S., 1996. Palaeoclimatology and palaeoceanography from laminated sediments. Geol. Soc. Spec. Pupl., 116.

Kemp, A.E.S. and Baldauf, J.G., 1993. Vast Neogene Laminated Diatom Mat Deposits from the Eastern Equatorial Pacific-Ocean. Nature, 362(6416): 141-144.

Kemp, A.E.S., Pearce, R.B., Koizumi, I., Pike, J. and Rance, S.J., 1999. The role of mat-forming diatoms in the formation of Mediterranean sapropels. Nature, 398(6722): 57-61.

Kemp, A.E.S., Pearce, R.B., Pike, J. and Marshall, J.E.A., 1998. Microfabric and microcompositional studies of Pliocene and Quaternary sapropels from the eastern Mediterranean. Proc. ODP Sci. Res., 160: 349-364.

Kemp, A.E.S., Pike, J., Pearce, R.B. and Lange, C.B., 2000. The "Fall dump" - a new perspective on the role of a "shade flora" in the annual cycle of diatom production and export flux. Deep-Sea Res. Part II-Top. Stud. Oceanogr., 47(9-11): 2129-2154.

Kremling, K., 1983. The behaviour of Zn, Cd, Cu, Ni, Co, Fe, and Mn in anoxic Baltic waters. Mar. Chem., 13: 87-108.

Kreyszic, E., 1999. Advanced engineering mathematics. John Wiley & Son Inc., New York.

Krinsley, D.H., Pye, K., Boggs, S. and Tovey, N.K., 1998. Backscattered scanning electron microscopy and image analysis of sediments and sedimentary rocks. Cambridge University Press, Cambridge, 193 pp.

Kulik, D.A., Kersten, M., Heiser, U. and Neumann, T., 2000. Application of Gibbs energy minimization to model early- diagenetic solid-solution aqueous-solution equilibria involving authigenic rhodochrosites in anoxic Baltic Sea sediments. Aquatic Geochemistry, 6(2): 147-199.

Kullenberg, G., 1981. Physical oceanography. In: A. Viopio (Editor), The Baltic Sea. Elsevier Sci. Publ. Co., Amsterdam.

Lepland, A. and Stevens, R.L., 1998. Manganese authigenesis in the Landsort Deep, Baltic Sea. Mar. Geol., 151: 1-25.

Manheim, F.T., 1961. A geochemical profile in the Baltic Sea. Geochim. Cosmochim. Acta, 25: 52-70.

Margalef, R., 1967. The food web in the pelagic environment. Helg. Wiss. Meeresunters., 15: 548-559.

Marshall, J., Kushnir, Y., Battisti, D., Chang, P., Hurrell, J.W., McCartney, M. and Visbeck, M., 1997. Atlantic Climate Variability, CLIVAR, (http://geoid.mit.edu/accp/avehtml.html).

Matley, C. and Wilson, T.S., 1946. The Harlech Dome north of the Barmouth Esturary. Quart. J. Geol. Soc. London, 102: 1-40.

Matthäus, W., 1990. Mixing across the primary Baltic halocline. Beitr. Meereskd., 61: 21-31.

Matthäus, W., 1995. Natural variability and human impacts reflected in long-term changes in the Baltic deep water conditions - A brief review. Dtsch. Hydrogr. Z., 47: 47-65.

Matthäus, W. and Franck, H., 1992. Characteristics of major Baltic inflows-a statistical analysis. Cont. Shelf Res., 12: 1375-1400.

Matthäus, W. and Lass, H.U., 1995. The Recent Salt Inflow into the Baltic Sea. Journal of Physical Oceanography, 25(2): 280-286.

Matthäus, W., Nausch, G., Lass, H.U., Nagel, K. and Siegel, H., 1999. The Baltic Sea in 1998 - Characteristic features of the current stagnation period, nutrient conditions in the surface layer and exceptionally high deep water temperatures. Deutsche Hydrographische Zeitschrift, 51: 67-84.

Matthäus, W., Nehring, D., Lass, H.U., Nausch, G., Nagel, K. and Siegel, H., 1996. The Baltic Sea in 1996 - Continuation of stagnation and decreasing phosphate concentrations. Dtsch. Hydrogr. Z., 48(2): 161-174.

Matthäus, W. and Schinke, H., 1994. Mean atmospheric circulation patterns associated with major Baltic inflows. Dtsch. Hydrogr. Z., 46: 321-399.

Maynard, J.B., Okita, P.M., May, E.D. and Martinez-Vera, A., 1990. Palaeogeographic setting of late Jurassic manganese mineralization in the Molango district, Mexico. Int. Assoc. Sedimentol. Spec. Publ., 11: 17-30.

McQuoid, M.R. and Hobson, L.A., 1997. A 91-year record of seasonal and interannual variability of diatoms from laminated sediments in Saanich Inlet, British Columbia. Journal of Plankton Research, 19(2): 173-194.

Morad, S. and Al-aasm, I.S., 1997. Conditions of rhodochrosite-nodule formation in Neogene-Pleistocene deep-sea sediments: evidence from O, C and Sr isotopes. Sediment. Geol., 114(295-304).

Mörner, N.A., 1995. The Baltic Ice Lake-Yoldia Sea transition. Quat. Int., 27: 95 - 98.

Morris, R.J., Niemi, A., Niemistö, L. and Poutanen, E.L., 1988. Sedimentary record of seasonal production and geochemical fluxes in a nearshore coastal embayment in the northern Baltic Sea. Finnish Mar. Res., 256: 77-94.

Mucci, A., 1988. Manganese uptake during calcite precipitation from seawater: Conditions leading to the formation of a pseudokutnahorite. Geochim. Cosmochim. Acta, 52: 1859-1868.

Nehring, D., Matthaus, W., Lass, H.U., Nausch, G. and Nagel, K., 1995a. The Baltic Sea 1994 - Consequences of the hot summer and inflow events. Dtsch. Hydrogr. Z., 47(2): 131-144.

Nehring, D., Matthaus, W., Lass, H.U., Nausch, G. and Nagel, K., 1995b. The Baltic Sea in 1995 - Beginning of a new stagnation period in its central deep waters and decreasing nutrient load in its surface layer. Dtsch. Hydrogr. Z., 47(4): 319-327.

Nesterov, E.S., 1998. Characteristic features of ocean and atmosphere in different phases of the North Atlantic Oscillation. Russ. Meteorol. Hydrol., 8: 58-65.

Neumann, T., Christiansen, C., Clasen, S., Emeis, K.C. and Kunzendorf, H., 1997. Geochemical records of salt-water inflows into the deeps of the Baltic Sea. Cont. Shelf Res., 17: 95-115.

Nordberg, K., Gustafsson, M., Filipsson, H.L., Harland, R. and Roos, P., in review. Climate and hydrography variations and marine benthic hypoxia in Koljö Fjord, Sweden. submitted to Marine Geology.

Nordberg, K., Gustafsson, M. and Krantz, A.-L., 2000. Decreasing oxygen concentrations in the Gullmar Fjord, Sweden, as confirmed by benthic foraminifera, and the possible association with NAO. J. Marine Syst., 23: 303-316.

Okita, P.M., Maynard, J.B., Spiker, E.C. and Force, E.R., 1988. Isotopic evidence for organic matter oxidation by manganese reduction in the formation of stratiform manganese carbonate ore. Geochim. Cosmochim. Acta, 52: 2679-2685.

Paillard, D., Labeyrie, L. and Yiou, P., 1996. Macintosh program performs time-series analysis. Eos Trans. Am. Geophys. Union, 77: 379.

Pearce, R.B., Kemp, A.E.S., Koizumi, I., Pike, J., Cramp, A. and Rowland, S.J., 1998. A laminae-scale, SEM-based study of a late Quaternary diatom-ooze sapropel from the Mediterranean ridge, Site 971. Proc. ODP Sci. Res., 160: 333-348.

Pedersen, T.F. and Price, N.B., 1982. The Geochemistry of manganese carbonate in Panama basin sediments. Geochim. Cosmochim. Acta, 46: 59-68.

Pike, J. and Kemp, A.E.S., 1996a. Preparation and analysis techniques for studies of laminated sediments. In: A.E.S. Kemp (Editor), Palaeoclimatology and Paleoceanography from Laminated Sediments. Geol. Soc. Spec. Pupl., London, pp. 37-48.

Pike, J. and Kemp, A.E.S., 1996b. Records of seasonal flux in Holocene laminated sediments from the Gulf of California. In: A.E.S. Kemp (Editor), Palaeoclimatology and Plaeoceanography from laminated sediments. Geol. Soc. Spec. Publ., London, pp. 157-169.

Pike, J. and Kemp, A.E.S., 1997. Early Holocene decadal-scale ocean variability recorded in Gulf of California laminated sediments. Paleoceanography, 12(2): 227-238.

Pike, J. and Kemp, A.E.S., 1999. Diatom mats in Gulf of California sediments: Implications for the paleoenvironmental interpretation of laminated sediments and silica burial. Geology, 27(4): 311-314.

Piker, L., Schmaljohann, R. and Imhoff, F., 1998. Dissimilatory sulfate reduction and methane production in Gotland Deep sediments (Baltic Sea) during a transition from oxic to anoxic bottom water (1993-1996). Aquat. Microb. Ecol., 14: 183-193.

Pingitore, N.E., Eastman, M.P., Sandidge, M., Oden, K. and Freiha, B., 1988. The coprecipitation of manganese with calcite: an experimental study. Mar. Chem., 25: 107-120.

Pohl, C. and Hennings, U., 1999. The effect of redox processes on the partitioning of Cd, Pb, Cu, Mn between dissolved and particulate phases in the Baltic Sea. Mar. Chem., 65: 41-53.

Postma, D. and Appelo, C.A.J., 2000. Reduction of Mn-oxides by ferrous iron in a flow system: Column experiment and reactive transport modelling. Geochim. Cosmochim. Acta, 64(7): 1237-1247.

Rahm, L., 1988. Hydrographic properties of the eastern Gotland Basin. Beitr. Meereskd., 58: 47-58.

Raukas, A., 1995. Evolution of the Yoldia Sea in the eastern Baltic. Quat. Int., 27: 99 - 102.

Rines, J.E.B. and Hargraves, P.E., 1988. The Chaetoceros ehrenberg (Bacillariophyceae) flora of Narrangansett Bay, Rhode Island, USA. Bibliotheca Phycologyca, 195 pp.

Rogers, J.C., 1997. North Atlantic storm track variability and its association to the North Atlantic Oscillation and Climate Variability. J. Clim., 10: 1635-1647.

Round, F.E., Crawford, R.M. and Mann, P.G., 1990. The Diatoms: Biology and Morphology of the genera. Cambridge University Press, Cambridge, 747 pp.

Salonen, V.-P., Grönlund, T., Itkonen, A. and Sturm, M., 1995. Geochemical record on early diagenesis of recent Baltic Sea sediments. Mar. Geol., 129: 101-109.

Sancetta, C., 1989. Spatial and temporal trends of diatom flux in the British Colombian fjords. J. Plankton Res., 11(3): 503-520.

Sancetta, C., 1996. Laminated diatomaceous sediments: controls on formation and strategies for analysis. Geol. Soc. Spec. Pupl., 116: 17-21.

Sancetta, C., Villareal, T.A. and Falkowski, P., 1991. Massive fluxes of rhizosolenid diatoms: a common occurrence? Limnol. Oceanogr., 36: 1452-1457.

Schinke, H. and Matthäus, W., 1998. On the causes of major Baltic inflows-an analysis of a long time series. Cont. Shelf Res., 18: 67-97.

Schmutz, C., Luterbacher, J., Gyalistras, D., Xoplaki, E. and Wanner, H., 2000. Can we trust proxy-based NAO index reconstructions. Geophys. Res. Let., 27(8): 1135-1138.

Sivkov, V.V., Emeis, K.C., Endler, R., Zhurov, Y. and Kuleshov, A., 1998. Observations of the Nepheloid layers in the Gotland Deep (August 1994). In: K.C. Emeis and U. Struck (Editors), Gotland Deep Experiment (GOBEX). Status report on investigations concerning benthic processes, sediment formation and accumulation. Meereswiss. Ber., Warnemünde, **34**, pp. 84-96.

Smetacek, V., 2000. Oceanography - The giant diatom dump. Nature, 406(6796): 574-575.

Sohlenius, G., 1996. The history of the Baltic proper since the Late Weichselian deglaciation as recorded in sediments. Quaternaria A, 3: 34.

Sohlenius, G., Emeis, K.C., Andrén, E., Andrén, T. and Kohly, A., 2001. Development of anoxia during the Holocene fresh-brackish water transition in the Baltic Sea. Mar. Geol., 177: 221-242.

Sohlenius, G., Sternbeck, J., Anden, E. and Westman, P., 1996a. Holocene history of the Baltic Sea as recorded in a sediment core from the Gotland Deep. Mar. Geol., 134: 183-201.

Sohlenius, G., Wastegård, S. and Sternbeck, J., 1996b. Evidence of benthic colonisation during formation of laminated sediments in the Gotland Deep, Baltic Sea. Quaternaria, A(3): paper IV.

Sohlenius, G. and Westman, P., 1998. Salinity and redox alternations in the northwestern Baltic proper during the late Holocene. Boreas, 27(2): 101-114.

Sternbeck, J., 1997. Kinetics of rhodochrosite crystal growth at 25°C: The role of surface speciation. Geochim. Cosmochim. Acta, 61: 785-793.

Sternbeck, J. and Sohlenius, G., 1997. Authigenic sulphide deposits and carbonate mineral formation in Holocene sediments of the Baltic Sea. Chem. Geol., 135: 55-73.

Sternbeck, J., Sohlenius, G. and Hallberg, R.O., 2000. Sedimentary trace elements as proxies to depositional changes induced by a Holocene fresh-brackish water transition. Aquat. Geochem., 6(3): 325-345.

Suess, E., 1979. Mineral phases formed in anoxic sediments by microbial decomposition of organic matter. Geochim. Cosmochim. Acta, 43: 337-352.

Sugisaki, R., Sugitani, K. and Adachi, M., 1991. Manganese carbonate bands as an indicator of hemipelagic sedimentary environments. J. Geol., 99: 23-40.

Sviridov, N.I., Sivkov, V.V., Rudenko, M.V. and Trimonis, E.S., 1997. Geological evidence of bottom currents in Gotland Basin of the Gotland Basin. Oceanol., 37: 838-844.

Taylor, K.G. and Macquaker, J.H.S., 2000. Early diagenetic pyrite morphology in a mudstone-dominated succession: the Lower Jurassic Cleveland Ironstone Formation, Eastern England. Sediment. Geol., 131: 77-86.

Thomson, D.J., 1982. Spectrum estimation and harmonic analysis. IEEE Proc., 70: 1055-1096.

Thomson, D.J., 1990. Time series analysis of Holocene climate data. Phil. Trans. R. Soc. Lond. A, 330: 601-616.

Thomson, J., Higgs, N.C., Jarvis, I., Hydes, S., Colley, S. and Wilson, T.R.S., 1986. The behaviour of manganese in Atlantic carbonate sediments. Geochim. Cosmochim. Acta, 50: 1807-1818.

van Santvoort, P., de Lange, G., Thomson, J., Cussen, H., Wilson, T.R.S., Krom, M. and Ströhle, K., 1996. Active post-depositional oxidation of the most recent sapropel (S1) in sediments of the eastern Mediterranean Sea. Geochim. Cosmochim. Acta, 60(21): 4007-4024.

Villareal, T.A., Altabet, M.A. and Culver-Rymszoa, K., 1993. Nitrogen transport by vertically migrating diatom mats in the North Pacific Ocean. Nature, 363: 709-712.

Villareal, T.A. and Carpenter, E.J., 1989. Nitrogen-fixation, suspension characteristics and chemical composition of rhizosolenia mats in the central North Pacific. Gyre Biol. Oceanogr., 6: 387-405.

Walker, G.T. and Bliss, E.W., 1932. World weather V. Mem. Roy. Meteor. Soc., 4(53-84).

Wastegård, S., Andrén, T., Sohlenius, G. and Sandgren, P., 1995. Different phases of the Yoldia Sea in the north-western Baltic Proper. Quat. Int., 27: 121-129.

Westman, P. and Sohlenius, G., 1999. Diatom stratigraphy in five offshore sediment cores from the northwestern Baltic proper implying large scale circulation changes during the last 8500 years. Journal of Paleolimnology, 22(1): 53-69.

Xu, X., Huang, H. and Liu, B., 1990. Manganese deposits of the Proterozoic Datangpo Formation, South China: Genesis and paleogeography. Int. Assoc. Sedimentol. Spec. Publ., 11: 39-50.

Yemelyanov, E.M., Trimonis, E.S., Lukashina, N.P. and Slobodyannik, V.M., 1995. Stratigraphy and composition of the stratotype core from the Gotland Deep (Baltic Sea). Oceanol., 35: 99-104.

Zenkevitch, L., 1963. Biology of the Seas of the USSR. George Allen and Unwin Ltd., London, 270 pp.

APPENDICES

CONTAINS ONE DATA CD-ROM, THAT INCLUDES ALL DATA COLLECTED AS PART OF THIS STUDY, AND A FULL ELECTRONIC COPY OF THIS THESIS, ACCEPTED MANUSCRIPTS AND FIGURES.

A. Fabric Logs

B. Energy Dispersive X-Ray Microanalysis Data

C. Foraminifera Analysis Data

D. Stable-Isotope-Mass-Spectrometry Data

E. Ion-Coupled-Plasma-Mass-Spectrometry Data

F. Bioturbation Index Data

G. X-ray Diffraction Traces

H. Manuscripts Accepted for Publication

All Files presented are formatted for PC and can be viewed using MS Word 97 (.doc), CorelDraw 5 (.cdr), CorelPhotoPaint 5 (.jpg), or MS Excel 97 (.xls) respectively.